Deciphering the assembly pathway of type IV pili in *Myxococcus xanthus*

Dissertation
zur Erlangung des Doktorgrades
der Naturwissenschaften
(Dr. rer. nat.)

dem Fachbereich Biologie
der Philipps-Universität Marburg
vorgelegt von

Carmen Friedrich
aus Kirchen (Sieg)

Marburg an der Lahn, Oktober 2013

Die Untersuchungen zur vorliegenden Arbeit wurden von Oktober 2010 bis Juni 2013 am Max-Planck-Institut für terrestrische Mikrobiologie unter der Leitung von Prof. Dr. Lotte Søgaard-Andersen durchgeführt.

Vom Fachbereich Biologie der Philipps-Universität Marburg (Hochschulkennziffer: 1180) als Dissertation angenommen am 02.10.13

Erstgutachterin: Prof. Dr. Lotte Søgaard-Andersen

Zweitgutachterin: PD Dr. Sonja-Verena Albers

Weitere Mitglieder der Prüfungskommission:

Prof. Dr. Andrea Maisner

Prof. Dr. Michael Bölker

Tag der mündlichen Prüfung: 19.11.13

Die während der Promotion erzielten Ergebnisse sind zum Teil in folgenden Originalpublikationen veröffentlicht worden:

- Outside-in assembly pathway of the type IV pili system in *Myxococcus xanthus*
Carmen Friedrich, Iryna Bulyha & Lotte Søgaard-Andersen (2013) J Bacteriol.

- The ubiquitous peptidoglycan-binding protein TsaP functions in surface assembly of type IV pili
Katja Siewering, Samta Jain, Carmen Friedrich, M.T.Webber-Birungi, Ina Binzen, Alexander Wagner, Stuart Huntley, Jörg Kahnt, Andreas Klingl, Egbert J. Boekema, Lotte Søgaard-Andersen and Chris van der Does (manuscript in preparation).

Table of contents

Abstract

Type IV pili (T4P) are hairlike surface structures, present on a variety of different bacteria. They are polymers involved in diverse functions such as motility, adherence, protein secretion, DNA uptake and in many pathogens they are found to be the primary colonization factor. Especially their role in virulence makes T4P particularly relevant for studying pilus function and assembly.

The T4P machinery consists of 12 conserved proteins building an envelope-spanning macromolecular machinery, which localizes polarly in *Myxococcus xanthus*. Although most of the proteins have been known and studied for a long time, the precise mechanism of how and in which order the individual components are assembled to generate a macromolecular machinery remain largely unknown. Here we uncovered a sequential, outside-in assembly pathway starting with the outer membrane (OM) PilQ secretin, and proceeding inwards over the periplasm and inner membrane (IM) to the cytoplasm. Specifically, by taking advantage of the cell biology tools for studying T4P in *M. xanthus*, we carried out one of the largest screens comprising 11 of the 12 proteins of the T4P machinery by systematically profiling the stability and localization of T4P proteins in the absence of each individual other T4P protein in combination with mapping direct protein-protein interactions. Using these approaches, we show that assembly of the T4P machinery initiates with the formation of the PilQ secretin ring, assisted by its pilotin Tgl, in the OM. Oligomeric PilQ serves as an assembly platform for further T4P components. PilQ recruits TsaP, a peptidoglycan binding protein, as well as PilP by direct interactions with PilP. PilP, in turn, recruits the IM proteins PilN and PilO. PilP/PilO/PilN likely make up a complex aligning IM and OM components of the T4P machinery. The PilP/PilO/PilN complex recruits cytoplasmic PilM by direct interaction between PilN and PilM and recruits PilC, presumably by direct interaction between PilC and PilO. Finally, the ATPases PilB and PilT that power extension and retraction of T4P, localize independently of other T4P machinery proteins.

In this study, we elucidate the assembly process and functional interactions between T4P proteins. This work lays the basis for further understanding of these functionally highly versatile surface structures. Interestingly, the assembly of the type II and III secretion systems also initiates from the OM secretin and proceeds inwards. Thus, an outside-in assembly pathway is emerging as a conserved feature in secretin-containing trans-envelope export machines.

Zusammenfassung

Type-IV-pili (T4P) sind haar-ähnliche Zellanhänge und kommen auf der Oberfläche von einer Vielzahl von verschiedensten Bakterien vor. Sie sind Polymere, welche an diversen Funktionen beteiligt sind, wie z.B an der Fortbewegung von Zellen, Anheftung an diverse Oberflächen, Protein-Sekretion, DNA-Aufnahme und in vielen pathogenen Bakterien werden sie primär zur Kolonisierung von Wirtszellen genutzt. Vor allem ihre Rolle als Pathogenitätsfaktor begründet das starke Interesse an der Erforschung von T4P.

Die T4P-Maschinerie besteht aus mindestens 12 Proteinen, welche zusammen einen makromolekularen Komplex bilden, der die komplette Zellhülle durchspannt. In *Myxococcus xanthus* wird dieser Komplex an beiden Zellpolen ausgebildet. Obwohl die meisten beteiligten Proteine schon vor langer Zeit identifiziert und seitdem studiert wurden, ist es bis heute noch unklar wie und in welcher Reihenfolge die einzelnen Komponenten miteinander interagieren, um den Multiprotein-Komplex zu assemblieren. Die Ergebnisse dieser Arbeit führten uns zu der Hypothese, dass die T4P-Maschinerie von Außen nach Innen aufgebaut wird. Die Assemblierung beginnt mit dem Sekretin PilQ in der äußeren Membrane und setzt sich fort über Proteine im Periplasma, der inneren Membran bis hin zu zytoplasmatischen Komponenten. Wir haben uns die diversen, verfügbaren zellbiologischen Methoden in *M. xanthus* zu Nutze gemacht und eine der umfassendsten Untersuchungen des T4P-Systems durchgeführt. Dabei haben wir systematisch 11 der 12 Proteine auf Ihre Abhängigkeit untereinander bezüglich ihrer Stabilität und Lokalisation untersucht. Zudem wurden direkte Proteininteraktionen *in vitro* studiert. Mit dieser Vorgehensweise konnten wir ein Modell zur Assemblierung der T4P-Maschinerie erstellen. Der Aufbau beginnt mit PilQ in der äußeren Membran, welches mit Hilfe von Tgl einen oligomerischen Ring bildet, welcher eine Art Assemblierungsplattform für weitere Komponenten darstellt. Zunächst wird TsaP vom PilQ-Multimer rekrutiert und verankert den Komplex vermutlich zum Peptidoglycan mit Hilfe der LysM-Domäne in TsaP. Des Weiteren werden PilP, sowie die beiden Proteine PilN und PilO in der inneren Membran rekrutiert, welche zusammen als Komplex innere und äußere Membran überbrücken und damit vermutlich die Proteine in beiden Membranen aufeinander ausrichtet. Dann werden weitere Komponenten in den Komplex integriert, wie PilC, vermutlich durch direkte Interaktion mit PilO und ebenfalls PilM wird durch direkte Interaktion mit PilN mit der T4P-Maschinerie verbunden. Die ATPasen PilB und PilT, die die Energie zur Extension und Retraktion der T4P bereitstellen, lokalisieren unabhängig von allen Komponenten des T4P-Komplexes und interagieren vermutlich nur transient.

In dieser Arbeit haben wir den Assemblierungsprozess, als auch direkte Interaktionen zwischen verschiedenen T4P-Proteinen untersucht, welches eine Grundlage für die weitere Erforschung dieser funktionell vielseitigen Strukturen schafft. Bemerkenswert ist die Tatsache, dass die Assemblierung des Type-II- als auch des Type-III-Sekretionssystems, ebenfalls mit dem Sekretin Protein in der äußeren Membran initiiert wird und sich weiter nach innen fortsetzt. Daher stellt sich die Frage, ob die Assemblierung von Außen nach Innen einen konservierten Mechanismus für den Aufbau von Zellhüll-durchspannenden Multi-Proteinkomplexen darstellt.

Abbreviations

ATP/ADP	Adenosin tri-/diphosphate
a.u.	arbitrary unit
BACTH	Bacterial Adenylate Cyclase-based Two-Hybrid
Bfp	Bunlde forming pili
bp	base pairs
BSA	Bovine serum albumin
CC	Coiled coil
Cm	Chloramphenicol
C-terminus	Carboxyl-terminus
CTT	Casitone Tris medium
ECM	Extracellular matrix
EM	Electron microscopy
EPS	Extracellular polysaccharides
EPEC	Enteropathogenic *E. coli*
EPS	Exopolysaccharides
FAC	Focal adhesion complexes
Frz	Frizzy
Gsp	General secretory pathway
GTP/GDP	Guanosine tri-/ diphosphate
h	hours
IM	Inner membrane
IPTG	Isopropyl β-D-1-thiogalaktopyranoside
Km	Kanamycin
LPS	Lipopolysaccharides
MANT-ATP	2'-/3'-O-(N'- Methylanthraniloyl) adenosine-5'-O-triphosphate
min	minutes
N-terminus	Amino-terminus
OM	Outer membrane
PMF	Proton motive force
pN	piconewton
s	seconds
SDS-PAGE	Sodium dodecyl sulfate polyacrilamide gel electrophoresis
Sec	secretory
sfGFP	superfolder green fluorescent protein
T2SS	Type II secretion system
T3SS	Type III secretion system

T4P	Type IV pili
Tad	Tight adherence pili
Tcp	Toxin co-regulated pili
TLC	Thin layer chromatography
TPR	tetratricopeptide repeat
YFP	Yellow fluorescent protein
WT	Wild type

1 Introduction

Type IV pili (T4P) are one of the most abundant surface structures and present on Gram-positive and Gram-negative bacteria (Pelicic, 2008). Recent studies suggest that also archaea possess T4P like surface structures (Ghosh & Albers, 2011). Interestingly, type II secretion systems (T2SS) and T4P likely share a similar architecture despite extensive sequence divergence of the individual components, suggesting a common evolutionary origin (Peabody *et al.*, 2003). Presumably, the T4P/T2SS system originated early in evolution and emerged as a successful system for trans-envelope protein transport and evolved to perform distinct functions by adapting to the respective, specialized requirements of different systems and organisms.

The biological significance of T4P arises from the variety of functions, which they can perform, including adhesion to biotic or abiotic surfaces (Craig & Li, 2008), biofilm formation (Klausen *et al.*, 2003, O'Toole & Kolter, 1998), cellular motility (Bradley, 1980, Henrichsen, 1983, Wall & Kaiser, 1999) and DNA-uptake during transformation (Averhoff & Friedrich, 2003). As T4P are expressed by a range of plant, animal and human pathogens, where they mediate the attachment to host cells (Mattick, 2002), they are important virulence factors. Therefore, understanding and investigating the assembly and function of T4P is crucial for understanding their role during pathogenesis and might uncover new targets for antibacterial drugs.

1.1 Type IV pili (T4P)

As the name pilus (Latin for “hair”) implies, T4P are thin, hair-like structures that are 5-8 nm in width and several microns in length (Craig & Li, 2008). They are polymerized fibers, predominantly composed of thousands of copies of the major pilin. Additionally, pili may contain minor pilins, which are less abundant. T4 pilins are synthesized as precursor proteins carrying a type III leader peptide that is cleaved off in the mature protein. The pilin subunits are anchored in the inner membrane (IM) from which they can be incorporated into the base of the extending pilus. T4P are rapidly assembled and in some cases disassembled (~500-700 subunits/s) (Clausen *et al.*, 2009, Skerker & Berg, 2001) and can withstand forces of up to 150 pN (Clausen et al., 2009). A pore in the outer membrane (OM), called secretin allows the passage of the assembled pilus to the exterior of the cell (Wolfgang *et al.*, 2000). The machinery required for biogenesis and function of T4P is a macromolecular, multiprotein complex spanning the whole cell envelope and is powered by ATP hydrolysis (Jakovljevic *et al.*, 2008, Sakai *et al.*, 2001, Turner *et al.*, 1993).

A number of distinct features of pilin subunits and assembly system has lead to the subdivision into type IVa and type IVb pili. T4aP are found in *Pseudomonas, Neisseria, Dichelobacter, Thermus, Myxococcus, Bdellovibrio* and *Shewanella* (Pelicic, 2008). So far, T4bP have been characterized best in bacteria that colonize the human intestine, like enteropathogenic, enterohemorrhagic and enterotoxigenic *Escherichia coli*, *Salmonella enteric* serovar Typhi and *Vibrio cholera* (Giltner *et al.*, 2012). The T4bP subclass includes bundle forming pili (Bfp), toxin co-regulated pili (Tcp), R64 thin pili and another subtype, called tight adherence pili (Tad or Flp pili) (Pelicic, 2008). T4b and Tad pili are typically not involved in cellular motility and for a long time it has been elusive if T4bP can retract as most of the systems are missing the ATPase providing the energy for retraction. Hence, T4bP probably function primarily in adhesion and cell aggregation. In contrast, T4aP are highly dynamic structures cycling between extension and retraction. Upon retraction T4aP can generate forces of up to 150 pN per pilus (Clausen et al., 2009). Bundles of T4P have been shown to generate even higher forces in the nanonewton range when retracting in a cooperative manner (Biais *et al.*, 2008). T4aP and T4bP can be distinguished by sequence and length of the mature pilin subunit and their leader peptides (Faast *et al.*, 1989). While the leader peptides of T4a pilins are generally short with six to seven residues, the leader peptides of the T4b subfamily are longer with 15 to 30 residues. Moreover, in the T4aP system, the N-terminus is methylated on a phenylalanine, whereas the methylated residue is variable for T4b pilins (Craig *et al.*, 2004). The mature pilin in the T4bP subfamily is composed of around 180 to 200 residues, while the type IVa pilins are smaller with 150 to 175 residues. An exception is the Tad pilus with pilins composed of only 50 to 80 residues (Kachlany *et al.*, 2001). The assembly machineries of T4aP and T4bP share five to six core components (Table 1): the pilin subunit, a prepilin peptidase, a traffic ATPase, providing the energy for extension of T4P, an integral IM protein of unknown function and an integral OM protein, called secretin that forms the pore in the OM. Many of the T4P systems also contain a retraction ATPase. However, it is rarely detected in T4bP systems

1.1.1 Type IV Pilins

PilA is the major pilin subunit and is synthesized as a precursor in the cytoplasm, targeted to the IM presumably by the Sec system as it was shown for several pseudopilins (Arts *et al.*, 2007, Francetic *et al.*, 2007). Due to their hydrophobic α-helical N-terminus, pilins remain in the IM where they are processed by the prepilin peptidase (Nunn & Lory, 1991). The leader peptide is cleaved at the cytoplasmic side of the IM and the new N-terminus is methylated. Both actions are required for the

incorporation of the subunits into the pilus. The conserved, hydrophobic N-terminus performs two functions: It is a transmembrane domain and also mediates fiber formation via hydrophobic association (Craig *et al.*, 2003). There is a reservoir of pilins in the IM from which they are incorporated into the base of the extending pilus. Likewise, pilus retraction involves the removal of pilins at the base of the pilus and incorporation into the IM (Morand *et al.*, 2004).

So far, several crystal structures of pilins have been solved and revealed that all type IV pilins share a similar architecture. To date only full-length structures of T4aP subunits have been solved (Hartung *et al.*, 2011, Craig et al., 2003, Parge *et al.*, 1995). For T4b pilins and some T4a pilin structures the hydrophobic N-terminus was removed to improve solubility of the protein to obtain crystals (Audette *et al.*, 2004, Balakrishna *et al.*, 2006, Ramboarina *et al.*, 2005). In essence, pilins are composed of two major domains; the N-terminal α-helical domain, called α1, and the globular head domain (Figure 1). While the C-terminal half of the α1 domain (α1-C) is embedded in the globular head domain, the hydrophobic N-terminal half (α1-N) is protruding from the globular head domain. α1-N is suggested to mediate pilus assembly by forming hydrophobic helical bundles in the central core of the assembled filament (Craig et al., 2004) (Figure 2).

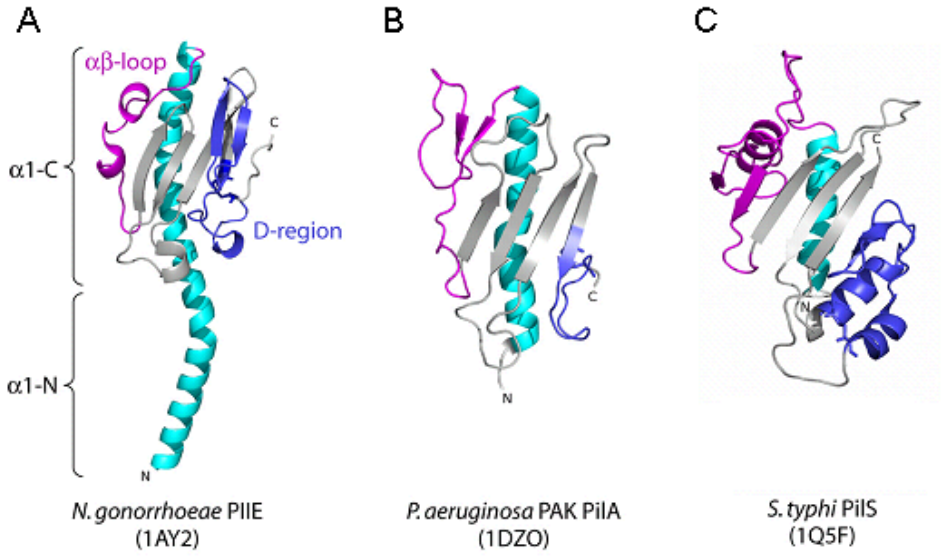

Figure 1 – Comparison of type IV pilin structures. The comparison of different crystal structures of type IVa and type IVb pilins revealed a similar overall architecture. The α1 helix shown in cyan is divided into the α1-C and α1-N domain. The αβ-loop, which connects the α1 domain and the β-sheet (grey) is marked in magenta. The variable D-region formed by the disulfide-bond of two conserved cysteine residues is highlighted in blue. A) Structure of the full-length major pilin PilE from *N. gonorrhoeae* (T4aP). B) Structure of the globular head domain of PilA from *P. aeruginosa* strain PAK (T4aP). C) Structure of the globular head domain of PilS from *S. typhi* (T4bP). Figure modified from Giltner et al. (2012).

In the full length structures of *P. aeruginosa* PAK and gonoccocal (GC) pilins, α1 was shown to have a shallow S-shaped curve (Craig et al., 2003, Parge et al., 1995) generated by the residues Pro22 and Gly/Pro42. The curvature is suggested to contribute to the flexibility of the α1 domain that is important for packing of the pilus fiber. The α1 structure of the T4b pilins may be less curved, as the residues at position 22 and 42 are neither proline nor glycine. Though, it is suggested that the flexibility of the T4b pilins is accomplished by a looser packing in the filament (Giltner et al., 2012). The globular head domain generally consists of a 4- to 7-stranded antiparallel β-sheet and the α1-C domain. The region connecting the N-terminal α1 helix to the β-sheet in the head domain is called the αβ-loop and is located on one side of the head domain (Figure 1). It is one of the regions in T4 pilins that exhibits variability in sequence, length and structure (Craig et al., 2004). The second variable region is the disulfide-bonded loop or D-region, which is built from two conserved cysteines and is thought to be the receptor binding loop during attachment to host cells in PAK pili (Farinha *et al.*, 1994) (Figure 1). Both regions on the globular domain are suggested to be involved in pilin subunit interactions and to define the surface chemistry of the fiber, contributing to the diverse functions of T4P (Craig et al., 2004). As pilus fibers are exposed on the cell surface, where they are involved in the attachment to host cells, they are undergoing intensive investigation as a vaccine target. T4 pilins have been shown to be immunogenic and provoke serological responses (Sheth *et al.*, 1995, Sun *et al.*, 1991). However, pathogenic bacteria such as *Neisseria* or *Pseudomonas* species have developed strategies to avoid the immune recognition e.g. antigenic variability, phase variation or post-translational modifications (Hagblom *et al.*, 1985, Segal *et al.*, 1985, Comer *et al.*, 2002). Antigenic variation, especially in the D-region, can be achieved by inter- and intra-strain sequence variation as a result of intergenic recombination, horizontal gene transfer and homologous recombination or point mutations. Phase variation is a phenomenon observed in *Neisseria* species, which describes the variation between hyperpiliated and nonpiliated strains probably due to a recombination event affecting the major pilin subunit (Criss *et al.*, 2005). This might help *Neisseria* cells to escape immune recognition after initial attachment to host cells mediated by T4P.

1.1.2 Pilus fiber

A common feature of all type IV pilins is the ability to reversibly polymerize into fibers. Based on the present crystal structures and cryo-electron microscopy data, models describing the molecular architecture of T4P were obtained. In these models, the α1 helices are twisted in a helical manner building the core of the pilus fiber,

anchoring the globular head domains, which build up the outer surface (Craig & Li, 2008) (Figure 2). T4aP from *N. gonorrhoeae* are modeled as a 3-start left-handed helix, 1-start right handed or 4-start right handed helix with 3.6 subunits per turn (Craig *et al.*, 2006). The pilus has an outer diameter of around 60 Å, which fits the size of the secretin channel with an opening of ~65 Å (Collins *et al.*, 2001). Current models for the T4bP fiber support a wider structure of approximately 90 Å in width and a 3-start left-handed helix (Craig et al., 2006) or a right-handed 1-start helix (Li *et al.*, 2012) (Figure 2). This is likely due to the bulky C-termini of the T4b pilins, which prevents tighter packing of the fiber and therefore also reduces the resistance to heat and proteases compared to T4aP (Li et al., 2012).

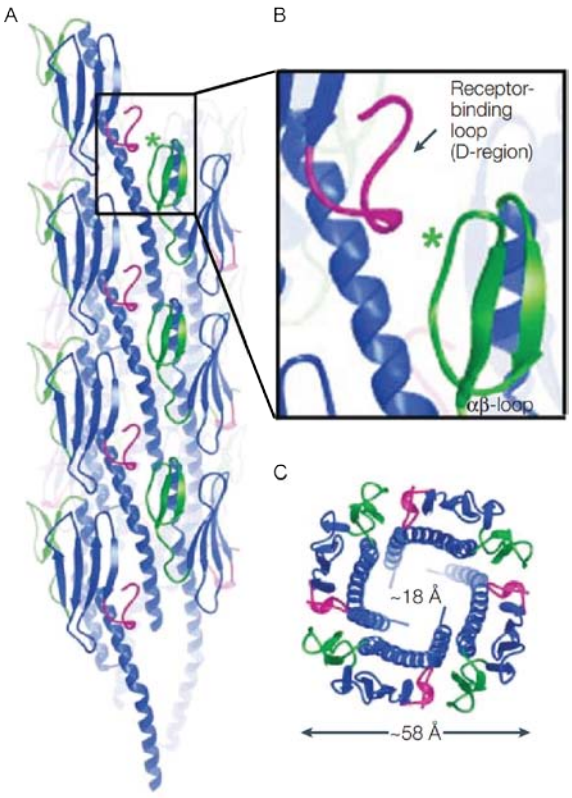

Figure 2 – Assembly model for PAK pili A) Ribbon diagram of the *P. aeruginosa* PAK pilus assembly model. Interactions between the αβ-loop (green) and the D-region (magenta) are shown in the 3-start strands. The D-region is buried in the filament and is only exposed at the tip of the fiber. A detailed view of the boxed area is shown in (B). B) Detailed view of the interaction site of the D-region and the αβ-loop. The green asterix shows the position of a disaccharide in the GC pilin structure. C) End-view of the PAK pilus model. This figure is modified from Craig et al. (2004).

A recent study on T4aP in *N. gonorrhoeae* revealed that pili can undergo force-induced structural changes (Biais *et al.*, 2010). Under strain, the pilus gets longer and thinner while residues, which are usually buried in the fiber, get surface exposed. Importantly, this conformational transition is reversible, as the pili regain their original structure upon

release of the force. The reversible transition might prevent detachment or breaking of T4P during shearing forces (Biais et al., 2010).

How the pilin subunits are extracted from the membrane and incorporated into the pilus, as well as mechanisms for initiation of pilus assembly or retraction remain to be elucidated. Referring to the similarity of T4P and the T2SS, it was shown that the T2SS assembles the major pseudopilin PulG (also called GspG) into periplasmic filaments, which may drive protein secretion in a piston-like manner. Upon overexpression of PulG, surface exposed pili were observed (Sauvonnet *et al.*, 2000) supporting the similarity between both systems. For the T2SS it is suggested that the minor pseudopilins self-assemble and build an initiation complex allowing the subsequent polymerization of the major pseudopilins beneath this complex (Cisneros *et al.*, 2012a). It is unclear whether the minor pilins work in a similar manner in the T4P system. To address this question Cisneros et al. expressed minor pilins in a T2SS and showed that they were able to initiate pseudopilus assembly, suggesting that minor pilins presumably also function in the initiation of pilus assembly in the T4P system (Cisneros *et al.*, 2012b). A recent publication revealed another function for minor pilins. ComP, one out of three minor pilins in *Neisseria* species, was shown to specifically bind to DNA in *N. meningitidis,* suggesting T4P bind and pull in DNA via ComP during DNA uptake (Cehovin *et al.*, 2013).

1.1.3 T4P assembly machinery

The assembly machineries for T4a and T4b pili systems share 5-6 core components and in addition, each system has its own specialized proteins. An overview of the conserved components of both systems and the nomenclature in different organisms is given in Table 1.

Table 1 – Nomenclature of key Type IV biogenesis components.[1]

Bacteria	Pilin subunit	Prepilin peptidase	Assembly ATPase	Retraction ATPase	Inner membrane protein	Secretin
Type IVa pili						
Pseudomonas aeruginosa	PilA, PilE	PilD	PilB	PilT, PilU	PilC	PilQ
Neisseria gonorrhoeae	PilE	PilD	PilF	PilT	PilG	PilQ
N. meningitidis	PilE	PilD	PilF	PilT	PilG	PilQ
Francisella tularensis	PilE	PilD	PilF	PilT	PilG	PilQ
Non-typeable *Haemophilus influenzae*	PilA	PilD	PilB		PilC	ComE
Myxococcus xanthus	PilA	PilD	**PilB***	PilT	**PilC***	PilQ
Clostridium perfringens (Gram positive)	PilA1, PilA2	PilD	PilB	PilT		None
Dichelobacter nodosus	FimA	FimP	FimN	PilT	FimO	PilQ
Type IVb pili						
Vibrio cholerae	TcpA, MshA	TcpJ	TcpT		TcpE	TcpC
Enteropathogenic *Escherichia coli* (EPEC)	BfpA	BfpP	BfpD	BfpF	BfpE	BfpB
Enterotoxigenic *E. coli* (ETEC)	CofA	CofP	CofH		CofI	CofD
Enterotoxigenic *E. coli* (ETEC)	LngA	LngP	LngH			LngD
Salmonella Typhi	PilS	PilU			PilR	

[1] **This table is modified from Craig and Li (2008). * indicates proteins that were added.**

As the main focus of this study is on T4aP from *M. xanthus*, from now on we refer to these as T4P and the nomenclature of the *M. xanthus* system is used throughout the text.

Biogenesis and function of T4P require a set of 12 conserved proteins, which span the entire cell envelope (Figure 3). In addition to the core components PilA, PilB, PilT, PilC, PilD and PilQ, the proteins PilM, PilN, PilO, PilP, Tgl and TsaP are only conserved among T4aP systems (Pelicic, 2008), (Figure 7).

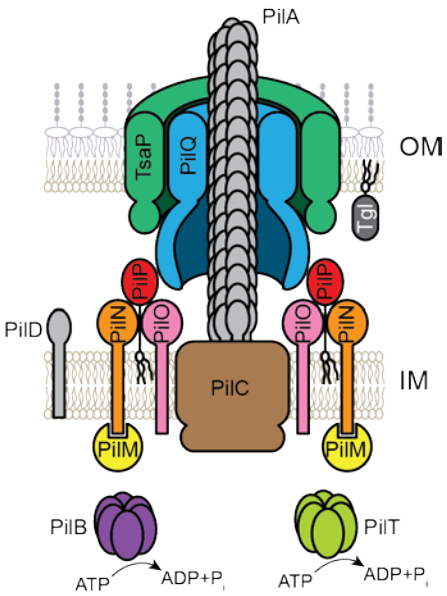

Figure 3 - Model of the T4P machinery. See text for details. Proteins are not drawn to scale. OM, outer membrane; IM, inner membrane. The figure is modified from Friedrich et al. (2013).

Prepilin peptidase PilD

After synthesis and incorporation of the pilin subunits in the IM they are processed by the prepilin peptidase PilD (Nunn & Lory, 1991). Prepilin peptidases constitute a family of bilobed aspartate proteases located in the IM that cleave the leader peptide of T4 prepilins and T4 prepilin-like proteins probably at the cytoplamsic side of the IM (Strom *et al.*, 1993). This cleavage is essential for the incorporation of the subunits into the pilus fiber (Strom & Lory, 1991). The new N-terminus is subsequently methylated by PilD.

Secretion ATPases PilB and PilT

Polymerization and depolymerization of the pilin subunits requires the hydrolysis of ATP. The energy required for pilus extension is provided by the cytoplasmic motor ATPase PilB (Turner et al., 1993). The ATPase activity of PilT enables pilus retraction (Wolfgang *et al.*, 1998, Merz *et al.*, 2000) and PilT is one of the few proteins that is not required for surface piliation, as a Δ*pilT* mutant still assembles pili (Wu & Kaiser, 1997, Whitchurch *et al.*, 1991). Both ATPases belong to the superfamily of secretion ATPases that are also found in T2SS and archaeal surface structures (Planet *et al.*, 2001, Peabody et al., 2003). Structural comparison of different members of this family revealed that the subunits of the ATPases share a bilobed structure with an N-terminal and C-terminal domain, connected by a flexible hinge region. The nucleotide is bound in the cleft between the two domains via conserved Walker A and Walker B boxes, as well as Asp and His box motifs in the C-terminal domain. PilB and PilT were shown to form hexameric rings. Crystal structures of PilT revealed that several invariant arginines play a critical role in PilT function. Satyshur et al. suggest that six arginine residues from two adjacent subunits in the hexamer form an arginine wire around the ATP-binding site (Satyshur *et al.*, 2007). The arginines in the N-terminal domain of one subunit might drive conformational changes by interaction with ATP in the C-terminal binding site of the adjacent subunit, and may lead the released P_i out of the active site. Satyshur and colleagues speculate that the arginines may act as an arginine finger in this motor that communicates the presence of ATP between adjacent subunits (Satyshur et al., 2007). Hence, the chemical energy from ATP hydrolysis is hypothesized to be converted into mechanical force via large domain movements in PilT, and is then transduced over the IM to enable pilus assembly or disassembly. Whether these motions in a cytoplasmic protein are transduced by direct interactions with the pilin subunits or indirectly through interaction with proteins of the IM remains unclear.

Platform protein PilC

A potential interaction partner of the two ATPases is the polytopic IM protein PilC, also called the platform protein. PilC is a member of the PilC/GspF family that is conserved in T2SS, T4P systems and archeal systems. Although PilC is one of the core components of the T4P machinery, its exact function remains largely unknown. Currently, there are different reports on the role of PilC. Whereas PilC is important for surface piliation in *P. aeruginosa* (Takhar *et al.*, 2013), studies on *N. meningitidis* revealed that PilC (PilG in *N. meningitidis*) is dispensable for pilus assembly, as the *pilC/pilT* double mutant is piliated (Carbonnelle *et al.*, 2006). Investigating the structure and oligomeric state of PilC in different organisms revealed that PilC presumably forms a tetrameric bilobed structure (Karuppiah *et al.*, 2010, Collins *et al.*, 2007). However, there are discrepancies describing the topology of the protein. While Karuppiah and colleagues propose a three transmembrane helix model, Collins and co-workers favor a four transmembrane helix model. Obviously, the number of transmembrane helices is important for the topology and to identify which domains are facing the cytoplasm or periplasm constituting potential interaction sites for other proteins of the T4P machinery. In *P. aeruginosa*, PilB polar localization and protein stability was shown to depend on the presence of PilC (Takhar et al., 2013, Chiang *et al.*, 2005). Furthermore, it was shown that the N-terminal domain of PilC can pull down PilB from whole cell extracts of *P. aeruginosa*, suggesting that the two proteins interact (Takhar et al., 2013). It is assumed that PilC mediates the interaction with PilB or PilT, transducing the energy for extension or retraction of the pilus over the IM. Indeed, a bacterial adenylate cyclase-based two-hybrid (BACTH) screen revealed direct interactions between PilC and the pilin subunit (Georgiadou *et al.*, 2012). However, the contradictory data on the importance of PilC in pilus assembly complicate the current understanding of PilC function in the T4P machinery and requires further research.

Secretin PilQ

PilQ builds a large, multimeric, ring-like complex, which belongs to the superfamily of GspD secretins. They are present in T2SS, T3SS, T4P systems, DNA-uptake systems and filamentous bacteriophage extrusion systems (Linderoth *et al.*, 1996). Secretins are integral OM proteins building the pores (50-80 Å in width) that allow the passage of folded proteins, oligomeric fibers or DNA. All secretins contain a conserved C-terminal domain that is important for OM integration and oligomerization (Figure 4). The N-terminal domain is more diverse among different secretins (Martin *et al.*, 1993). 3D structures suggest that this domain extends into the periplasm forming the sides of a secretin chamber (Reichow *et al.*, 2010) (Figure 5). The N-terminal part

is divided into different subdomains (Figure 4) and is thought to provide system and species specific features (Berry *et al.*, 2012). The N0 domain exhibits an αβ-type fold and is followed by one or several homologous repeat domains, called N1-N5. These domains are thought to line the walls of the periplasmic chamber. The extreme N-terminal region consisting of two β-domains, named B1 and B2, are only found in T4P secretins. 3D reconstructions by cryo-EM revealed that B1 and B2 form a kind of plug, closing the chamber on the periplasmic side (Berry et al., 2012, Collins *et al.*, 2004) (Figure 5). Therefore, the passage of a pilus fiber would require large domain movements. Collins and colleagues observed that T4P can induce structural changes in PilQ. They describe the induction of the dissociation of the cap feature and lateral movements of the arms upon interaction with purified pili (Collins *et al.*, 2005). Moreover, they showed that the PilQ complex was filled with pili and bound only to one end of the purified pilus fibers (Rumszauer *et al.*, 2006, Collins et al., 2005), suggesting that PilQ specifically recognizes and binds to the pilus and that the pilus fiber possesses a kind of polarity.

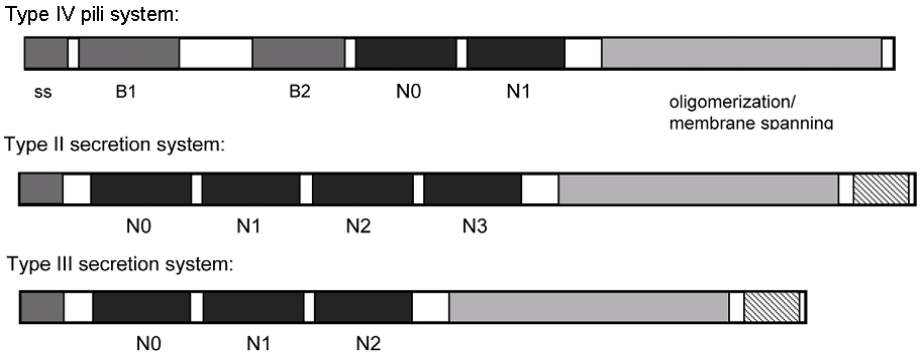

Figure 4 – Schematic illustration of domain structures in secretins. Comparison of the secretin domain organization among T4P system, T2SS and T3SS is based on secondary structure prediction and homology sequence alignments. The C-terminal domain is important for oligomerization and is embedded in the OM. B1 and B2 are special for T4P secretins and are predicted to provide interaction sites for system specific components. This figure is modified from Berry et al. (2012).

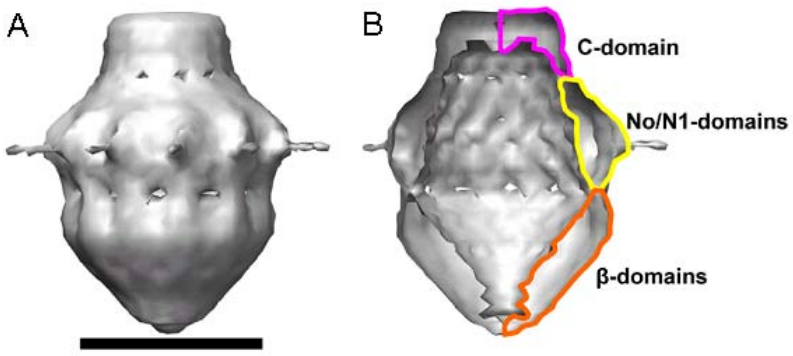

Figure 5 – 3D reconstruction of the PilQ complex by cryoelectron microscopy A) Surface contoured map of PilQ dodecamer. Scale bar 100 Å. B) Structure as shown in (A) with the front half of the volume removed to show domain boundaries of distinct structures within the density map. This figure is modified from Berry et al. (2012).

Pilotin Tgl

Oligomerization and presumably OM localization of many secretins require the help of another protein, called pilotin, which is one of the non-core components of the T4P machinery. In *M. xanthus* the pilotin protein is called Tgl. In different organisms, pilotins have been shown to be lipoproteins anchored in the OM (Carbonnelle *et al.*, 2005, Koo *et al.*, 2008, Rodriguez-Soto & Kaiser, 1997). Crystal structures of the Tgl homologs from *P. aeruginosa* (PilF) (Kim *et al.*, 2006) and *N. meningitidis* (PilW) (Trindade *et al.*, 2008) revealed that these proteins have six tetratricopeptide repeats (TPRs). TPRs in other proteins are usually involved in protein-protein-interactions (Andrade *et al.*, 2001). Tgl has not been crystallized so far, but sequence analysis showed six TPR domains in Tgl, suggesting that it folds similar to PilF or PilW .
It is currently unclear how Tgl or pilotins in general assist the secretin in multimer formation or OM localization.

Peptidoglycan binding protein TsaP

Electron microscopy analysis of PilQ multimers in the OM from *N. gonorrhoeae* revealed that the PilQ ring is surrounded by a second ring structure and spikes (Jain *et al.*, 2011). The second ring was recently proposed to consist of TsaP (Type IV pilus secretin associated protein). TsaP is conserved among T4aP systems and was shown to be important for surface piliation in *N. gonorrhoeae* (Siewering et al., manuscript in preparation). Upon deletion of *tsaP* in *N. gonorrhoeae* the second ring structure around PilQ and the spikes disappear (Figure 6). Moreover, lack of TsaP results in the formation of membrane protrusions filled with pili. Stability and OM association of TsaP seems to be highly dependent on PilQ whereas PilQ stability and oligomerization are not affected by lack of TsaP. In addition to domains of unknown function, TsaP contains a LysM domain. LysM domains have been reported to be involved in

peptidoglycan binding (Buist *et al.*, 2008). Consistently, tests for peptidoglycan binding of TsaP from *N. gonorrhoeae* were positive. The current idea is that TsaP anchors the secretin complex to the cell wall and helps to align PilQ with the IM complex, which is discussed in the following chapter (Siewering et al., manuscript in preparation).

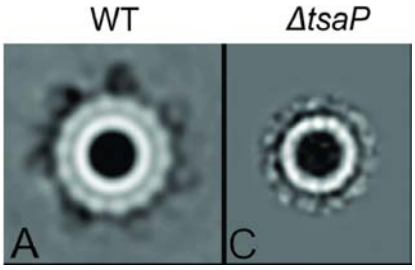

Figure 6 - Projection maps of single particle electron microscopy analysis of the secretin complex in isolated OMs from *N. gonorrhoeae*. Projection maps of class averages of single particle EM images were obtained from membranes isolated from the indicated strains. This figure is modified from Siewering et al., (manuscript in preparation).

PilM, PilN, PilO and PilP

The gene cluster *pilM/N/O/P/Q* is highly conserved among T4aP-expressing organisms (Pelicic, 2008). Mutagenesis studies revealed that each protein is required for T4P function (Rumszauer et al., 2006, Nudleman *et al.*, 2006, Martin *et al.*, 1995). Though, the exact function of PilM, PilN, PilO and PilP is not understood, they are suggested to form an cytoplasmic/IM complex, which bridges or aligns the OM secretin PilQ and the pilus assembly machinery in the IM (Ayers *et al.*, 2009). Similar to the platform protein PilC, there is some controversy concerning the role of PilM/N/O/P. While PilN/N/O/P seem to be essential for surface pilus expression in *N. meningitidis* (Carbonnelle et al., 2006), they seem to be dispensable in *P. aeruginosa* (Takhar et al., 2013).

PilP is a lipoprotein anchored in the IM (Balasingham *et al.*, 2007, Ayers et al., 2009) and was shown to interact directly with PilQ (Balasingham et al., 2007, Tammam *et al.*, 2013). 3D-reconstruction of transmission electron microscopy data of the PilP-PilQ complex suggested that PilP localizes around the cap region of the PilQ oligomer (Balasingham et al., 2007). Further structural characterization of PilP revealed that it has an N-terminal disordered region followed by a globular C-terminal domain possessing a simple β-sandwich type fold (Golovanov *et al.*, 2006, Tammam *et al.*, 2011). Interestingly, this fold is similar to the homology region (HR) of a protein from the T2SS, namely GspC, which interacts with its secretin GspD (Korotkov *et al.*, 2011). This domain of PilP was shown to be responsible for the direct interaction with the N0 domain of PilQ (Tammam et al., 2013). On the other hand PilP was shown to interact with PilN and PilO by its N-terminal disordered region (Tammam et al., 2013). PilN and

PilO are integral IM proteins with a short cytoplasmic N-terminus, one transmembrane helix and a large globular domain in the periplasm (Georgiadou et al., 2012, Sampaleanu *et al.*, 2009). While the N-terminus of PilN is highly conserved and the C-terminal sequence varies between different species, PilO exhibits stronger sequence conservation in the C-terminal periplasmic part and variations in the N-terminus. However, the secondary structure of PilN and PilO seems to be similar despite low sequence identity. The crystal structure of the periplasmic part of PilO revealed two structural domains (Sampaleanu et al., 2009). The core domain exhibits a ferredoxin-like fold, which is a widely distributed structural domain present in many different proteins with different functions and oligomerization states. Due to the extremely broad functional diversity of ferredoxin-like proteins, it is difficult to extrapolate functional properties between different proteins. The second domain is composed of coiled coil (CC) domains that are usually involved in protein-protein or protein-DNA interactions. Both domains are suggested to be involved in dimerization to form either homodimers or heterodimers with PilN (Sampaleanu et al., 2009). So far, only heterodimers of PilN and PilO were able to interact with PilP. Further studies in *P. aeruginosa* and *N. meningitidis* showed mutually stabilizing effects between PilN, PilO and PilP. However, the single interdependencies between the respective proteins differ among the two organisms (Georgiadou et al., 2012, Sampaleanu et al., 2009). Furthermore, a large scale BACTH interaction study in *N. meningitidis* revealed that PilN and PilO interact with the major pilin and that PilO interacts with PilC (Georgiadou et al., 2012), raising the question if the function of the IM complex exceeds the alignment function and is potentially involved in incorporation or removal of pilin subunits.

The last member of the IM complex is the cytoplasmic protein PilM. The conserved, cytoplasmic N-terminus of PilN was shown to interact with PilM (Georgiadou et al., 2012, Karuppiah & Derrick, 2011). Karuppiah and colleagues solved the crystal structure of PilM from *Thermus thermophilus* including a short peptide of PilN with the conserved N-terminal region, which folded nicely into the PilM structure. PilM possesses an actin-like fold and is structurally closely related to FtsA or MreB. Both proteins belong to the family of actin-like ATPases and usually polymerize upon ATP-binding. Until now, there is no evidence for polymerization of PilM. However, ATP-binding was observed for PilM from *T. thermophilus* (Karuppiah & Derrick, 2011). PilM is proposed to first bind ATP and sequentially associate with PilN. Intriguingly, the structure of PilM revealed another stretch of conserved residues on the opposite side of the PilN-binding side that is suggested to be an interaction site for another protein (Karuppiah & Derrick, 2011). Due to the similarity to the actin-like protein GspL from the T2SS that interacts with the secretion ATPase GspE (Sandkvist *et al.*, 1995), the

ATPases PilB or PilT are potential candidates for binding to this conserved region. As mentioned, PilM is a non-core component that is only found in T4aP system. Strikingly, a recent publication by Yamagata und colleagues uncovered the relationship between PilM and a protein of the bundle forming pili machinery from enteropathogenic *E. coli* (EPEC) that is a T4bP (Yamagata *et al.*, 2012). The N-terminal part of BfpC (N-BfpC) was crystallized and revealed that despite lack of sequence similarity between PilM and N-BfpC, they share a similar structure. In fact, N-BfpC is more closely related to the cytoplasmic part of GspL, which was also shown to have an actin-like fold (Abendroth *et al.*, 2004) like PilM. The discovery of the relationship between these proteins raises the question if PilM or actin-like proteins play a more central role in the T4P machinery and can be designated as a core component of the T4P system.

In conclusion PilM/N/O/P/Q build up a cell envelope spanning complex, which is thought to be connected to PilC and the motor proteins in the cytoplasm. The complex of PilN/O/P/Q was also shown to interact with the pilin subunits. Tammam and co-workers propose that this interactions is either required for local enrichment of PilA subunits at the site of pilus polymerization or contributes to the anchoring of the fiber. Furthermore, they propose a model in which all components of the PilM/N/O/P/Q complex are arranged in a circular manner (Tammam et al., 2013). It is clear that this arrangement would require space at the periplasmic side for the pilin subunits for incorporation or removal.

1.1.4 Relationship between T4P and T2SS

The components of the T4P and T2S machinery exhibit structural and functional similarities assuming that they share a common origin (Peabody et al., 2003, Russel, 1998). This relationship provides the advantage that data from one system might be instructive to understand the other system. Therefore, a more detailed look at the T2SS might help to understand the mechanism of the T4P machinery.

The T2SS is involved in the export of folded proteins from the periplasm over the OM into the extracellular milieu. The common architecture is obvious when comparing both systems (Figure 7). The T2SS can be subdivided into the pseudopilus, the OM complex (GspD, GspS), the IM complex (GspC/F/L/M) and the secretion ATPase (GspE) (Figure 7). The IM complex is thought to connect all subcomplexes and might convert the energy from ATP hydrolysis in the form of conformational changes into polymerization of the pseudopilus. The fiber is thought to act as a piston to export proteins through the secretin channel (Sauvonnet et al., 2000). Interestingly, PilM and PilN are composed of one protein in the T2SS, called GspL (Sampaleanu et al., 2009), which emphasizes the importance of the interaction between PilM and PilN.

While the relationship for some of the proteins was obvious, the relationship between PilM/N/O/P and GspL/M/C became clear after the crystal structure of the proteins were solved (Sampaleanu et al., 2009, Tammam et al., 2011).

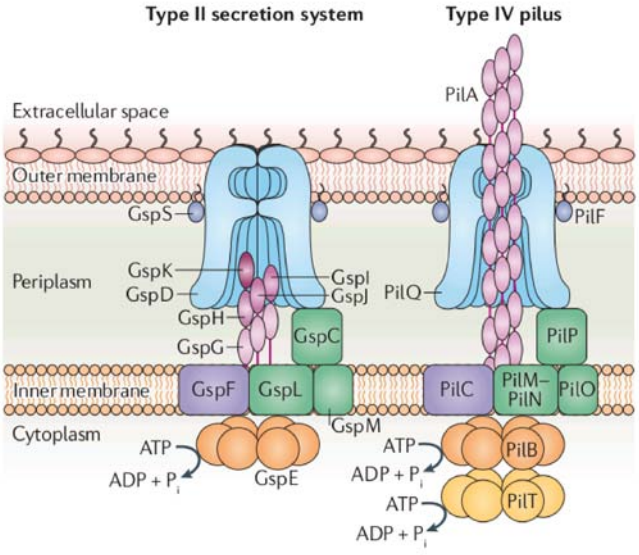

Figure 7 – Comparison of T2SS and T4P machineries. Related proteins are in the same color. For the T2SS, the general secretory pathway (Gsp) nomenclature is used. This figure is reproduced from Korotkov *et al.* (2012).

The interchangeability of the prepilin peptidase between both systems emphasizes their close relationship (Strom *et al.*, 1991). Furthermore, Cisneros and colleagues showed that the T2SS can assemble T4 pilins of a T4bP system (PpdD) into fibers using either minor pilins or minor pseudoplins for initiation (Cisneros et al., 2012b). Even though different pilins and pseudopilins can be recognized by the same machinery, the fibers formed could not accomplish the secretion of the respective substrate, suggesting that system and species specific properties or modifications on the (pseudo)pilins are required for correct function. Analyzing the similarity between pilins and pseudopilins, it has been shown that the homology is limited to the transmembrane segment while the globular domains differ significantly (Cisneros et al., 2012b). This suggests that the transmembrane segment plays a crucial role in interacting with the assembly machinery. Simultaneous expression of pilins and pseudopilins resulted only in fibers composed of one or the other subunit, but no mixed filaments. Cisneros and coworkers came to the conclusion that filament elongation requires the recognition between the specific major subunits (Cisneros et al., 2012b).

GspC and the secretin GspD interact in a manner similar to PilP and PilQ. GspC is important for the stability of GspL and GspM. The proteins GspE/F/L/M, corresponding to PilC/B/O/M-N in the T4P system seem to build a stable complex (Py *et al.*, 2001). GspM and GspL interact directly and require each other for stability

(Sandkvist *et al.*, 1999). Intriguingly, the ATPase GspE was shown to be recruited to the membrane by the cytoplasmic part of GspL and this interaction, together with the resulting membrane association of GspE seem to stimulate its ATPase activity 30-130 fold (Camberg *et al.*, 2007). Further, the platform protein GspF interacts with GspE and GspL (Py et al., 2001) and the major pseudopilin GspG interacts with GspL. (Gray *et al.*, 2011). The complex of GspC/L/M/F is proposed to transmit the energy, provided by the ATPase GspE over the IM to either act in gating the secretin pore or to promote pseudopilus assembly to drive protein secretion (Sandkvist et al., 1999).

1.2 *Myxococcus xanthus*

In this study, we examine the T4P structure with respect to assembly and function in the soil bacterium *Myxococcus xanthus*. In the last decades *M. xanthus* emerged as a model organism for studying motility, cellular polarity, social interactions, predation and development.

M. xanthus is a Gram-negative, rod-shaped bacterium belonging to the class of δ-proteobacteria. It has a complex life cycle involving three distinct cellular patterns; spreading colonies, predatory behavior and the starvation induced formation of spore-filled fruiting bodies (Dworkin, 1996) (Figure 8).

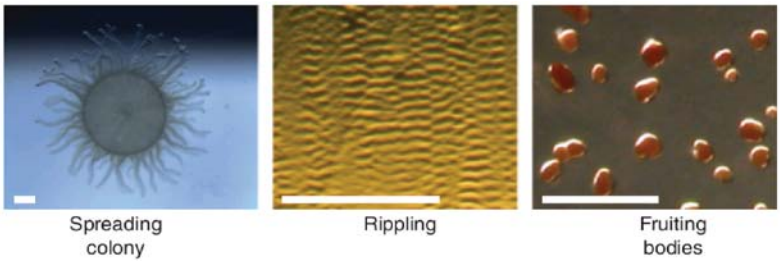

Figure 8 – The three distinct cellular patterns of *M. xanthus*. Scale bar in left, middle and right panel: 2 mm, 50 µm and 0.2 mm. Reproduced from Konovalova *et al.* (2010).

In the presence of nutrients cells grow, divide and spread out of the colony building a thin, film-like structure. They secrete antibiotics and digestive enzymes, which lyse neighboring cells and degrade macromolecules that serve as a food source. *M. xanthus* cells feed in a cooperative manner, as they preferably move in groups, which leads to a higher concentration of the secreted enzymes and antibiotics (Rosenberg *et al.*, 1977). *M. xanthus* cells are motile on solid surfaces, but are non-motile in liquid. In the presence of prey or less stringent starvation conditions *M. xanthus* cells exhibit a collective motility behavior, called rippling (Berleman *et al.*, 2006, Shimkets & Kaiser, 1982). During rippling, cells are organized into parallel lines of high cell density and these move perpendicular to the axis of the cell line, like

accordion waves. When cells of neighboring waves collide, cell reversals are induced and cells travel in the opposite direction until they hit a parallel wave. During this behavior, cells do not display any net movement (Sager & Kaiser, 1994). Berleman and colleagues proposed that rippling enables a more efficient cell lysis of prey organisms and subsequent absorption of nutrients (Berleman et al., 2006). Under starvation conditions, *M. xanthus* cells enter a developmental pathway, which requires a highly coordinated gene expression, intercellular signaling and coordinated cell movement. Cells move into aggregation centers that become multicellular fruiting bodies after 24 h of starvation (Figure 9). After 72 h, cells inside these fruiting bodies have differentiated into environmentally resistant, spherical spores (Shimkets, 1999). While a large portion of cells lyse during this process (Nariya & Inouye, 2008, Wireman & Dworkin, 1977), a small portion of the population remains outside of the fruiting bodies, these cells are referred to as peripheral rods (O'Connor & Zusman, 1991). Peripheral rods have been proposed to function as a kind of scout cells, searching for new food sources. When nutrients are available, the release of soluble nutrients through digestion by the peripheral rods might trigger spore germination (Zusman *et al.*, 2007). All three morphological patterns of *M. xanthus* require the ability of cells to actively move on a surface. For this purpose, *M. xanthus* possesses two motility systems.

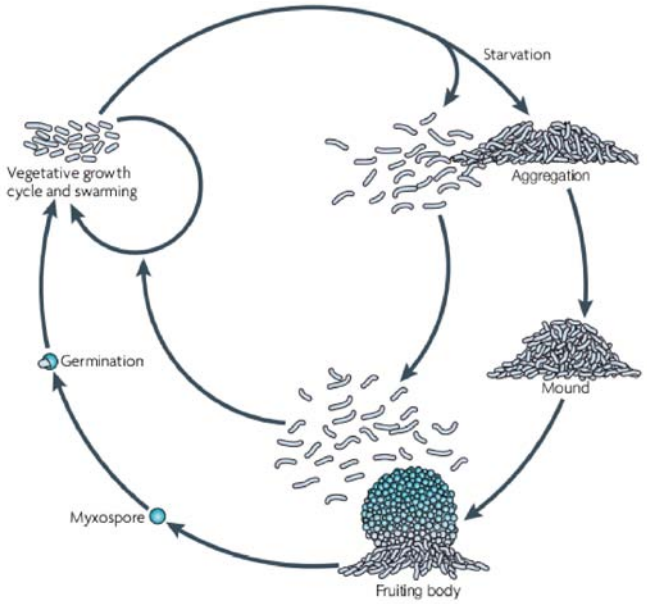

Figure 9 – Life cycle of *M. xanthus.* Graphic illustration of the different stages in the *M. xanthus* life cycle. This figure is reproduced from Zusman et al. (2007).

1.3 Gliding motility in *M. xanthus*

Bacterial motility is essential for a wide range of behaviors, including colony expansion, chemotaxis, predation, biofilm formation, virulence and development.

Bacteria have evolved different strategies for locomotion, like swimming, swarming, twitching or gliding. *M. xanthus* moves by gliding, which is the smooth movement of cells on solid surfaces in the direction of their long axis and independently of flagella (Henrichsen, 1972). Movement by gliding (2-4 µm/min) is approximately 1,000 times slower than flagella driven motility. Back in 1979, Hodgkin and Kaiser discovered that gliding in *M. xanthus* is driven by two distinct motility systems (Hodgkin & Kaiser, 1979) that work independently, but synergistically. If one system is knocked out, cells still remain motile by the means of the other system. The two motility modes were termed adventurous (A) and social (S) motility. A-motility enables the movement of single cells, whereas S-motility occurs exclusively in cell groups. Moreover, the two motors were shown to display specific selective advantages on different surfaces. While A-motility is favored on hard and dry surfaces, S-motility appears preferentially on wet and soft surfaces (Shi & Zusman, 1993). The mechanism underlying S-motility was shown to correlate with the presence of pili in 1979, although their role was unclear at that point of time (Kaiser, 1979). To date, there are different models proposed for the A-motility motor. However, the exact mechanism remains controversial.

1.3.1 A-motility

Currently, there are three different models proposed for the mechanism of A-motility. The first model is called the slime gun model and implies that a polyelectrolyte gel (slime) is actively secreted via nozzle-like structures at the lagging cell pole. Slime secretion is thought to propel the cells forward (Wolgemuth *et al.*, 2002). By now, there are two other models that are favored over the first model; the focal adhesion complex (FAC) model and the helical rotor model. In the FAC model, envelope spanning multiprotein complexes, including the proteins AglZ and AgmU, are localized in clusters along the cell body (Mignot *et al.*, 2007b, Nan *et al.*, 2010). They are built at the leading cell pole, attach to the substratum and stay stationary with respect to the substratum. Motor complexes powered by the proton motive force (PMF) are suggested to energize the FAC and in this way pushing a cell forward (Sun *et al.*, 2011). FAC formation was shown to depend on the cytoskeletal element MreB, suggesting that it builds a kind of track on which the FACs move along (Mauriello *et al.*, 2010) (Figure 10A). The helical rotor model describes a similar mechanism by which motor proteins move along a helical cytoskeletal track that deforms the cell surface, creating a kind of wave-like contours (Nan *et al.*, 2011). These surface waves exert force on the ventral side of a cell, in this way pushing a cell forward by a mechanism similar to the movement of snails. As the cytoskeletal track is helical, cells are suggested to rotate during movement. This mechanism is also suggested to be powered by PMF and to involve

flagella motor homologs, which carry different protein cargos, deforming the membrane (Nan et al., 2011) (Figure 10B).

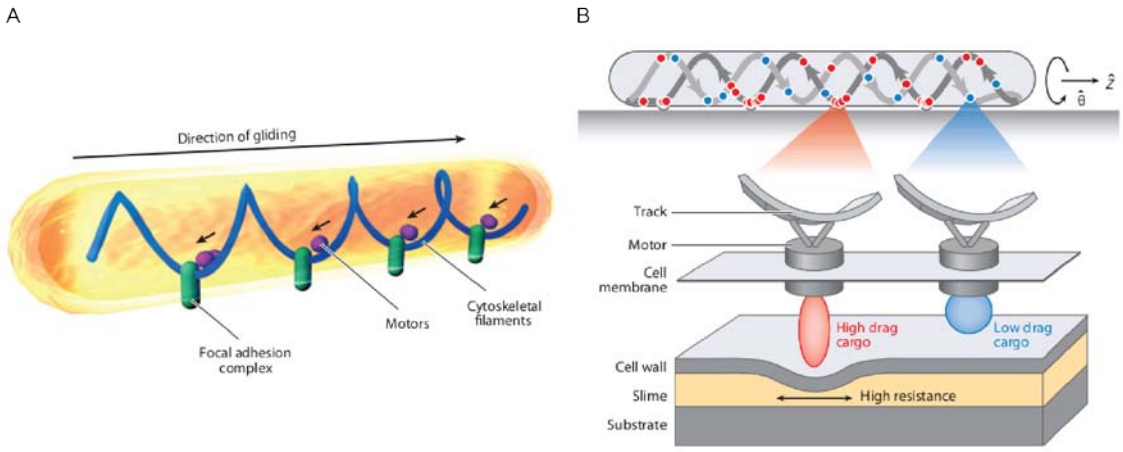

Figure 10 – Models for the mechanism underlying A-motility. A) In the focal adhesion model, large adhesion complexes penetrate the cell envelope, attach to the surface and are moved backwards along a cytoskeletal element. Motor proteins power this movement by pushing against the adhesion complexes (marked by black arrows). B) The helical rotor model describes different cargo proteins, which ride along a helical cytoskeletal element. High-drag cargos are proposed to deform the cell envelope, causing the helical movement of the cells. This figure is reproduced from Nan and Zusman (2011).

Although A-motility has been known for a long time and in the meantime there are around 40 genes identified to be involved in A-motility, the exact mechanism is not known and requires further studies.

1.3.2 S-motility

S-motility depends on the presence of T4P and is comparable to twitching motility in *P. aeruginosa,* which describes the jerky movement via T4P (Henrichsen, 1983). As *M. xanthus* moves smoothly, the term twitching was not used for *M. xanthus*. 5-10 T4P are built at the leading cell pole of *M. xanthus*. They undergo cycles of extension, attachment to a surface and retraction, and this set of events generates sufficient force to pull a cell forward (Merz et al., 2000, Skerker & Berg, 2001). The fact that S-motility only occurs in cell groups is due to the fact that the extracellular matrix of neighboring cells are generally used for attachment and stimulate retractions. Therefore, cells, which are within a distance of a T4P length, are able to move by means of T4P.

Extracellular matrix required for S-motility

Further requirements for T4P-dependent motility in *M. xanthus* are the lipopolysaccharide (LPS) O-antigen and the extracellular matrix (ECM) including extrapolysaccharides (EPS) and proteins. While the role for LPS is not understood, Li and colleagues showed that EPS are the binding target for T4P and trigger pilus retraction. They observed that sheared pili can bind to purified EPS and importantly, that the addition of EPS to an EPS deficient strain can restore T4P retraction (Li *et al.*, 2003). Moreover, when 1 % methylcellulose is added to cells, also isolated cells were shown to move by T4P (Hu *et al.*, 2011), suggesting that the methylcellulose can compensate for the absence of EPS as an anchoring substrate. However, cells failed to move in a coordinated manner, suggesting that EPS plays an important role in coordinating S-motility in cell groups (Hu et al., 2011). The accumulation of the ECM is highly regulated and involves the Dif chemosensory system, the histidine protein kinase SgmT together with the response regulator DigR and several transcriptional activators that presumably regulate the expression of genes coding for proteins of the ECM and genes involved in EPS biosynthesis (Black & Yang, 2004, Lancero *et al.*, 2005, Overgaard *et al.*, 2006, Yang *et al.*, 1998). Black and coworkers discovered that T4P act upstream of the Dif system and might serve as a sensor that mediates signal input into the Dif system. They propose a co-regulation of T4P and EPS, in which T4P recognize cells in their vicinity to regulate EPS production through the Dif chemotaxis pathway (Black *et al.*, 2006). Another protein that was identified to be involved in regulation of EPS production is FrzS. FrzS was known to be important for S-motility, but not for pilus assembly, and was thought to be involved in regulating pilus function, as it localizes to the leading cell pole (Mignot *et al.*, 2007a, Ward *et al.*, 2000). However, Berleman and coworkers revealed that a Δ*frzS* mutant can be rescued by the addition of purified EPS and furthermore, that *frzS* mutants are motile in 1 % methylcellulose (Berleman *et al.*, 2011). This observation excludes the possibility that FrzS is involved in pilus function and leads to the assumption that FrzS is involved in EPS biogenesis or secretion. How FrzS functions in EPS regulation remains unresolved.

The *pil*-genes

The majority of genes, which are required for the biogenesis and function of T4P in *M. xanthus* are encoded in the *pil*-gene cluster consisting of 17 genes (Figure 11). This is an exception to the rule, as genes of a T4aP system are usually scattered throughout the genome. The clustering of T4P genes is mainly observed for T4bP systems (Pelicic, 2008). To date there are two genes known, which are directly

involved in the assembly of T4P in *M. xanthus* and which do not localize to the *pil*-gene cluster, named Tgl and TsaP. 12 out of the 19 *pil* genes are highly conserved among T4aP systems, while the remaining seven genes are non-conserved, non-core proteins (Figure 11). As the conserved components of the T4P machinery were already depicted in section 1.1.3, the *M. xanthus* specific components and characteristics will be primarily discussed in this section.

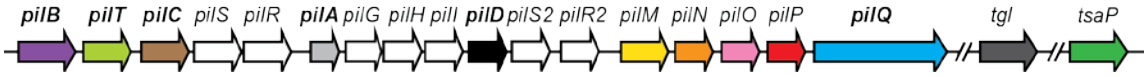

Figure 11 – *pil*-gene cluster plus *tgl* and *tsaP*. Gene names highlighted in bold are conserved core-components among T4P systems. Colored genes are conserved among T4aP systems and white genes are *M. xanthus* specific *pil*-genes.

pilS, *pilR* and the paralogs *pilS2* and *pilR2* code for two two-component systems, involved in the regulation of *pilA* expression and were named after their homologs in *P. aeruginosa*. Classic two component systems consist of a sensor histidine kinase and a response regulator. Generally, the sensor kinase recognizes an environmental signal, autophosphorylates on a conserved histidine residue and transfers the phosphate to a conserved aspartate residue of the response regulator. The phosphorylated response regulator is then able to regulate the expression of certain genes. PilR is a response regulator, responsible for *pilA* expression. PilS seems to be the sensor kinase although little is known about the signal(s) received by PilS. Interestingly, overexpression of PilS leads to the reduction of *pilA* expression, leading to the conclusion that PilS is a negative regulator of *pilA* expression (Wu *et al.*, 1997). In addition to *pilR/S*, the genes *pilR2/S2* seem to play an important but unknown role in pilus assembly, as an insertion mutant of *pilR2* leads to the loss of S-motility (Caberoy *et al.*, 2003).

pilG, pilH and *pilI* were each shown to be required for S-motility and T4P biogenesis (Wu *et al.*, 1998). None of the three genes show any homology to known genes of other T4P systems. They were shown to be co-transcribed and with overlapping initiation and termination codons. *pilH* displays similarity to members of the family of ABC-transporter proteins (Wu et al., 1998). It was speculated that *pilGHI* are involved in the export of PilA. However, this has not been verified and new models for PilA export have been developed as discussed in section 1.1.3.

pilM, pilN, pilO and *pilP* are the least characterized genes in *M. xanthus* despite their conservation among T4aP systems. A transposon screen revealed that the genes are important for T4P-dependent motility in *M. xanthus* (Nudleman et al., 2006). Furthermore, they were shown to be co-transcribed with *pilQ* (Bulyha, 2010). In-frame

deletions of the individual genes revealed that each gene is required for T4P-dependent motility, but mutants remained motile in terms of A-motility (Bulyha, 2010). Furthermore, the genes were shown to be dispensable for PilQ-multimer formation, as the multimer was detectable in each deletion mutant (Bulyha, 2010).

pilT paralogs

Analyzing the retraction velocities and forces of T4P in *M. xanthus*, Clausen et al. observed PilT-independent retractions at a low frequency. Genome analyses of *M. xanthus* revealed the presence of four *pilT* paralogs (Mxan_0415, Mxan_1995, Mxan_6705 and Mxan_6706). The paralogs share around 37-49 % sequence identity and 43-70 % sequence similarity (Clausen et al., 2009). Paralogs of other *pil*-genes could not be identified. The role of the *pilT*-paralogs in T4P function is not clear in *M. xanthus*. Also in other organisms, different numbers of PilT paralogs are found. Precedents for PilT paralogs are the PilU protein from *P. aeruginosa* or PilU and PilT2 from *Neisserial* species, although their role remains poorly understood, too. This is predominantly due to the fact that deletion mutants of *pilU* display different phenotypes in different species. While it is required for twitching motility in *P. aeruginosa* (Whitchurch & Mattick, 1994), it is dispensable for motility in *N. gonorrhoeae*, but mutants lacking PilU show increased adherence to host cells (Park *et al.*, 2002). Lack of PilT2 does not abolish twitching motility in *N. meningitidis* (Brown *et al.*, 2010), but was shown to affect the speed of single T4P retractions and therefore twitching motility in *N. gonorrhoeae* (Kurre *et al.*, 2012). In summary, PilU and PilT2 are required for full functionality of T4P, but the exact role remains to be elucidated.

Tgl transfer

The pilotin, which is important for oligomerization of the secretin PilQ in *M. xanthus* is called Tgl, which stands for "**t**ransient **gl**iding". Early on it was found that a small subset of motility mutants of *M. xanthus* could be transiently complemented when mixed with strains, which contained the respective wild type (WT) gene (Hodgkin & Kaiser, 1977). This stimulation was only phenotypic and not genotypic, as no DNA was transferred and cells became non-motile over time. Moreover, physical contact between cells and motility was shown to be required for this type of intercellular complementation, suggesting that cell-cell alignment facilitates the transfer (Wall & Kaiser, 1998, Wei *et al.*, 2011). Furthermore, it was demonstrated that OM lipoproteins are transferred from one cell to another in a structured biofilm (Nudleman *et al.*, 2005). Tgl is the only protein of the S-motility machinery, which was identified to be transferred, whereas there are several mutants of the A-machinery, which can be

complemented extracellularly. Strikingly, most of the proteins contain a type II signal sequence for lipoproteins. Wei and coworkers showed that a type II signal sequence for OM localization is sufficient for transfer from one cell to another (Wei et al., 2011). Specifically, they observed that the fluorescent protein mCherry fused to such a signal sequence was efficiently transferred from the red fluorescing donor cell to the green fluorescent marked recipient cells. Recent studies revealed that not only lipoproteins are transferred, but also lipids. Pathak and Wall proposed that the mechanism underlying this exchange is OM fusion (Pathak *et al.*, 2012). This hypothesis was supported by two recent publications, which visualized a network of OM extensions in the form of membrane vesicle chains or membrane tubes between *M. xanthus* cells (Ducret *et al.*, 2013, Remis *et al.*, 2013). Although these OM tubes are thought to fuse the OMs of adjacent cells, suggesting a continous connection of the periplasmic space, efficient transfer was only observed for OM lipids and proteins (Ducret et al., 2013). Compositional analysis of the vesicles revealed the presence of Tgl and other lipoproteins, which have been shown to be transferred (Remis et al., 2013).

Pathak and Wall identified two proteins that are important for OM exchange, called TraA and TraB. They are predicted to localize to the cell envelope. TraA has a PA14 lectin-like domain, usually implicated in glycan binding, a cysteine-rich tandem repeat region and a putative C-terminal region named MYXO-CTERM that was proposed to serve as a myxobacteria specific protein sorting tag for cell surface localization (Pathak et al., 2012). TraB encodes an OmpA/MotB-like domain that is presumably involved in peptidoglycan binding. The current model describes TraA as being a cell surface receptor possibly binding to the glycans on other cells. This could mediate cell–cell adhesion for OM fusion, which then allows the transfer of lipoproteins and lipids via lateral diffusion (Pathak et al., 2012). The function of TraB is not clear so far.

1.4 Inversion of cell polarity - Cellular reversals

M. xanthus cells move by gliding in the direction of their long axis implying that cells exhibit a cell polarity with a leading and a lagging cell pole. A fascinating feature of *M. xanthus,* making it a model organism for studying cellular polarity, is the inversion of the polarity on the average every few minutes (Blackhart & Zusman, 1985). During a reversal, a cell stops moving in one direction and then resumes gliding in the opposite direction, thus the leading pole becomes the lagging cell pole and vice versa. The frequency of these reversals are highly regulated to ensure i) that both motility motors generate force in the same direction and ii) that cells display net movement in a certain direction (Leonardy *et al.*, 2007).

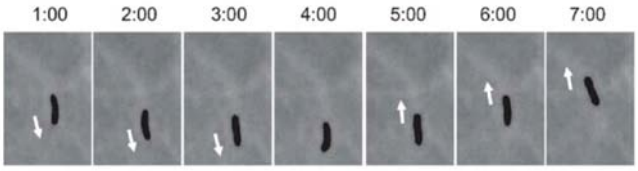

Figure 12 – Cellular reversals of *M. xanthus*. Time lapse recordings of a single cell moving on a solid surface. Time is indicated in min. White arrows indicate the direction of movement. Figure reproduced from Leonardy *et al.* (2008).

As T4P are only built at the leading cell pole, a cellular reversal involves the switching of T4P between both poles (Mignot *et al.*, 2005, Sun *et al.*, 2000). For this purpose, T4P are disassembled at the old leading pole and re-assembled at the new leading cell pole. This finding raised the question if the proteins of the T4P machinery also switch poles. Localization of several Pil-proteins was investigated and revealed that they localize to the poles. However, there are two subsets of proteins: the bipolarly localizing proteins and the predominantly unipolarly localizing proteins. The secretin PilQ, the IM platform protein PilC and the cytoplasmic, actin-like protein PilM localize in a symmetric pattern to both cell poles (Bulyha *et al.*, 2009, Nudleman et al., 2006). Whereas the two ATPases PilB and PilT mainly localize to one pole and switch poles during a cellular reversal (Bulyha et al., 2009). Therefore, pole switching of T4P was thought to involve preassembled complexes of the T4P machinery at both poles, which are activated at one pole at a time by the dynamically localizing ATPases. Strikingly, while the extension ATPase localizes to the leading cell pole, the ATPase PilT, which is providing the energy for pilus retraction is predominantly localizing to the lagging cell pole. However, Bulyha and colleagues showed that bursts of PilT periodically localize to the leading cell pole, possibly to enable pilus retraction (Bulyha et al., 2009). They assume that the spatial separation of PilB and PilT in combination with the periodic accumulation of PilT at the leading cell pole enable the temporal separation between pilus extension and retraction.

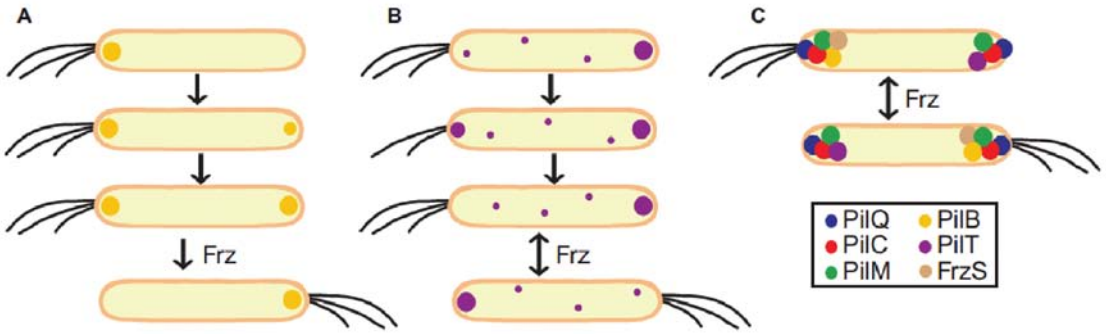

Figure 13 - Localization of stationary and dynamic T4P proteins. A) PilB localizes predominantly to the leading cell pole after a cellular reversal. After some time, PilB starts to accumulate in a bipolar manner. During a Frz-system induced cellular reversal (1.4.1), PilB switches to the new leading cell pole. B) PilT accumulates similar to PilB in an asymmetric manner with the main cluster at the lagging cell pole. Smaller PilT clusters resemble bursts of PilT accumulation at the leading cell pole. C) While PilQ, PilC and PilM localize to both poles and stay stationary upon a cellular reversal, PilB, PilT and FrzS localize mainly to one pole and switch poles during a cellular reversal, induced by the Frz-system. This figure is reproduced from Bulyha et al. (2009).

1.4.1 The Frizzy system controls cellular reversals

The frequency of cellular reversals is highly regulated to coordinate directed movement. The Frizzy (Frz) chemosensory system regulates the reversal frequency in *M. xanthus* (Blackhart & Zusman, 1985). Frz mutants display either hyper- or hyporeversing cells, which form abnormal, frizzy colonies and are incapable of fruiting body formation. The input signal of this chemosensory system is not known so far, but there are several hypotheses to which signals the Frz system might respond. As *M. xanthus* was shown to move towards attractants and move away from repellents (Kearns & Shimkets, 2001, Shi *et al.*, 1993), the reversals might fulfill a similar function like runs and tumbles in flagellated bacteria (Kaimer *et al.*, 2012). On the other hand, it has been shown that the reversal frequency is affected by cell-cell contact (Mauriello *et al.*, 2009), by contact with prey cells (Berleman *et al.*, 2008) and during development (Jelsbak & Sogaard-Andersen, 2003). The Frz system consists of seven proteins, which display similarity to proteins of the chemosensory system involved in regulating chemotaxis in *E. coli* (Bustamante *et al.*, 2004). Briefly, it includes FrzCD, a methyl accepting chemoreceptor that is methylated or demethylated by FrzF and FrzG, respectively (Astling *et al.*, 2006). Methylated FrzCD presumably activates FrzE, a histidine kinase, leading to its autophosphorylation (Inclan *et al.*, 2008). The phosphate group is then transferred to FrzZ, a response regulator, which is thought to serve as the output of the Frz pathway signaling to further proteins that determine cell polarity (Inclan *et al.*, 2007). In conclusion, an unknown environmental signal is possibly sensed by FrzCD or FrzF, which leads to a change in the FrzE autokinase activity and

subsequently to phosphorylation in FrzZ, which influences the reversal frequency. While the Frz system regulates the frequency of cellular polarity inversions, there are further proteins required to establish this polarity.

1.4.2 Establishing cell polarity – MglA and MglB

The effect of the Frz system on cellular reversals depends on the MglA/MglB module (Leonardy *et al.*, 2010, Zhang *et al.*, 2010). MglA is a small Ras-like GTPase, which was found to be essential for motility in *M. xanthus*. It acts as a nucleotide dependent molecular switch including MglA/GTP as the active form and MglA/GDP as the inactive form (Leonardy et al., 2010, Zhang et al., 2010). As Ras-like GTPases have a high affinity for nucleotides and low intrinsic GTPase acitivity, they require accessory proteins, called Guanine-nucleotide exchange factors (GEFs) and GTPase activating proteins (GAPs). MglA is encoded in an operon with MglB, which was shown to be MglA's cognate GAP. Together, MglA and MglB set up the polarity of cells. MglA-GTP localizes to the leading cell pole, whereas MglB localizes in bipolar clusters with the large cluster at the lagging cell pole. MglB excludes MglA from the lagging cell pole as it converts MglA/GTP to MglA/GDP, which localizes diffusely over the cell. Upon a cellular reversal, MglA and MglB switch poles in a Frz system dependent manner (Leonardy et al., 2010, Zhang et al., 2010) (Figure 14). Active MglA/GTP at the leading cell pole is thought to promote motility by setting up the correct polarity for the motility proteins, therefore stimulating T4P function and assembly of focal adhesion complexes.

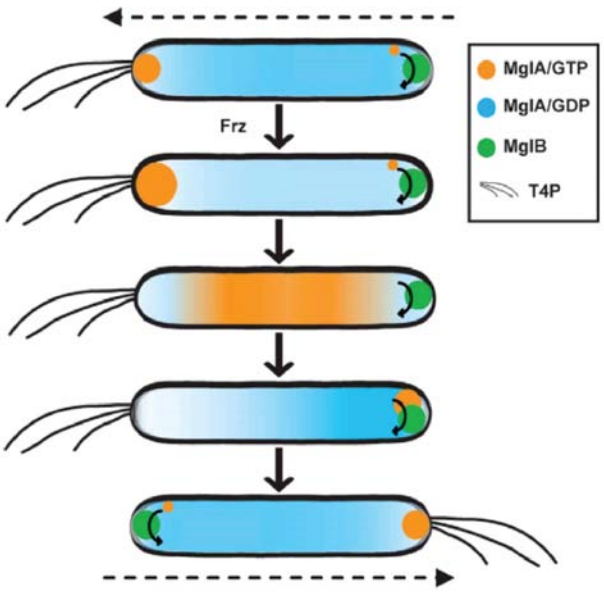

Figure 14 – Model of the polarity module MglA/MglB. Upon movement in one direction, the polarity is maintained with MglA at the leading and MglB at the lagging cell pole. MglB excludes active MglA/GTP from the lagging pole by promoting GTP hydrolysis (round arrow). When cellular reversals are induced via the Frz system, MglA/GTP accumulates at increased levels at the leading cell pole. Subsequently, MglA is released from the leading cell pole and relocates to the lagging cell pole. Upon interaction with MglB, the MglA/GTP concentration decreases. MglB relocates to the opposite pole and thus, polarity switching of the MglA/B module is completed. Figure reproduced from Leonardy et al. (2010).

Recent publications revealed a link between the Frz system, controlling polarity switching frequencies and the MglA/B module establishing the cell polarity. The response regulator RomR was shown to be essential for the correct localization of MglA and MglB (Keilberg *et al.*, 2012, Zhang *et al.*, 2012). Furthermore, mutations at the conserved aspartate residue of the receiver domain lead to either hypo- or hyperreversing cells, depending on the substitution (Leonardy et al., 2007). RomR was first discovered to be important for A-motility. Leonardy and colleagues showed that RomR localizes in a bipolar asymmetric pattern with the large cluster at the lagging cell pole and upon a reversal, RomR relocates between the poles (Leonardy et al., 2007). Recent publications revealed that RomR directly interacts with MglA and MglB. Moreover, RomR was suggested to interface with the output response regulator FrzZ (Keilberg et al., 2012, Zhang et al., 2012). Therefore, RomR is suggested to function between the Frz chemosensory system and the MglA/B polarity module. How exactly the output of the Frz system is converted via RomR and MglA/B to changes in polarity and directs the motility proteins, remains largely unknown.

1.4.3 SofG and bactofilins

A mechanism for polar localization of the two ATPases PilB and PilT was proposed by Bulyha *et al.* (2013). They could show that a small Ras-like GTPase, called SofG in combination with the bactofilin BacP are required to recruit PilB/T to the poles (Bulyha et al., 2013). SofG is a MglA paralog and localizes in one cluster in a subpolar region. Bactofilins are bacterial cytoskeletal proteins, which can polymerize in the absence of cofactors and form filament bundles (Kühn *et al.*, 2010). In *M. xanthus* they were shown to localize in two large subpolar patches, which are important for correct subpolar localization of SofG. Both proteins were discovered to be important for T4P-dependent motility. Moreover, BacP and SofG were shown to interact and to be important for pole-targeting of PilB and PilT. Currently, there are two working models. One describes that SofG binds to a BacP patch and interacts directly or indirectly with PilB or PilT. Then, SofG shuttles along the bactofilin filaments to transport PilB/T to the pole or retain them at the pole. The second scenario envisions that SofG is moved to the pole by depolymerization of the BacP filaments. However, BacP and SofG are not sufficient to regulate the localization of PilB/T to the opposite poles. It requires additionally a sorting module to differentiate between leading and lagging cell pole. This function is accomplished by the MglA/MglB module. Both SofG/BacP and MglA/B are required to target the proteins to the pole and sort the proteins to the leading or lagging cell pole, respectively (Bulyha et al., 2013).

1.5 Scope of this study

Type IV pili (T4P) are ubiquitous bacterial surface structures. T4P are of broad interest due to their functional diversity, as they are involved in a variety of processes such as attachment to eukaryotic host cells during pathogenesis, biofilm formation, cellular motility, protein secretion and DNA-uptake. Especially their role in virulence makes T4P highly relevant for studying pilus assembly and function.

The T4P machinery consists of 12 conserved proteins that assemble into an envelope-spanning macromolecular machinery that localizes polarly in *M. xanthus*. Although most of the proteins have been known and studied for a long time, the precise mechanism of how and in which order the individual components are assembled to generate a macromolecular machinery that spans from the cytoplasm to the outside remains to be elucidated.

To better understand the mechanism by which the T4P machinery functions, we used a combination of cell biological and biochemical approaches to study protein-protein interactions. We performed a large scale screen comprising 11 of the 12 proteins of the T4P machinery by systematically profiling the stability and localization of T4P proteins in the absence of each individual other T4P protein in combination with mapping direct protein-protein interactions *in vitro*.

Investigating the biology of T4P is crucial for understanding their role during pathogenesis and DNA-uptake, which can contribute to the distribution of multi-drug resistant bacteria. With this study we wanted to lay the basis for further understanding of these functionally highly versatile surface structures.

2 Results

2.1 PilM, PilN, PilO, PilP, PilQ and Tgl are each required for T4P-dependent motility in *M. xanthus*

To study the assembly pathway of the T4P machinery, we needed a basic knowledge of all proteins involved in this trans-envelope complex and their role in motility. While PilM, PilN, PilO and PilP (PilM/N/O/P) have been characterized in detail in other organisms, their role in *M. xanthus* had not been characterized in detail. PilM/N/O/P are thought to build an IM complex in *P. aeruginosa* and *N. meningitidis,* which is suggested to align IM and OM components. Due to the high structural similarity of the proteins among *M. xanthus, P. aeruginosa* and *N. meningitidis*, PilM/N/O/P are thought to fulfill a similar function in *M. xanthus.* Consistently, in-frame deletions of each gene result in the loss of T4P-dependent motility in *M. xanthus* (Bulyha, 2010). A *tgl* mutant was constructed by Nudleman et al. (2006) and shown to be deficient in S-motility and in PilQ multimer assembly, however, the gene was replaced by a tetracycline cassette. Therefore, we constructed a clean in-frame deletion and confirmed that deletion of *tgl* leads to the loss of S-motility (Figure 15). To verify that all observed defects in motility are due to the absence of each gene and to exclude polar effects, we complemented the motility defect by introducing each gene at the Mx8 *attB*-site with expression of the relevant genes from the constitutively active *pilA*-promoter. Complementation strains, together with WT and the individual deletion mutants were phenotypically analyzed on 0.5 % agar that favors cell movement by T4P. The deletion mutants showed smooth edges, indicating that cells cannot spread out of the colony using T4P-dependent motility. The WT and all complementation strains showed flares indicating that cells are mobile using T4P (Figure 15A). To monitor protein levels in the different strains, protein specific antibodies were raised against the purified proteins PilN, PilO and PilP. Immunoblot analysis confirmed that the proteins do not accumulate in the respective deletion mutants and that protein levels in the complementation strains were restored to levels comparable to those in WT (Figure 15B). The in-frame deletion of *pilQ* that has already been shown to be deficient in T4P-dependent motility (Wall *et al.*, 1999), was included in this analysis and complemented as described above. It should be noted that the protein level of Tgl in the complementation strain was higher compared to WT (Figure 15B), however, this did not have a dominant negative effect on T4P-dependent motility (Figure 15A).

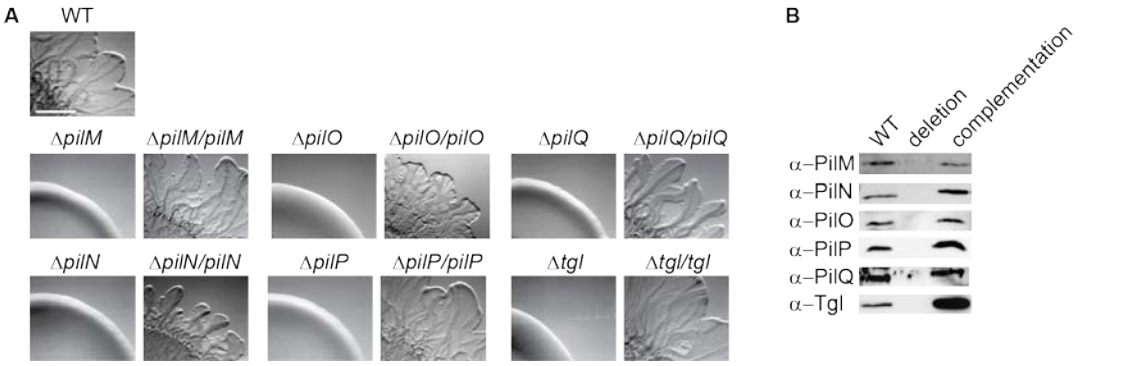

Figure 15 – PilM, PilN, PilO, PilP, PilQ and Tgl are required for T4P-dependent motility in *M. xanthus.* A) Motility phenotypes of the indicated mutants and complementation strains. Strains were incubated at 32 °C for 24 h on 0.5% agar/0.5% CTT which favors T4P-dependent motility. Scale bar 1 mm. B) Immunoblots of T4P protein accumulation. Total cell lysates from exponentially growing cultures were separated by SDS–PAGE (protein from 7 x 10^7 cells loaded per lane), and analyzed by immunoblotting using specific antibodies as indicated. For PilQ, only the heat- and detergent resistant oligomer is shown. The middle lane in each blot contains lysate from the relevant in-frame deletion mutant, and the last lane lysate from the relevant complementation strain.

2.2 PilD seems to be essential in *M. xanthus*

The prepilin peptidase PilD is a core component of the T4P system we planned to include it in our analyses. To date there is no deletion mutant of *pilD* available in *M. xanthus*. Therefore, we tried to generate an in-frame deletion as described in material and methods. While the plasmid generated for the in-frame deletion was incorporated via homologous recombination at the *pilD* site, a second homologous recombination to loop out the gene resulted only in WT genotypes. As all attempts to delete *pilD* failed, we suggest that it is essential in *M. xanthus*. Because we were unable to generate a *pilD* mutant, we did not include it in further analyses.

2.3 TsaP is required for efficient T4P-dependent motility in *M. xanthus*

TsaP was shown to be important for surface piliation in *N. gonorrhoeae* and is suggested to anchor the secretin ring to the peptidoglycan by its LysM domain (Siewering et al., manuscript in preparation). As the gene for TsaP is conserved among all T4aP organisms, we investigated the role of TsaP in *M. xanthus* (Mxan_3001). Bioinformatic analyses revealed that despite low sequence identity (18%), TsaP from *M. xanthus* and *N. gonorrhoeae* share a similar secondary structure (data not shown). Importantly, TsaP from *M. xanthus* also contains a conserved LysM motif (Figure 16). Due to the presence of a signal peptide, the potential peptidoglycan binding domain and its secondary structure, containing many ß-sheets (data not shown), we suggest that TsaP is either an integral or associated OM protein.

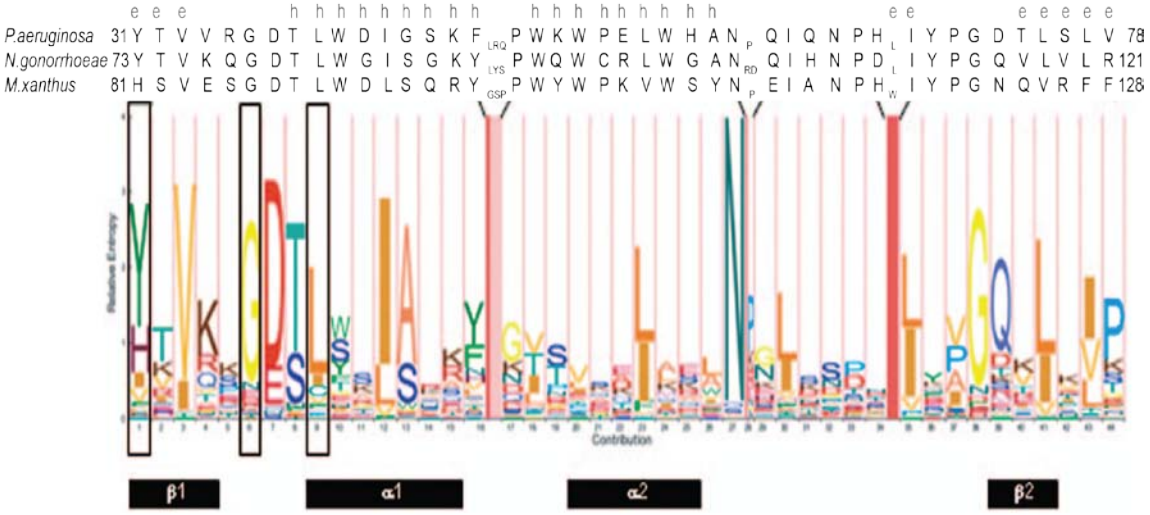

Figure 16 - Sequence comparison of LysM domains. Predicted LysM domain sequences from the indicated organisms were aligned to the LysM consensus sequence (Buist et al., 2008). Numbers at the start and end of the sequences indicate the amino acid position in the proteins. First row shows secondary structure prediction for the three indicated sequences by PROMALS3D. e=beta strand, h=alpha helix. Boxes below the sequence indicate regions with secondary structure for the LysM consensus sequence as defined by Mulder *et al.* (2006).

Characterization of TsaP from *M. xanthus* was carried out by Ina Binzen in the scope of her Bachelor thesis under my direct supervision (Binzen, 2012). An in-frame deletion of *tsaP* was constructed and analyzed for motility on hard and soft agar. While the *ΔtsaP* mutant showed normal A-motility (data not shown), T4P-dependent motility was significantly reduced. Only short flares were detected at the edge of the *ΔtsaP* colonies (Figure 17A). We were able to complement the motility defect by introducing the *tsaP* gene under control of the *pilA* promoter at the Mx8 *attB* site (Figure 17A). TsaP was purified to raise specific antibodies. Western blot analysis using TsaP-specific antibodies showed that TsaP does not accumulate in a *ΔtsaP* mutant and that TsaP levels were slightly overexpressed in the complementation strain when compared to WT (Figure 17B). However, this did not have a negative effect on motility. To analyze if the deletion of *tsaP* affects surface piliation, we performed transmission electron microscopy (TEM) on *ΔtsaP* cells to visualize T4P (Dr. A. Klingl, Philipps-Universität Marburg). As controls we included WT and the *ΔpilA* mutant that lacks T4P. TEM analyses revelead that the number of cells with T4P and the average number of pili per cell were decreased in the *ΔtsaP* mutant when compared to WT (Figure 17C/D). While in WT about 75% of the cells have three to nine T4P at a pole, the *ΔtsaP* mutant has in 65% of the cells no pili and in 35 % of the cells one to two polar T4P. These observations agree with the reduced S-motility in the *ΔtsaP* mutant and suggest that assembly, anchoring or surface excess of T4P are affected in the absence of TsaP.

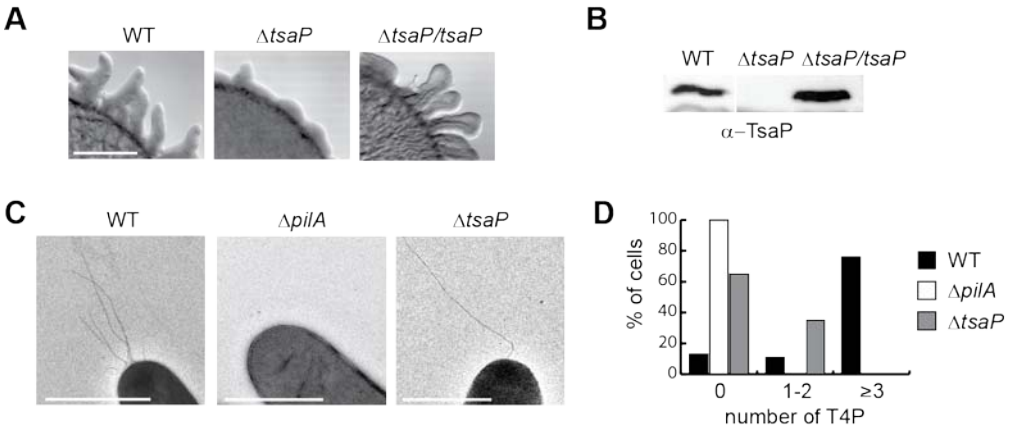

Figure 17 - TsaP is required for T4P-dependent motility. A) Motility phenotypes of the indicated strains on 0.5% agar/0.5% CTT favoring T4P-dependent motility. Scale bar 1 mm. B) Immunoblot detecting TsaP in the indicated strains using specific antibodies. C) Lack of TsaP reduces the number of T4P. Cells from exponentially growing cultures were visualized by TEM after staining with uranyl acetate (Dr. A. Klingl, Philipps-Universität Marburg). Scale bars 1 µm. D) Histogram summarizing the number of T4P per cell of the indicated strains (n= 19-55).

2.4 Mutually stabilizing effects between T4P proteins suggest the presence of an envelope spanning complex in *M. xanthus*

We next explored the interactions and interdependencies between individual T4P components. In *P. aeruginosa* and *N. meningitidis*, the Pil-proteins build a large, envelope-spanning multi-protein complex. However, comparison of both organisms revealed striking differences concerning the role of specific proteins in T4P assembly and the dependencies among each other (section 1.1.3). To elucidate how the Pil-proteins work together with TsaP and Tgl in *M. xanthus* to build the T4P machinery, we systematically profiled the stability of each protein in the absence of each individual other protein. Mutually stabilizing effects in which two or more proteins protect each other from degradation have been observed for several protein complexes. This approach had previously been successfully used to identify protein interactions in the case of membrane proteins belonging to complexes such as SecE/SecY, GspE/GspL from the T2SS or TonB/ExbB (Nishiyama *et al.*, 1992, Sandkvist et al., 1999, Skare & Postle, 1991).

To determine protein levels of the pilin subunit PilA in the available deletion mutants, we performed an immunoblot with PilA specific antibodies. Briefly, cells from exponentially growing cultures were harvested and total cell lysates were separated by SDS–PAGE (protein from 7 x 10^7 cells loaded per lane). Protein levels of PilA were detected via immunoblotting using specific α-PilA antibodies. As shown in Figure 18, the protein was detected at comparable levels in each deletion strain except for the *ΔpilA* strain, confirming specificity of the antibodies.

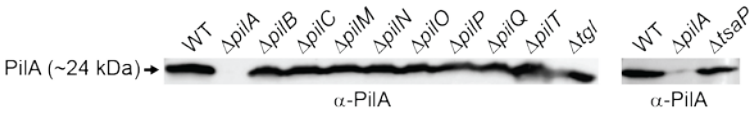

Figure 18 – PilA protein accumulation in in-frame deletion mutants. Immunoblot analysis with the indicated strains was done as described in Figure 15B using PilA specific antibodies. The blot with the *tsaP* deletion mutant was done separately including control strains WT and *ΔpilA* to confirm specificity of the antibody.

Further, we wanted to analyze the stability of PilB, which is the cytoplasmic ATPase providing the energy for T4P extension. An immunoblot with PilB specific antibodies was performed as previously done for PilA. PilB protein levels comparable to WT were detected in all tested deletion mutants except for the *pilB* deletion mutant (Figure 19), suggesting that PilB does not require any of the tested proteins for stability. These results are in agreement with the hypothesis that the two ATPases PilB and PilT only transiently interact with the T4P machinery to enable extension or retraction of the pili, respectively. It seems likely that a temporary interaction does not involve mutually stabilizing effects. Next, we determined the accumulation of the cytoplasmic retraction ATPase PilT in all deletion strains. PilT protein levels were detected at levels comparable to WT in all tested deletion mutants, indicating that none of the other proteins are required for PilT stability (Figure 19). This fits with the stability data of the extension ATPase PilB, which also accumulated in all deletion strains.

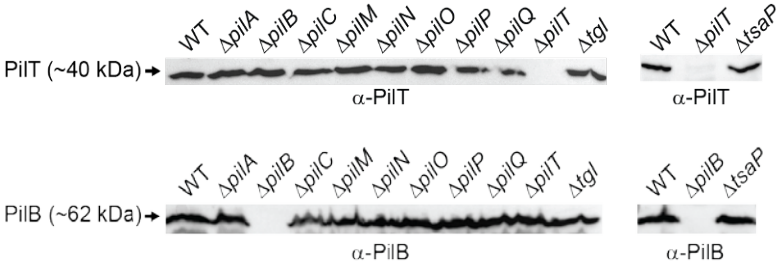

Figure 19 – PilB and PilT protein accumulation in in-frame deletion mutants. Immunoblot analysis with the indicated strains was done as described in Figure 15B using PilB and PilT specific antibodies, respectively.

The conserved IM platform protein PilC is suggested to be part of an IM complex in *N. meningitidis*, as direct interactions with PilO were detected in BACTH experiments (Georgiadou et al., 2012). Whether PilC interacts in a similar manner with PilO in *M. xanthus* was not previously known. However here, immunoblots using PilC specific antibodies showed that PilC accumulates in all tested deletion mutants at levels comparable to the WT strain (Figure 20), suggesting that there are no mutually stabilizing effects between PilC and the tested proteins. Though, these results do not argue against an interaction between PilC and PilO in *M. xanthus* as not all interactions go along with stabilizing effects.

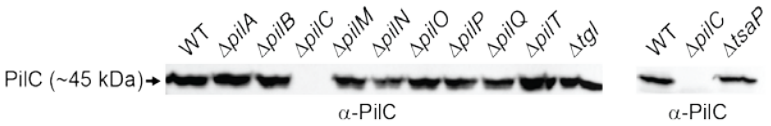

Figure 20 - PilC protein accumulation in in-frame deletion mutants. Immunoblot analysis with the indicated strains was done as described in Figure 15B using PilC specific antibodies. The blot with the *tsaP* deletion mutant was done separately including control strains WT and *ΔpilC* to confirm specificity of the antibody.

Determining the protein levels of the cytoplasmic actin-like protein PilM in the panel of T4P deletion strains revealed that PilM requires IM proteins PilN and PilO, the IM lipoprotein PilP, the OM secretin PilQ and its pilotin Tgl for full stability (Figure 21). The fact that *pilM* is co-transcribed with *pilN, pilO, pilP* and *pilQ* raised the question of whether the in-frame deletion interferes with the expression of the operon or the stability of the transcript instead of actual protein stability. However, polar effects in the mutants were already excluded by the complementation by ectopic expression of each individual gene. Interference by one of the other proteins at the level of PilM translation cannot be excluded, but seems unlikely, as all proteins contain a signal peptide and are secreted. The observation that two OM proteins, namely PilQ and Tgl affect the level of PilM in the cytoplasm points out that this experimental set up cannot distinguish between direct and indirect effects. Presumably, the OM proteins affect other proteins, possibly in the IM, which then affect cytoplasmic PilM accumulation. It is also unclear if the effect of Tgl on PilM stability occurs directly or indirectly via PilQ, as Tgl is required for the multimerization of PilQ (Figure 25).

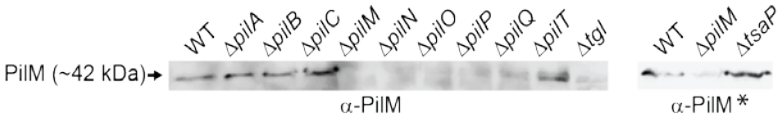

Figure 21 - PilM protein accumulation in in-frame deletion mutants. Immunoblot analysis with the indicated strains was done as described in Figure 15B using PilM specific antibodies. The blot with the *tsaP* deletion mutant was reproduced from Binzen (2012) (indicated by a star)

PilN was shown to be part of an IM complex in *N. meningitidis* and *P. aeruginosa*. In *M. xanthus*, immunoblot analysis with PilN specific antibodies revealed that PilN accumulated at decreased levels in the absence of PilO, PilP, PilQ and Tgl, and the absence of PilM had a minor effect on PilN levels (Figure 22). The stabilizing effects observed here suggest that PilN might also be part of an IM complex in *M. xanthus* consisting of PilN/O/P and that possibly also involves cytoplasmic protein PilM. Notably, the hypothesized complex seems to additionally require the OM secretin and Tgl. All other tested mutants have PilN protein levels compared to WT suggesting

they are not necessary for PilN stability (Figure 22). Although PilN is important for PilM stability (Figure 21), PilM affects PilN levels only to a minor degree, demonstrating that the stabilizing effects are not always equally affecting the stability of both interaction partners.

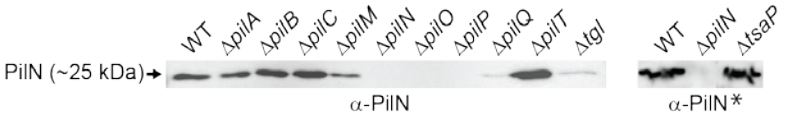

Figure 22 - PilN protein accumulation in in-frame deletion mutants. Immunoblot analysis with the indicated strains was done as described in Figure 15B using PilN specific antibodies. The blot with the *tsaP* deletion mutant was reproduced from Binzen (2012) (indicated by a star)

Determining the protein levels of the IM protein PilO in the *pil* deletion mutant strains revealed that the absence of IM protein PilN, lipoprotein PilP, secretin PilQ and pilotin Tgl results in decreased levels of PilO (Figure 23). These results are in agreement with previous studies from *N. meningitidis,* which showed that PilN and PilO require each other and both proteins require PilP for stability (Georgiadou et al., 2012). The dependency of PilO on PilQ and Tgl coincides with the data obtained for PilN, confirming that the potential IM complex requires the OM subcomplex of PilQ and Tgl for stability or incorporation into the T4P machinery. All other tested mutants showed PilO protein levels similar to WT (Figure 23).

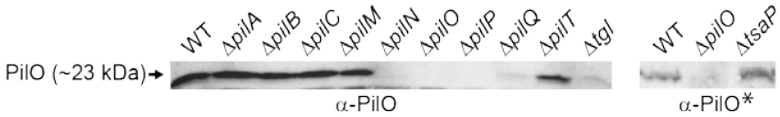

Figure 23 - PilO protein accumulation in in-frame deletion mutants. Immunoblot analysis with the indicated strains was done as described in Figure 15B using PilO specific antibodies. The blot with the *tsaP* deletion mutant was reproduced from Binzen (2012) (indicated by a star).

The lipoprotein PilP is anchored in the IM and is thought to connect OM and IM components of the T4P machinery in other species. Analysis of PilP accumulation in the different deletion mutants revealed stabilizing effects by PilQ and Tgl. All other tested mutants showed protein levels indistinguishable from WT (Figure 24). Interestingly, neither PilN nor PilO are required for PilP accumulation, showing that the stabilizing effects can be unidirectional since PilN and PilO require PilP for stability even though the reverse is not true.

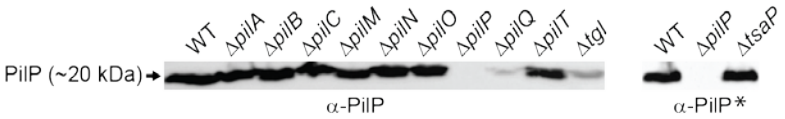

Figure 24 - PilP protein accumulation in in-frame deletion mutants. Immunoblot analysis with the indicated strains was done as described in Figure 15B using PilP specific antibodies. The blot with the Δ*tsaP* mutant was reproduced from Binzen (2012) (indicated by a star).

Further, immunoblot analysis was performed for the secretin PilQ, which builds the pore in the OM to allow the passage of the pilus. PilQ monomers accumulated in all tested deletion mutants, whereas oligomeric PilQ complexes were detected in all tested mutants except for the *tgl* deletion mutant (Figure 25). This is in agreement with previous studies that demonstrate that Tgl is the pilotin of PilQ required for oligomerization (Nudleman et al., 2006).

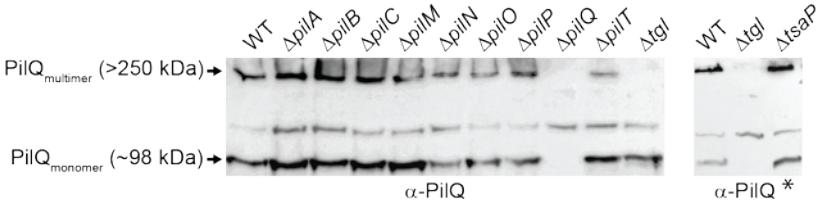

Figure 25 - PilQ monomer and multimer protein accumulation in in-frame deletion mutants. Immunoblot analysis with the indicated strains was done as described in Figure 15B using PilQ specific antibodies. The blot with the Δ*tsaP* mutant was reproduced from Binzen (2012) (indicated by a star).

Immunoblot analysis of Tgl displayed protein levels comparable to the WT strain in all tested deletion mutants (Figure 26). This suggests that Tgl does not require any of the tested proteins for stability even though it is required for the stability of other T4P components. Given that the role of Tgl in the stability of other proteins phenocopies the effects observed with PilQ, we speculate that Tgl might act indirectly via its effect on the multimerization of PilQ.

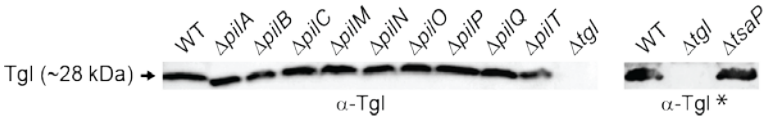

Figure 26 - Tgl protein accumulation in in-frame deletion mutants. Immunoblot analysis with the indicated strains was done as described in Figure 15B using Tgl specific antibodies. The blot with the Δ*tsaP* mutant was reproduced from Binzen (2012) (indicated by a star).

Finally, accumulation of TsaP in the absence of each T4P component was analyzed by immunoblotting (Binzen, 2012). The peptidoglycan binding protein TsaP, which putatively anchors the secretin to the cell wall, was shown to depend on PilQ and

Tgl for stability, as decreased protein levels were only detected in the absence of these two proteins (Figure 27).

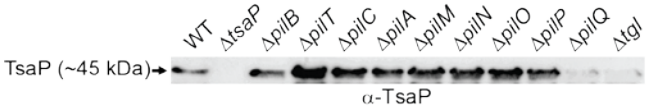

Figure 27 – TsaP protein accumulation in in-frame deletion mutants. Immunoblot analysis with the indicated strains was done as described in Figure 15B using TsaP specific antibodies. The blot was reproduced from Binzen (2012).

While each of the observed stabilizing effects shed some light on potential interactions, when considered together, we can begin to understand that the T4P machinery in *M. xanthus* builds a multi-protein complex. Briefly, stabilizing effects were observed between PilM/N/O/P/Q, TsaP and Tgl, while PilB/T/C/A accumulate completely independently, meaning that they did not affect and were unaffected by any other protein (Figure 28). The stabilizing effects between proteins of all subcelllar compartments support the hypothesis of a protein complex spanning the whole cell envelope. Strikingly, most effects observed, seemed to act in an outside-in manner, as OM proteins PilQ and Tgl are required for stably accumulating PilN/O/P in the IM and these proteins in turn, stabilize PilM in the cytoplasm (Figure 28). Hence, there seems to be an accumulation hierarchy from the OM, over the periplasm and the IM to the cytoplasm. Interestingly, TsaP, which is thought to anchor PilQ to the peptidoglycan is unstable in the absence of PilQ and Tgl, suggesting that TsaP association occurs solely with the assembled secretin.

Although these data suggest the existence of a multi-protein complex, it cannot tell us which proteins directly interact with each other. Furthermore, the fact that a protein is stable in the absence of another protein does not exclude the possibility that these proteins interact. Proteins may also be mislocalized in the absence of a protein interaction partner.

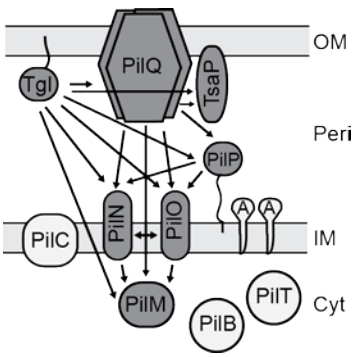

Figure 28 - T4P protein map summarizing stabilizing effects between the single components. Proteins in grey participate in stabilizing effects, while proteins in white accumulate independently of all tested proteins. OM=outer membrane, Peri=periplasm, IM=inner membrane, Cyt=cytoplasm.

2.5 PilN, PilO, PilP, PilQ and TsaP localize in a bipolar manner

Since some of the T4P proteins have been shown to localize in a bipolar manner, we investigated the localization of individual T4P proteins in the absence of each T4P protein. This cell biological approach allows the study of T4P protein assembly in the context of the complete machinery, preserving correct stoichiometry. Protein localization of a T4P component might be affected in the absence of an interaction partner and therefore prohibiting incorporation into the T4P machinery. Hence, localization analyses can provide a tool to indirectly study protein interactions. Fluorescent reporter strains or immunofluorescence microscopy to investigate the localization of the proteins PilA, PilB, PilC, PilM, PilQ and PilT are already established for *M. xanthus* (Bulyha et al., 2009, Nudleman et al., 2006, Yang *et al.*, 2010). So far, all localized proteins localize to one or both poles, except for the pilin PilA, which localizes throughout the whole cell envelope. While PilC, PilM and PilQ localize to both poles, PilB and PilT were predominantly found at one pole. Previous work has not addressed the localization of PilN, PilO or PilP in *M. xanthus.*

To investigate the localization of PilN, immunofluorescence microscopy using PilN specific antibodies and a fluorophore conjugated secondary antibody was performed. In parallel, we tried to investigate the localization of PilN using a fluorescent fusion with superfolder GFP (sfGFP). sfGFP can fluoresce in the periplasmic space in contrast to GFP or YFP (Dinh & Bernhardt, 2011), that generally fail to fold properly when exported in an unfolded manner via the Sec system (Feilmeier *et al.*, 2000). The fusion protein was expressed from the *pilA* promoter, which has already been successfully used for the complementation experiments (Figure 15). As PilN has a signal peptide at the N-terminus, sfGFP was fused to the C-terminus of PilN. To ensure proper folding of both PilN and sfGFP, we introduced a linker between the proteins as recommended by Dinh and Bernhardt (2011).

Using immunofluorescence microscopy with PilN specific antibodies, we could observe bipolar clusters in approximately 40 % of the WT cells (Figure 29). These clusters were absent in the deletion mutant of *pilN*, therefore, the signals observed in WT were specific.

The fluorescent fusion PilN-sfGFP was introduced at the Mx8 *attB* site in WT and in the deletion mutant of *pilN* to check for complementation of motility and hence, functionality of the fusion protein. However, no motility and no fluorescent signals could be detected in *M. xanthus* cells carrying the localization construct (Figure 29A). Immunoblot analysis confirmed that the protein was not expressed in the cells (Figure 29B), suggesting that fusion to sfGFP leads to the degradation of the protein or the

protein is not expressed. As already shown from the stability analysis, PilN requires further interaction partners for stability (Figure 22). We suggest that fusion to sfGFP prevents interactions to other stabilizing proteins resulting in the degradation of PilN.

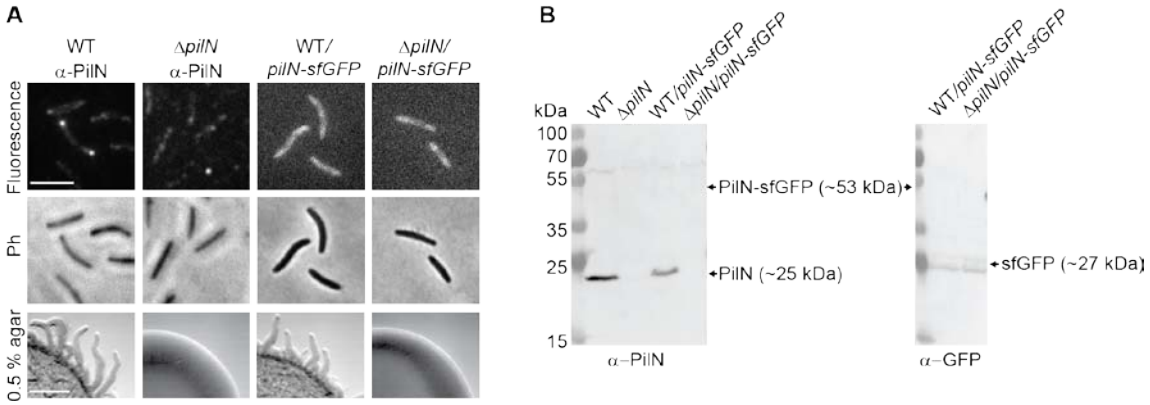

Figure 29 – PilN localizes to both poles. A) PilN localization was investigated by immunofluorescence and sfGFP-fusion in WT and *ΔpilN* as indicated. Upper and second rows show fluorescent and phase contrast images, respectively. For live-cell imaging of the strains containing the fluorescent fusion, cells from exponentially growing cultures were transferred to a 1.5% agar pad on a microscope slide and imaged by fluorescence microscopy. For immunofluorescence, cells were fixed and imaged by immunofluorescence microscopy using α-PilN antibodies. Scale bar 5 µm. The lower row shows motility phenotypes of the indicated strains on 0.5% agar/0.5% CTT, which favors T4P-dependent motility. Assay was done as described in Figure 15A. Scale bar 1 mm. B) Immunoblots detecting PilN and GFP in the indicated strains using specific antibodies. Blots were carried out as described in Figure 15B. Molecular weight markers are indicated in the left blot and are applicable for the right blot. Calculated molecular masses of proteins are shown in parentheses.

Next, PilO localization was investigated by immunofluorescence and sfGFP fusion. Immunofluorescence was essentially done as described for PilN. Using PilO specific antibodies, we could not detect clear signals in WT cells that were absent in the deletion mutant. We tested two available antisera for PilO in different dilutions to find the right ratio between specific signals and unspecific background noise. Also different paraformaldehyde concentrations were tested for fixation. Specific fluorescent signals could be detected under none of the tested conditions (Figure 30A). As PilO and PilN share a similar topology, the fluorescent fusion for PilO was constructed as described for PilN. PilO-sfGFP was introduced into WT and the *pilO* deletion mutant. Both strains showed bipolar foci when analyzed by fluorescence microscopy (Figure 30A). Introducing the construct into the deletion mutant restored motility, suggesting that the PilO-sfGFP fusion is functional and that the observed foci reflect where the functional activity occurs. Western blot analysis revealed that the full length protein PilO-sfGFP is expressed (Figure 30B). As the fusion protein could not be detected in the WT background using PilO-specific antibodies, a blot with GFP-specific antibodies was performed as well. This blot showed that the full-length protein is also expressed in

the WT background (Figure 30B). Furthermore, it showed some degradation of the fusion protein, as GFP alone was detected at around 27 kDa. However, the complementation of motility and the agreement with the bipolar localization pattern of PilM, PilN and PilQ, led us to conclude that the observed localization pattern of PilO is not artificially caused by the cleaved GFP. These data support our hypothesis that PilO is part of the bipolar, stationary complexes together with PilC/M/N/Q.

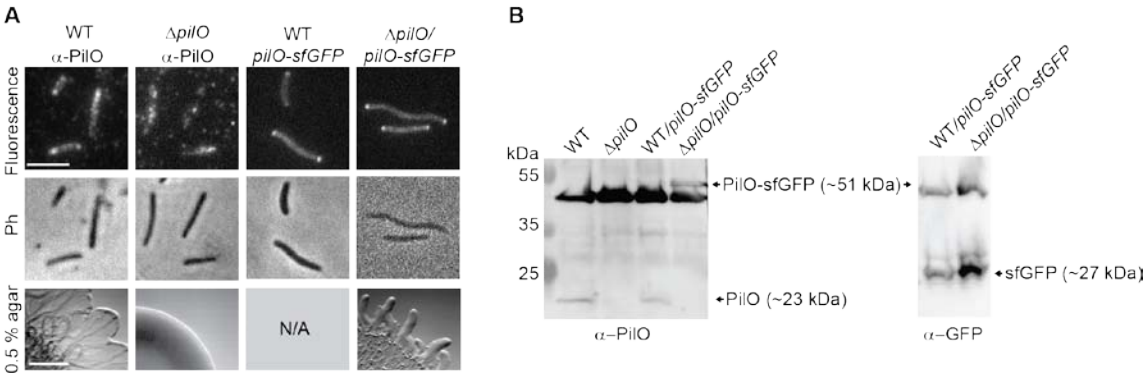

Figure 30 - PilO localizes to both poles. A) PilO localization was determined by immunofluorescence and sfGFP-fusion in WT and *ΔpilO* strains as indicated. Upper and second row show fluorescent and phase contrast images, respectively. Scale bar 5 µm. Microscopy was performed like described in Figure 29A. The lower row shows motility phenotypes of the indicated strains on 0.5% agar/0.5% CTT which favors T4P-dependent motility. Assay was done as described in Figure 15A. Scale bar 1 mm. B) Immunoblots detecting PilO and GFP in the indicated strains using specific antibodies. Blots were done as described in Figure 15B. Molecular weight markers are indicated in the left blot and are applicable for the right blot. Calculated molecular masses of proteins are shown in parentheses.

Similar to PilN and PilO, we analyzed the localization of PilP via immunofluorescence and fluorescent fusion. Using immunofluorescence microscopy, we could rarely detect specific signals. Bipolar signals could be detected in less than 10 % of the cells in WT (Figure 31A). As these bipolar signals were absent in the *ΔpilP* strain, we suggest that the signals are specific. However, 10 % of cells with specific signals are not sufficient to analyze the localization of a protein and especially effects on localization in different mutant backgrounds. Hence, a fluorescent fusion construct was used to visualize PilP. As the N-terminus of PilP carries a signal peptide II, which is cleaved off, followed by a lipid modification, which anchors PilP presumably in the IM, a C-terminal fusion was chosen. sfGFP was used, as PilP resides in the periplasmic space. The fusion construct was introduced into WT cells and the Δ*pilP* strain and analyzed by fluorescence microscopy. Bipolar signals could be observed in both strain backgrounds confirming the bipolar signals observed in immunofluorescence (Figure 31A). Introducing the fusion into the *ΔpilP* mutant restored motility to WT levels, suggesting that the fusion protein is active. Besides the full-length fusion protein the immunoblot showed some cleavage of the fusion protein, as PilP

alone could be detected in the deletion background. It is not clear if the cleaved protein or the fusion protein is accountable for the complementation effect. However, the combination of immunofluorescence and fluorescence microscopy of the PilP-sfGFP fusion leads us to propose that PilP localizes in a bipolar manner, as has been shown for PilC/M/N/O/Q.

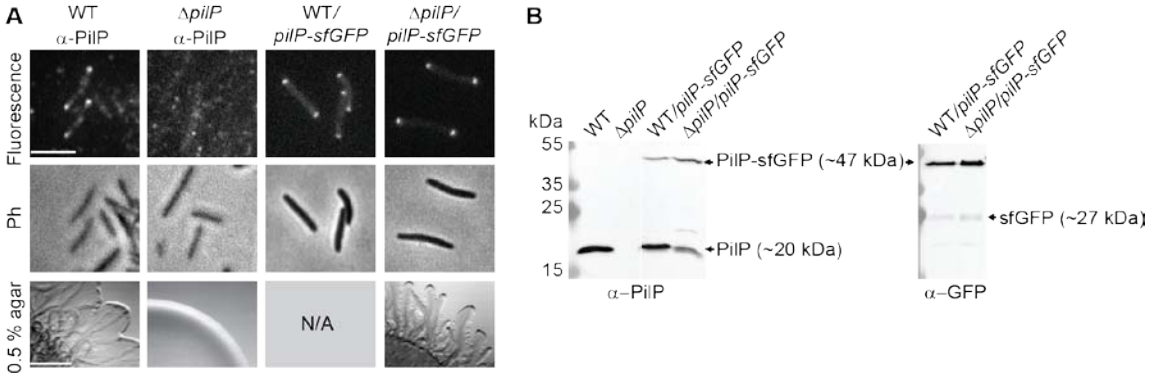

Figure 31 - PilP localizes to both poles. A) PilP was localized by immunofluorescence and sfGFP-fusion in WT and *ΔpilP* strains as indicated. Upper and second row show fluorescent and phase contrast images, respectively. Scale bar 5 µm. Microscopy was performed as described in Figure 29A. The lower row shows motility phenotypes of the indicated strains on 0.5% agar/0.5% CTT which favors T4P-dependent motility. Assay was done as described in Figure 15A. Scale bar 1 mm. B) Immunoblots detecting PilP and GFP in the indicated strains using specific antibodies. Molecular weight markers are indicated in the left blot and are applicable for the right blot. Calculated molecular masses of proteins are shown in parentheses.

PilQ localization was determined by immunofluorescence by Nudleman et al. (2006), as well as by Bulyha et al. (2009). However, in our hands PilQ localization via immunofluorescence only yielded a low percentage of cells with bipolar signals (Figure 32). Interestingly, when PilQ was localized in the Δ*tsaP* mutant via immunofluorescence, this resulted in a significantly increased number of cells showing clear bipolar foci (I. Binzen, MPI Marburg) (Figure 32), suggesting that TsaP interferes with immunodetection by blocking the binding sites for the PilQ antibodies. To validate the bipolar localization in the presence of functional TsaP, we decided to localize PilQ with a fluorescent fusion. Similar to PilN, PilO and PilP, PilQ was fused C-terminally to sfGFP under control of the *pilA* promoter. The construct was introduced at the Mx8 *attB* site in WT and the *ΔpilQ* strain. Microscopic analysis showed three different localization patterns; diffuse, unipolar and bipolar. In a WT background the majority of the cells showed one polar cluster (Figure 34C). Unipolar and diffuse localization patterns where seen in equal ratios in the remaining cells. In the Δ*pilQ* mutant, bipolar clusters were only observed in 3% of cells. Unipolar and diffuse localization patterns were observed in similar ratios in the remaining cells (Figure 34C). To analyze at which pole the unipolar cluster is located, time lapse movies were recorded. This revealed that there is

no correlation between the position of the unipolar cluster and the direction of movement, as some cells had the unipolar cluster at the leading cell pole whereas others showed one cluster at the lagging cell pole (Figure 33). Furthermore, no relocation of this cluster was observed during a cellular reversal (Figure 33). Immunoblot analysis showed that the fusion protein was expressed in both WT and *ΔpilQ* backgrounds (Figure 32B). However, motility assays revealed that PilQ-sfGFP is not functional, as motility in a *ΔpilQ* mutant could not be restored. However, the protein did not have a dominant negative effect on motility, as motility was not reduced in WT expressing the fusion protein (Figure 32).

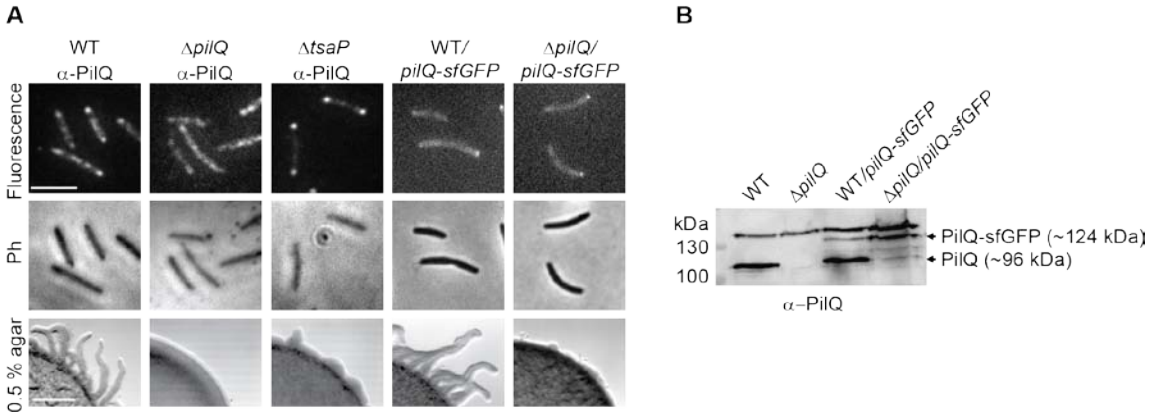

Figure 32 – PilQ localizes in a bipolar manner. A) PilQ was localized by immunofluorescence and sfGFP-fusion in WT, *ΔtsaP* and *ΔpilQ* strains as indicated. Upper and second row show fluorescent and phase contrast images, respectively. Scale bar 5 µm. Microscopy was performed like described in Figure 29A. The lower row shows motility phenotypes of the indicated strains on 0.5% agar/0.5% CTT which favors T4P-dependent motility. Assay was done as described in Figure 15A. Scale bar 1 mm. B) Immunoblots detecting PilQ in the indicated strains using specific antibodies. Blots were done as described in Figure 15B. Molecular weight markers are indicated on the left side. Calculated molecular masses of proteins are shown in parentheses.

Given that the fluorescent fusion of PilQ does not display the correct localization pattern, we took advantage of an approach that was used to determine the localization of the PulD secretin of the T2SS in *E. coli* (Buddelmeijer *et al.*, 2009). They discovered that the secretin fused to mCherry only showed the correct subcellular localization in the presence of high levels of its pilotin protein PulS. Therefore, we designed a localization construct, which co-expressed the pilotin TgI with PilQ-sfGFP. TgI was cloned under the *pilA* promoter followed by the intergenic region between *pilP* and *pilQ,* and the gene for *pilQ-sfGFP*, thereby, creating an artificial operon. Again, this construct was introduced into WT and *ΔpilQ* and analyzed by fluorescence microscopy. Overexpression of TgI significantly increased the number and the intensity of bipolar clusters. The majority of the cells in the WT background showed bipolar foci and only a small portion of cells with unipolar clusters or diffuse localization (Figure 34A/C). In

contrast, the fusion in the *ΔpilQ* background showed again a large fraction of cells with unipolar clusters (Figure 34A/C). The different distribution of localization patterns observed in WT and *ΔpilQ* strain backgrounds suggests that the native PilQ present in the WT promotes correct localization of PilQ-sfGFP.

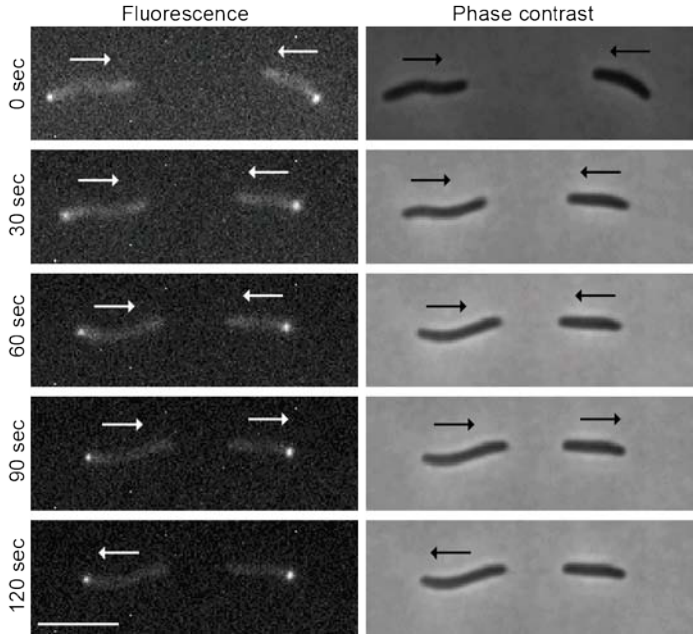

Figure 33 – Unipolar cluster position of PilQ-sfGFP and direction of movement do not correlate. Cells from an exponentially growing culture were transferred to a 1.5% agar pad on a microscope slide imaged by fluorescence and phase contrast microscopy at 30 sec intervals. White arrows indicate the direction of movement of each cell. Strain used, SA4099 (*ΔpilQ/pilQ-sfGFP*). Scale bar 5 µm.

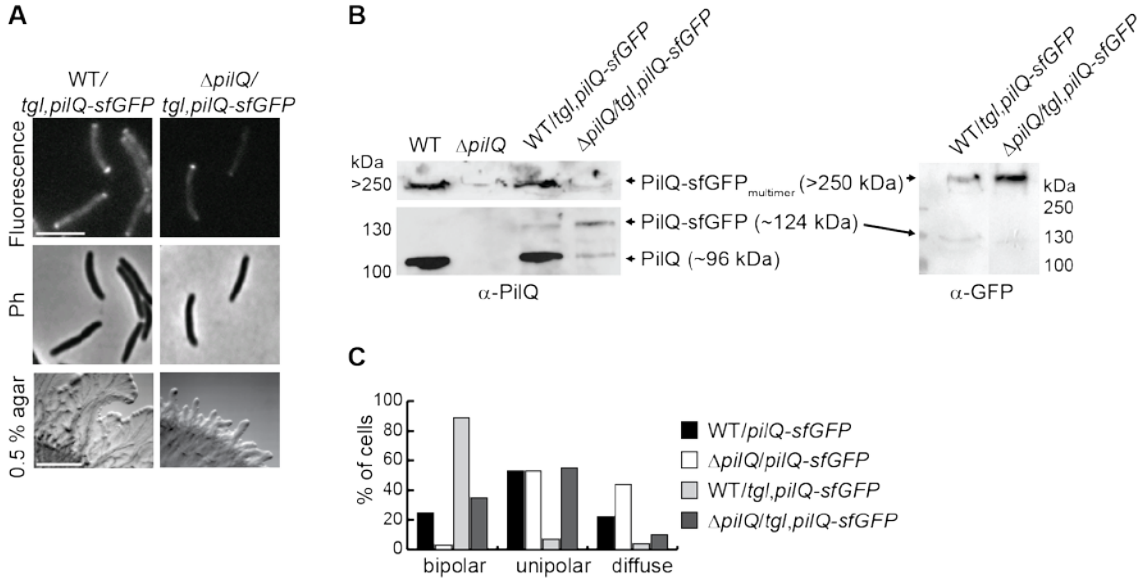

Figure 34 – Co-expression of Tgl promotes bipolar localization of PilQ-sfGFP. A) PilQ was localized as a sfGFP-fusion co-expressed with Tgl in WT and and *ΔpilQ* strain backgrounds as indicated. The upper and second rows show fluorescent and phase contrast images, respectively. Microscopy was performed as described in Figure 29. Scale bar 5 µm. The lower row shows motility phenotypes of the indicated strains on 0.5% agar/0.5% CTT, which favors T4P-dependent motility. Scale bar 1 mm. B) Immunoblots detecting PilQ and GFP in the indicated strains using specific antibodies

as indicated. Molecular weight markers are indicated. Calculated molecular masses of proteins are shown in parentheses. C) Distribution of localization patterns of PilQ-sfGFP in the indicated strains. (n=57-233)

Immunoblot analysis showed that the fusion protein was expressed, although protein levels were reduced when compared to PilQ expression in WT. Importantly, PilQ-sfGFP was incorporated into multimers, as multimers could be detected using GFP specific antibodies (Figure 34B). Motility in the *ΔpilQ* mutant was partially restored by PilQ-sfGFP, as small flares were observed on soft agar (Figure 34A), suggesting that PilQ-channels could be formed by PilQ-sfGFP at low efficiency, allowing the passage and function of T4P. Motility of the WT strain expressing the fusion construct showed normal motility, comparable to WT. Since PilQ-sfGFP, coexpressed with TgI in the WT background strain reflects best the bipolar localization of PilQ, this set-up was chosen for further analyses.

Next, we analyzed the localization of TsaP, the predicted secretin anchoring protein. Immunofluorescence microscopy and a C-terminal fluorescent fusion to mCherry revelead that TsaP localizes in a bipolar manner (Figure 35) (Binzen, 2012). TsaP-mCherry was introduced into WT and the *ΔtsaP* mutant. The motility defect of the *ΔtsaP* mutant could only be partially complemented when compared to WT (Binzen, 2012). In addition, motility of the WT strain, containing the fusion construct, seemed to be slightly reduced, suggesting a dominant negative effect on motility. The mCherry-tag might disturb the function of TsaP. Protein levels of TsaP-mCherry were increased in WT and *ΔtsaP* strain backgrounds when compared to native TsaP levels, however, this is presumably not negatively affecting motility, as overexpression of the proteins did not affect motility in our complementation assay (Figure 17).

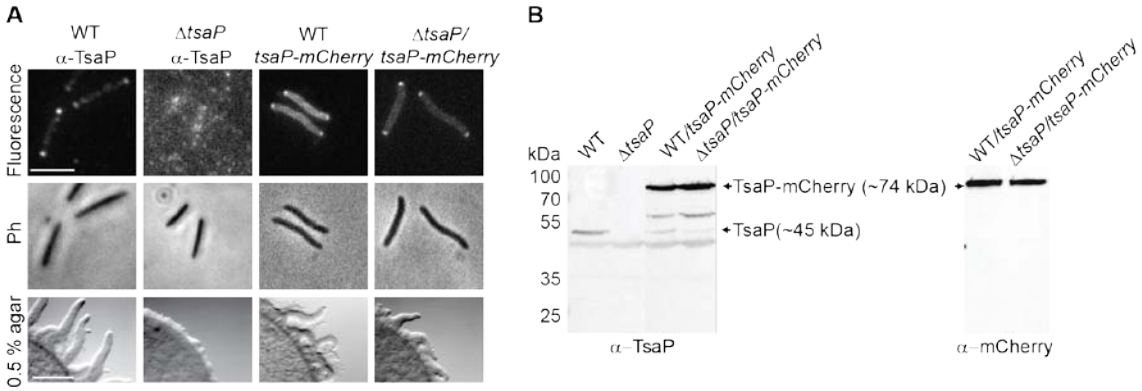

Figure 35 - TsaP localizes in a bipolar manner. A) TsaP was localized by immunofluorescence and mCherry-fusion in WT and *ΔtsaP* strains as indicated. Scale bar 5 µm. The lower row shows motility phenotypes of the indicated strains Scale bar 1 mm. (Pictures were taken by I. Binzen, MPI Marburg). B) Immunoblots detecting TsaP or mCherry in the indicated strains using specific antibodies. Immunoblot was reproduced from Binzen (2012). Molecular weight markers are indicated on the left side. Calculated molecular masses of proteins are shown in parentheses.

2.6 Tgl localizes throughout the cell envelope

Because Tgl is important for the multimerization of PilQ, we wanted to include it in our analyses. Therefore, we tried to perform immunofluorescence microscopy as done by Nudleman et al. (2006). Using Tgl specific antibodies, we were unable to observe a unipolar localization as it was proposed by Nudleman and colleagues. As no specific signals could be seen in WT and lower dilutions of the Tgl-specific antibodies only resulted in a higher level of background fluorescence in WT an deletion strain, we decided to test the complementation strain, which is overexpressing Tgl (Figure 15B). This strain showed fluorescent signal over the whole cell that was absent in both WT and the deletion mutant (Figure 36). The weaker signal in the cell body compared to the cell border suggests that the signal is located in the cell envelope. As this localization is at odds with the published unipolar localization, we wanted to confirm these results using a fluorescent fusion for Tgl. Due to the N-terminal signal peptide type II, which localizes Tgl to the OM via a lipid anchor, we designed a sfGFP fusion, as in the case of PilO and PilP.

We then introduced the localization construct for Tgl into WT and the *Δtgl* mutant. Microscopy analysis revealed a localization pattern identical to that observed via immunfluorescence microscopy, i.e. an envelope signal throughout the cell (Figure 36). Motility was complemented by the fluorescent construct in the Δ*tgl* mutant. However, immunoblot analysis showed that the fusion protein was partially cleaved and a band corresponding to the size of Tgl was detected (Figure 36). Therefore, we cannot distinguish whether the fluorescent fusion is active, as motility might have been restored by the Tgl freed from its fluorescent tag. Importantly, there was no GFP alone

detected in the blot using GFP-specific antibodies (Figure 36), suggesting that the fluorescent envelope signal reflects the localization of the full-length Tgl-sfGFP protein. Although Tgl was overexpressed in both experimental set ups due to the expression from the *pilA* promoter, we propose that the combination of both experiments provides evidence supporting a uniform localization of Tgl throughout the OM.

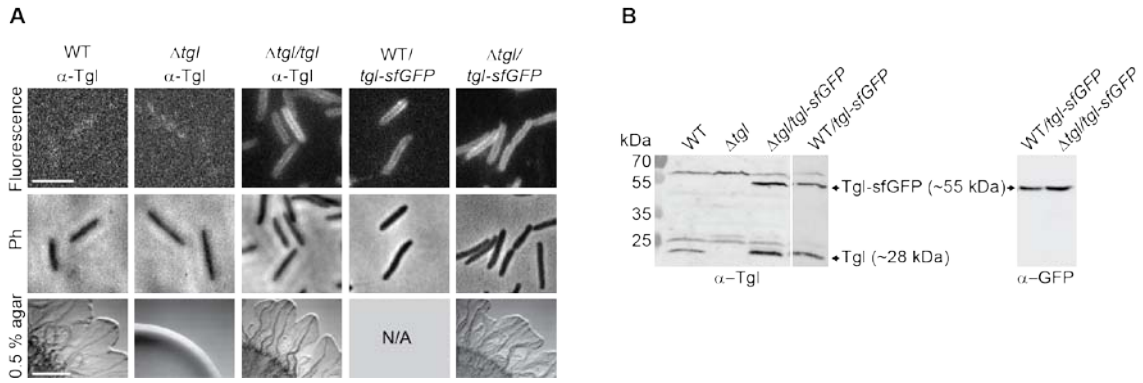

Figure 36 – Tgl localizes uniformly throughout the cell envelope. A) Tgl was localized by immunofluorescence and sfGFP-fusion in WT, *Δtgl* and *Δtgl/tgl* strains as indicated. Upper and second row show fluorescent and phase contrast images, respectively. Microscopy was performed like described in Figure 29A. Scale bar 5 µm. The lower row shows motility phenotypes of the indicated strains on 0.5% agar/0.5% CTT which favors T4P-dependent motility. Assay was done as described in Figure 15A. Scale bar 1 mm. B) Immunoblots detecting Tgl and GFP in the indicated strains using specific antibodies. Blots were done as described in Figure 15B. Molecular weight markers are indicated on the left side and are applicable for the right blot. Calculated molecular masses of proteins are shown in parentheses.

Furthermore, a unipolar localization would imply that Tgl switches poles during a cellular reversal as reported for other unipolarly localized proteins (Bulyha et al., 2009, Mignot et al., 2005). We cannot think of a mechanism, which allows a lipoprotein anchored in the OM to switch from one pole to another in the time period of a cellular reversal (~30 s). An alternative mechanism could be that Tgl is only synthesized during cell division, when the new cell pole requires the multimerization of PilQ. This would imply that Tgl is fully degraded at the old pole within one cell cycle, resulting in a unipolar localization pattern. To test this possibility, we blocked protein biosynthesis using chloramphenicol and observed that Tgl is stable for at least 6 h (Figure 37). As one cell cycle is approximately 5 h, we conclude that this excludes one way of generating a unipolar localization of Tgl. Therefore, combined with the above localization data, we suggest that Tgl localizes uniformly throughout the OM.

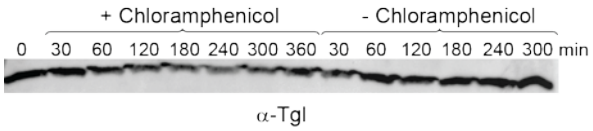

Figure 37 – Determination of half life ($T_{1/2}$) of Tgl. DK1622 WT cells were grown in 1.0% CTT medium. At t= 0 min, the culture was split in two and chloramphenicol added to one at a concentration of 25 µg/ml, which inhibits protein synthesis under these conditions (Konovalova *et al.*, 2012). At the indicated time-points, samples were harvested. Protein from 7×10^7 cells were loaded per lane, separated by SDS-PAGE and Tgl levels determined by immunoblotting using α-Tgl antibodies.

During the microscopy analysis of the fluorescent fusion, we noticed fluorescent tracks of moving *M. xanthus* cells and fluorescent cell appendages (Figure 38). We speculate that this is Tgl-sfGFP, which is deposited in so called outer membrane vesicles (OMVs, section 1.3.2). The OMVs are often organized in chains that can be seen by electron microscopy (Figure 38). As fluorescent signals exterior to cells could not be seen with any of the other used fusions, this is another hint that the observed signals reflect the correct localization of Tgl, anchored in the OM.

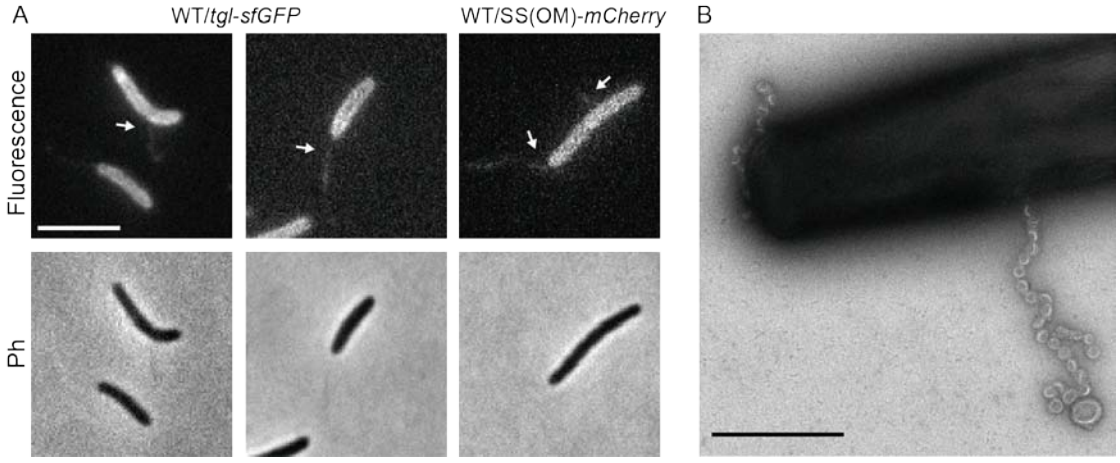

Figure 38 - Outer membrane vesicles of *M. xanthus*. A) OM localization of Tgl-sfGFP and mCherry with a signal sequence type II for OM localization (Wei et al., 2011). OMVs are indicated by white arrows. Upper and lower rows show fluorescent and phase contrast images, respectively. Microscopy was performed as described in Figure 29A. Scale bar 5 µm. B) Transmission electron microscopy picture of a WT cell after fixation with glutaraldehyde and negative staining with uranyl acetate (Dr. A. Klingl, Philipps-Universität Marburg). Scale bar 1 µm.

2.7 Localization of T4P proteins in the absence of each individual other T4P protein

After validating the localization of individual T4P proteins, we wished to use protein localization to analyze the interdependencies for localization between the individual components of the T4P machinery. Investigating the localization of PilB/C/M/N/O/P/Q/T and TsaP in the available deletion mutants would demonstrate whether polar recruitment and presumably incorporation into the T4P envelope

complex requires the presence of another protein. Due to their uniform cell envelope localization, PilA and Tgl were excluded from this approach.

The extension ATPase PilB was shown to accumulate in all deletion mutants, therefore, PilB localization was investigated in all of these strains. Immunofluorescence with specific α-PilB antibodies was performed as done by Bulyha et al. (2009). In WT, cells with unipolar and bipolar clusters could be observed. In contrast, these signals were absent in the Δ*pilB* mutant, confirming the specificity of the observed signals. When staining PilB in the different deletion mutants, signals comparable to WT were observed (Figure 39), suggesting that none of the tested proteins are required for polar PilB localization. To confirm that PilB localization is independent of the complete T4P machinery at the poles, we constructed an in-frame deletion of *pilT/C/M/N/O/P/Q* and checked again for PilB localization. In agreement with our previous data, we observed polar clusters in this mutant strain (Figure 39).

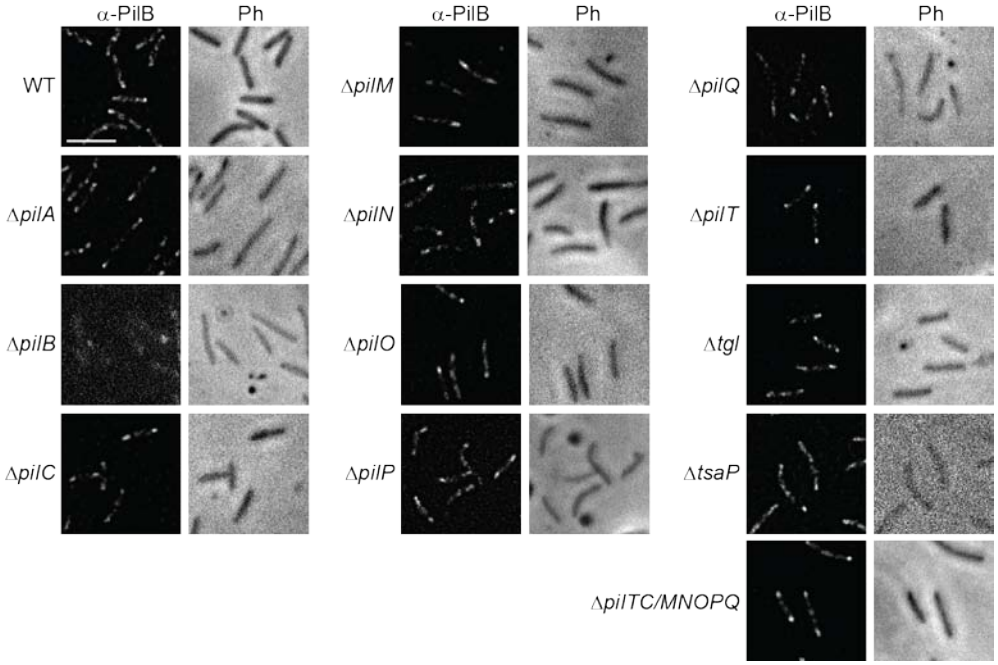

Figure 39 – PilB independently localizes to the pole(s). PilB was visualized by immunofluorescence in WT and the indicated deletion strains. Left and right rows show fluorescent and phase contrast images, respectively. Microscopy was performed as described in Figure 29A. All pictures were deconvolved using Huygens Essentials. Scale bar 5 µm.

A functional YFP-PilT fusion was used to investigate the localization of the retraction ATPase PilT and its dependency on other T4P proteins. YFP-PilT accumulated at comparable levels in all tested strains (Figure 41). Furthermore, polar localization could be observed in the *ΔpilT* mutant as well as in a strain lacking PilB, PilC, PilM, PilN, PilP, PilP and PilQ (Figure 40). Similarly, YFP-PilT localized polarly independently of Tgl and TsaP (Figure 40). In agreement with the localization data for

the extension ATPase PilB, PilT is not recruited to the pole(s) by any of the tested T4P components.

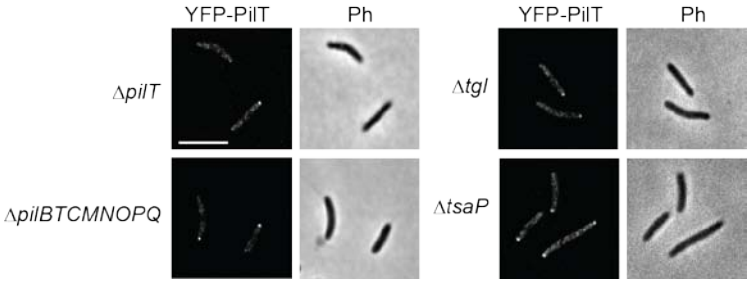

Figure 40 – Polar PilT localization is independent of all tested proteins. PilT localization was analyzed using an YFP-PilT fusion. The fusion was introduced into the indicated strains. Left and right rows show fluorescent and phase contrast images, respectively. Microscopy was performed like described in Figure 29A. All pictures were deconvolved using Huygens Essentials. Scale bar 5 µm.

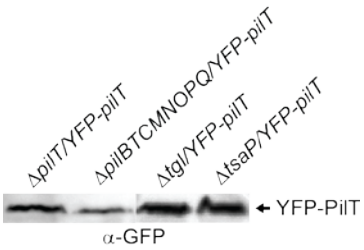

Figure 41 – YFP-PilT accumulates in all tested deletion strains. Immunoblot detecting YFP-PilT in the indicated strains using GFP specific antibodies. Blot was done as described in Figure 15B.

PilC localization was investigated by immunofluorescence as done by Bulyha et al. (2009). Bipolar PilC foci were observed in WT as well as in the deletion mutants of *pilA, pilB, pilM, pilT* and *tsaP* (Figure 42). Strikingly, although PilC was stable and accumulated in the *tgl, pilQ, pilP*, *pilO* and *pilN* deletion mutants, PilC localization was altered in the absence of any one of these five proteins. Bipolar localization could be detected in fewer cells and the observed clusters were fainter than those in WT (Figure 42). This suggests that although PilC accumulation does not depend on PilN/O/P/Q and Tgl, it requires these proteins for proper incorporation into the T4P assemblies.

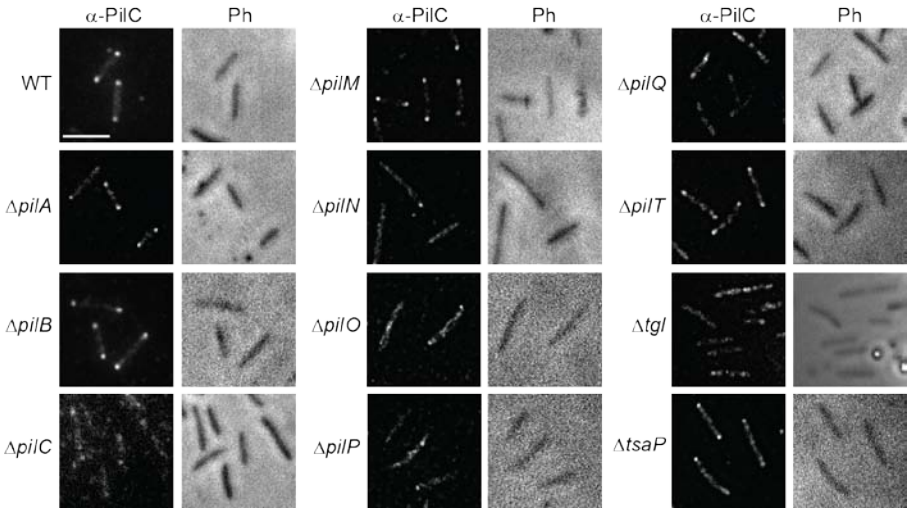

Figure 42 - PilC polar localization requires PilN, PilO, PilP, PilQ and Tgl. PilC was visualized by immunofluorescence in WT and the indicated deletion strains. Left and right rows show fluorescent and phase contrast images, respectively. Microscopy was performed like described in Figure 29A. All pictures were deconvolved using Huygens Essentials. Scale bar 5 µm.

To localize PilM, we performed immunofluorescence microscopy as described previously by Bulyha et al. (2009). PilM does not accumulate in the *ΔpilN*, *ΔpilO*, *ΔpilP*, *ΔpilQ* and *Δtgl* mutants (Figure 21). Hence, these mutants were excluded from the localization experiment. In the remaining five mutants bipolar PilM localization occured at levels and frequencies indistinguishable from WT (Figure 43). This supports the accumulation experiment results in that PilM protein levels were observed indistinguishable from WT in these mutants (Figure 21).

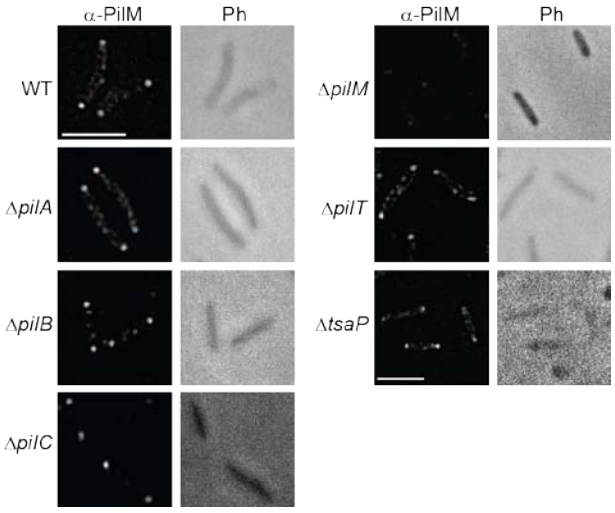

Figure 43 – Bipolar PilM localization is independent of PilA, PilB, PilC, PilT and TsaP. PilM localization was detected by immunofluorescence in WT and the indicated deletion strains. Left and right rows show fluorescent and phase contrast images, respectively. Microscopy was performed like described in Figure 29A. All pictures were deconvolved using Huygens Essentials. Scale bars 5 µm. *Δtsap* scale bar applies only to that image pair.

PilN localization was determined by immunofluorescence microscopy in WT and six of the eleven in-frame deletion mutants. Because PilN does not accumulate in the *ΔpilO, ΔpilP, ΔpilQ* and *Δtgl* mutants (Figure 22), these strains were excluded from the localization analyses. In the remaining in-frame deletion mutants and WT, comparable numbers and intensities of bipolar PilN foci were observed (Figure 44), suggesting that PilA, PilB, PilC, PilM, PilT and TsaP are dispensable for bipolar PilN localization.

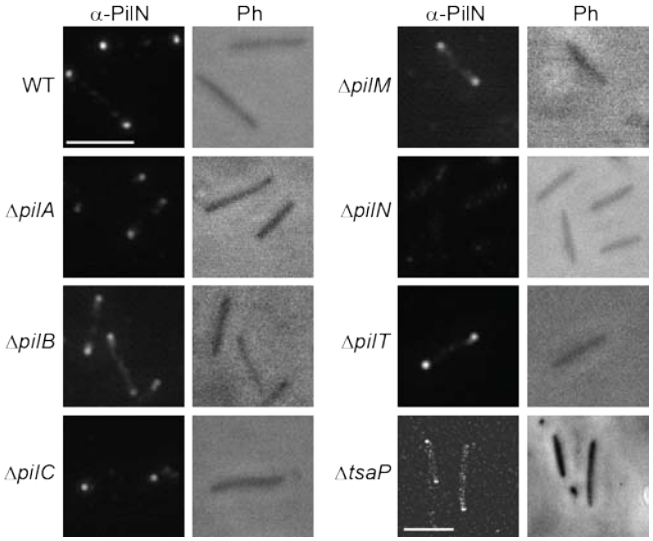

Figure 44 - Bipolar PilN localization is independent of PilA, PilB, PilC, PilM, PilT and TsaP. PilN localization was determined by immunofluorescence in WT and the indicated deletion strains. Left and right rows show fluorescent and phase contrast images, respectively. Microscopy was performed like described in Figure 29A. The picture of the *ΔtsaP* mutant was taken by I. Binzen (MPI Marburg). Pictures were deconvolved using Huygens Essentials. Scale bars 5 µm. *Δtsap* scale bar applies only to that image pair.

Next, PilO-sfGFP was introduced into the different deletion strains to analyze its dependency on the different T4P proteins in terms of localization. We also included the deletion strains of *pilN/P/Q* and *tgl* in which native PilO was shown to be highly unstable (Figure 23). Western blot analysis revealed that PilO-sfGFP accumulated in WT and in all in-frame deletion mutants, although protein levels were slightly reduced in the *ΔpilN* and *ΔpilP* mutants (Figure 46) suggesting that the sfGFP-tag partially rescues PilO from degradation in the *Δtgl*, *ΔpilN/P/Q* mutants. Although, PilO-sfGFP accumulated, no polar clusters were detectable in any one of these mutants (Figure 45). In all other strains bipolar PilO-sfGFP clusters were detected, except that the polar clusters in the *ΔtsaP* mutant were fainter (Figure 45).

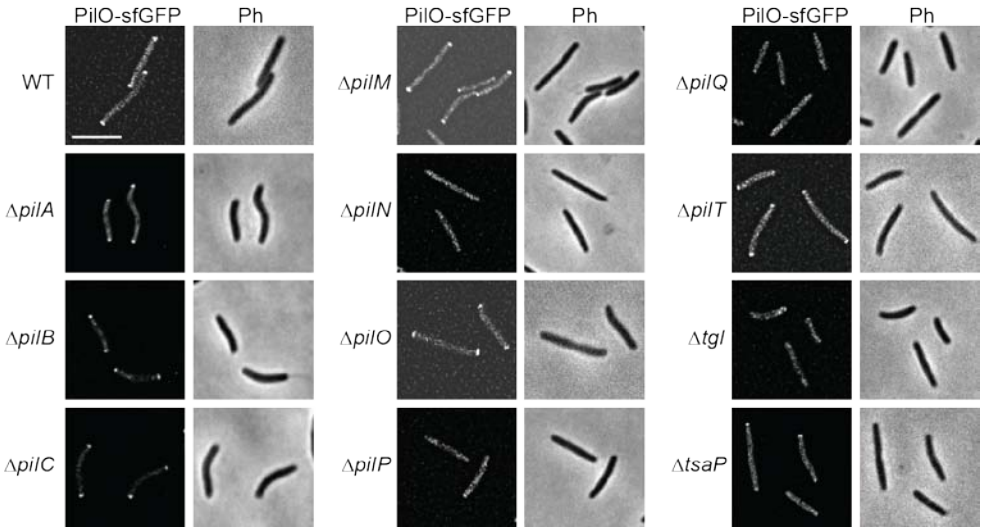

Figure 45 – PilO bipolar localization depends on PilN, PilP, PilQ and Tgl. PilO was visualized by fluorescence microscopy using an sfGFP-fusion protein in WT and the indicated deletion strains. Left and right rows show fluorescent and phase contrast images, respectively. Microscopy was performed like described in Figure 29A. All pictures were deconvolved using Huygens Essentials. Scale bar 5 µm.

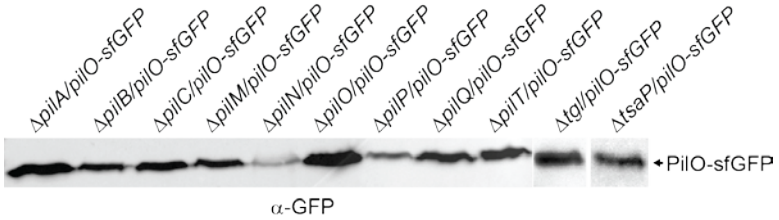

Figure 46 – PilO-sfGFP protein levels in different deletion mutants. Immunoblot detecting PilO-sfGFP in the indicated strains using GFP specific antibodies. Blot was done as described in Figure 15B.

PilP localization was determined using PilP-sfGFP, which was introduced into the different deletion mutants. Although native PilP was shown to be degraded in the absence of PilQ and Tgl (Figure 24), immunoblotting revealed that PilP-sfGFP accumulated at similar levels in all deletion strains and WT (Figure 48). Again, the fusion to sfGFP seems to rescue PilP from proteolytic degradation. However, mainly diffuse signals of PilP-sfGFP were observed in deletion mutants of *pilN, pilO* and *pilQ* and showed only faint polar clusters in the deletion mutant of *tgl* (Figure 47). In the remaining strains PilP bipolar localization could be observed comparable to WT.

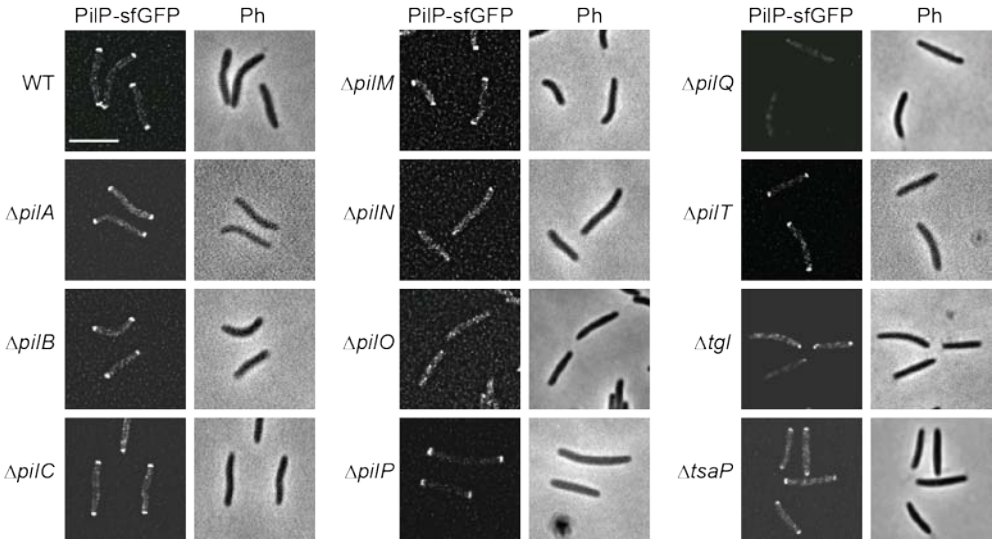

Figure 47 - Bipolar PilP localization depends on PilN, PilO, PilQ and Tgl. PilP localization was investigated by fluorescent microscopy using an sfGFP-fusion protein in WT and the indicated deletion strains. Left and right rows show fluorescent and phase contrast images, respectively. Microscopy was performed like described in Figure 29A. All pictures were deconvolved using Huygens Essentials. Scale bar 5 µm.

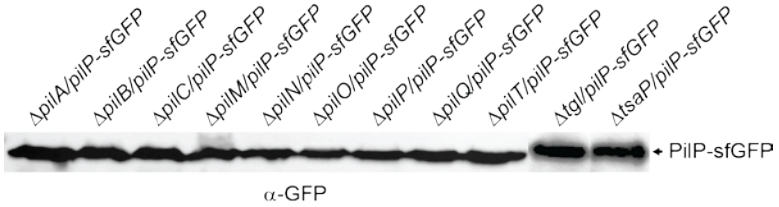

Figure 48 - PilP-sfGFP protein levels in different deletion mutants. Immunoblot detecting PilP-sfGFP in the indicated strains using GFP specific antibodies. Blot was done as described in Figure 15B.

PilQ localization was examined using PilQ-sfGFP co-expressed with Tgl as it resembles best the bipolar localization of PilQ. Immunoblotting confirmed that monomeric and multimeric PilQ-sfGFP accumulated in WT as well as in all in-frame deletion mutants except for the *tgl* deletion mutant (Figure 50). Furthermore, all tested deletion strains displayed bipolar PilQ localization similar to that in WT (Figure 49). Expressing PilQ-sfGFP in the absence of extra Tgl in a *Δtgl* mutant, resulted in diffuse signals throughout the cells (Figure 49). Since Tgl localizes uniformly throughout the cell envelope, we speculate that Tgl does not act as a polar targeting factor for PilQ. Ratherbecause Tgl is required for PilQ oligomer formation, we suggest that only oligomeric PilQ localizes to or can be retained at the poles.

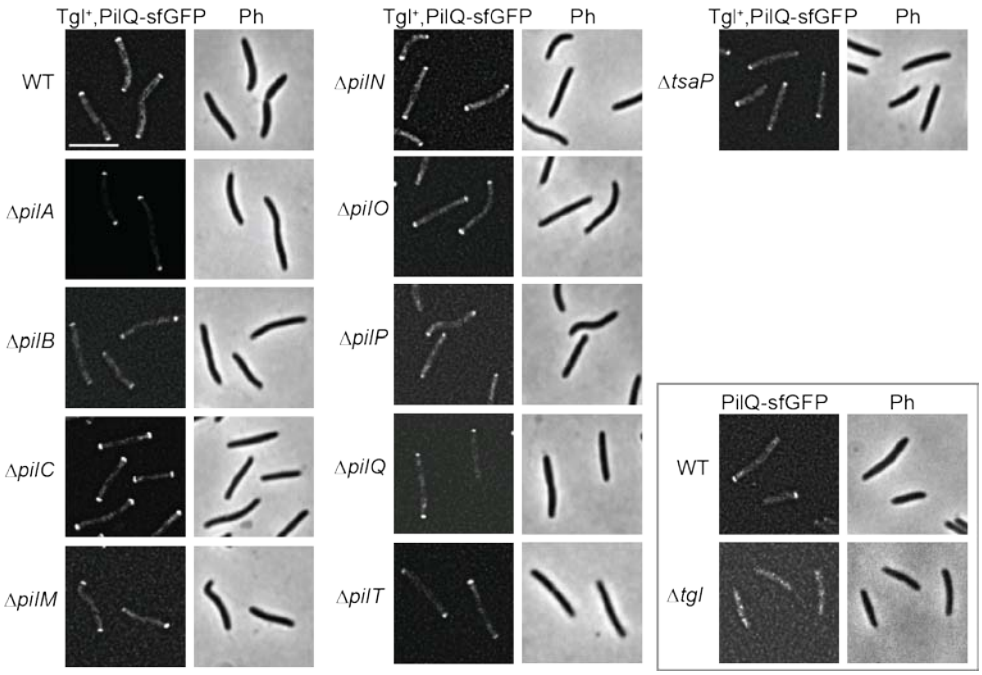

Figure 49 – Polar PilQ localization is independent of all tested proteins except for Tgl. PilQ localization was investigated using an sfGFP-fusion and co-expression with Tgl in WT and the indicated deletion strains. Strains containing the PilQ-sfGFP fusion without co-expression of Tgl are shown in the grey box. Left and right rows show fluorescent and phase contrast images, respectively. Microscopy was performed like described in Figure 29A. All pictures were deconvolved using Huygens Essentials. Scale bar 5 µm.

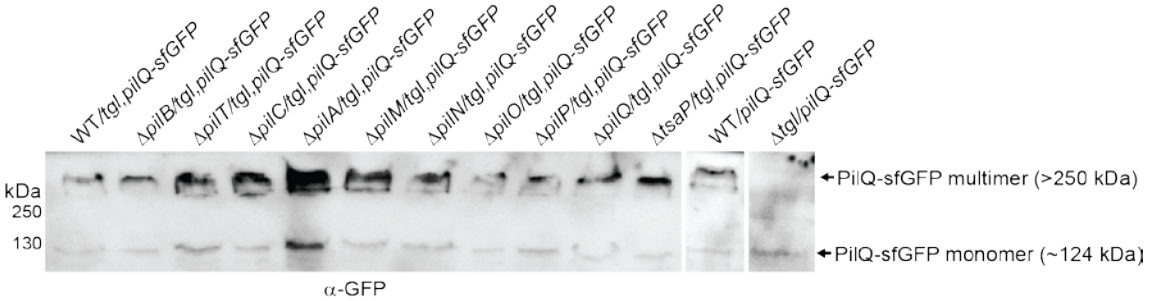

Figure 50 - PilQ-sfGFP protein levels in different deletion mutants. Immunoblot detecting PilQ-sfGFP in the indicated strains using GFP specific antibodies. Blot was done as described in Figure 15B. Molecular weight markers are indicated on the left. Calculated molecular masses of the detected proteins are indicated in parenthesis.

Localization of the LysM-domain protein TsaP was determined using a functional TsaP-mCherry fusion. The fusion protein accumulated in all tested deletion strains (Figure 52). TsaP-mCherry localized to both poles in all deletion strains except for the deletion mutants of *pilQ* and *tgl*. This is in agreement with previous results showing that TsaP requires these two proteins for stability (Figure 27). Interestingly, in the *ΔpilA* strain, polar clusters of TsaP-mCherry were fainter than those in WT (Figure 51). However, we had the impression that the envelope signals were increased in this strain, which might mask the polar signal.

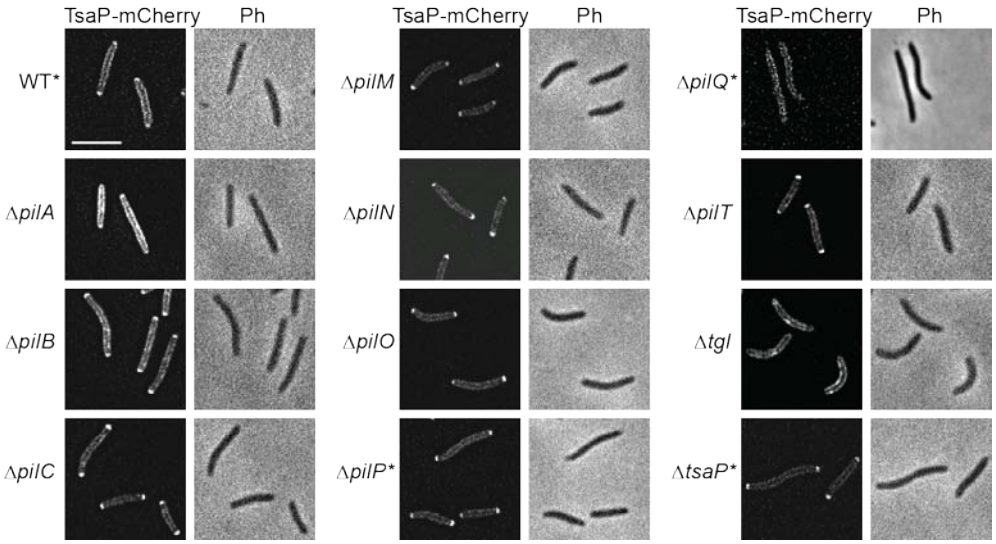

Figure 51 - Polar TsaP localization depends on PilQ and Tgl. TsaP localization was analyzed using a functional TsaP-mCherry fusion. The fusion was introduced into the indicated strains. Left and right rows show fluorescent and phase contrast images, respectively. Microscopy was performed like described in Figure 29A. * indicates pictures that were taken by I. Binzen (MPI Marburg). All pictures were deconvolved using Huygens Essentials. Scale bar 5 µm.

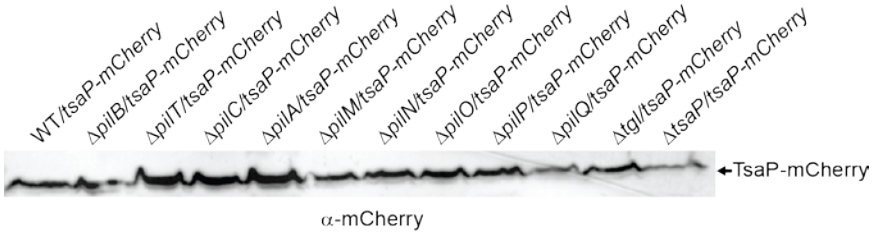

Figure 52 – TsaP-mCherry accumulates in all tested deletion mutants. Immunoblot detecting TsaP-mCherry in the indicated deletion mutants using mCherry specific antibodies. Blot was done as described in Figure 15B.

The systematic localization approach used here, revealed new insights into interdependencies and potential interactions between T4P components, which were not observed in the protein stability approach. Additionally, the experiments confirmed some of the data from the stability approach, as proteins that were not stable in certain deletion strains were not able to localize to the poles even though they were stabilized by the added fluorophores. To get an overview of all localization experiments and to quantify the observed effects, the distribution of the localization patterns in the different strains was determined by grouping cells into three categories; cells with polar clusters, faint polar clusters or diffuse signals (Figure 53).

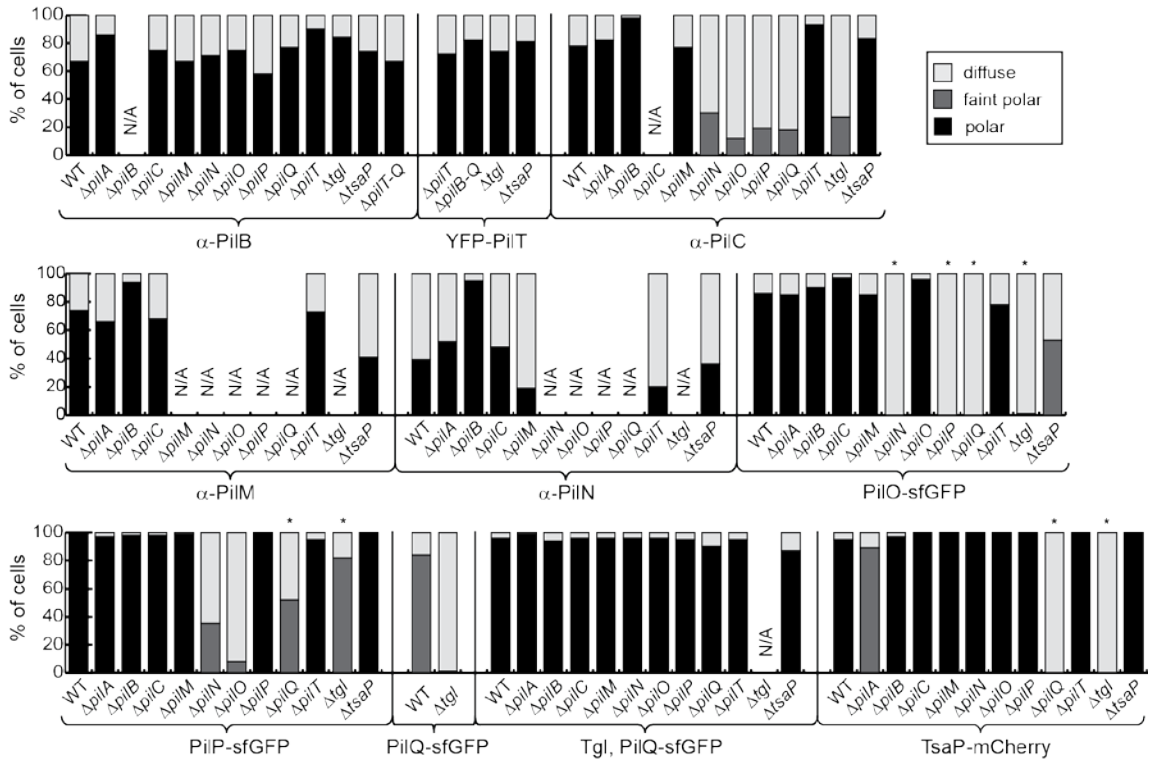

Figure 53 – Distribution of localization patterns of different T4P proteins in the indicated in-frame deletion mutants. Immunofluorescence microscopy was used to analyze the localization of PilB, PilC, PilM and PilN. PilO, PilP, PilQ and TsaP were localized using the indicated sfGFP/mCherry-tagged fusion proteins. Patterns of fluorescence signals were grouped into three categories. The histograms illustrate the distribution of localization patterns of the indicated proteins in the indicated in-frame deletion mutants (n=57-317). * indicates in-frame deletion mutants in which the relevant native protein does not accumulate (Figure 27 - Figure 26). Strains marked N/A= not applicable were not analyzed because the relevant protein does not accumulate.

Using the combination of data from the stability and localization approach, we can draw certain conclusions about the T4P assembly (Figure 54). PilC, which accumulates independently of all tested components, depends on the OM subcomplex of PilQ and Tgl as well as the IM proteins PilN/O/P to localize to the poles. PilB and PilT are the only proteins that accumulate and localize independently of all other components. Interestingly, these two proteins are the only ones localizing dynamically to the poles. The outside-in T4P assembly model that we inferred from the stability experiments was only partially observed by protein localization. PilQ and Tgl are again on top of the hierarchy, as they affect the localization of PilC/O/P and TsaP, but are unaffected in the absence of these four proteins. The observation that PilN and PilO are required for correct localization of PilP suggests that these three proteins require each other for correct incorporation into the trans-envelope T4P machinery. This mutual dependency among PilN/O/P supports the hypothesis of an IM complex in *M. xanthus* like previously shown for *N. meningitidis* and *P. aeruginosa*.

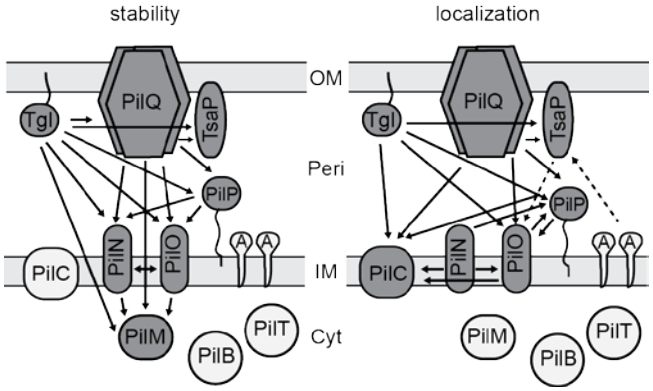

Figure 54 - T4P protein maps summarizing the data obtained from the stability and localization approaches. Proteins in grey affect or are affected by other T4P proteins, while proteins in white accumulate or localize independently of all tested proteins and do not affect the accumulation or localization of any other protein. Stippled lines indicate minor effects. OM=outer membrane, Peri=periplasm, IM=inner membrane, Cyt=cytoplasm.

2.8 PilN recruits PilM to the poles

The cytoplasmic protein PilM is critical for T4P function and was shown to depend on PilN/O/P/Q and Tgl for stability (Figure 21) and could not be localized in all these deletion mutants. How does PilM connect to other members of the T4P? To adress this question, we tried to place PilM in our T4P-model by a different approach taking advantage of the recently solved X-ray structure of PilM from *T. thermophilus* (Karuppiah & Derrick, 2011).

PilM was crystallized in complex with the cytoplasmic, N-terminal 15 residues of PilN. These residues are highly conserved among PilN proteins from different organisms, suggesting that the binding between PilM and PilN occurs similarly in these organisms (Figure 55B). To test *in vivo* whether the cytoplasmic N-terminus of PilN is required to recruit PilM to the T4P machinery in *M. xanthus*, three single substitutions were made in the predicted binding site for PilN in PilM (D203A, V204D and R388A; [Figure 55A, C]). Each substitution was introduced into the YFP-PilM construct, which is functional and localizes bipolarly (Bulyha et al., 2009). Although all mutant proteins accumulated at levels comparable to the WT fusion (Figure 55D), none of the three mutant proteins was able to restore motility in a non-motile Δ*pilM* mutant (Figure 55E). Furthermore, all three proteins failed to localize to the poles (Figure 55E), suggesting that the mutated residues interfere with polar recruitment of PilM presumably by PilN.

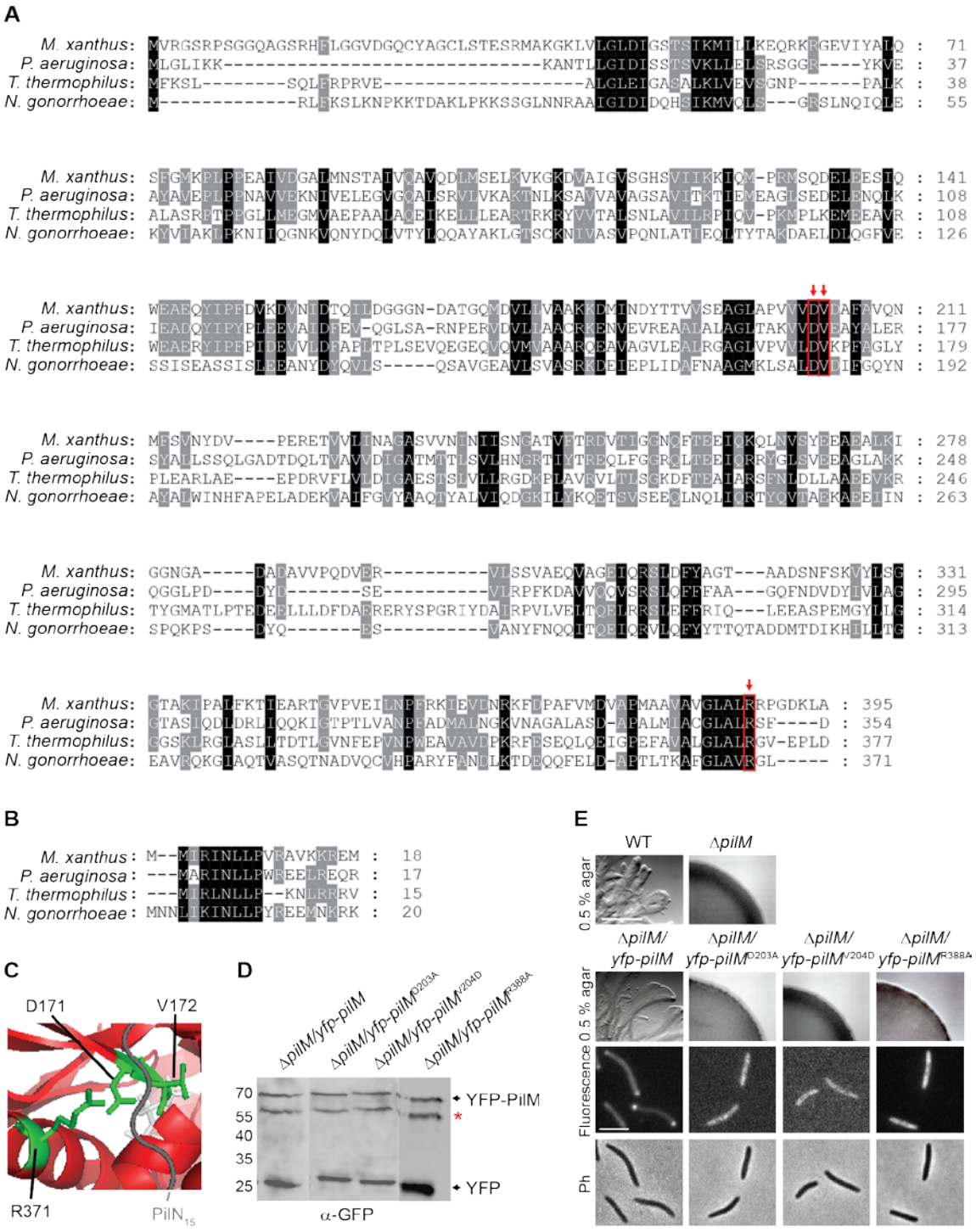

Figure 55 – PilN recruits PilM to the poles. A) Alignment of PilM proteins from *M. xanthus, P. aeruginosa, T. thermophilus* and *N. gonorrhoea*. Residues are shaded according to conservation. White on black residues are 100% conserved and white on grey residues are 75% conserved. Residues marked with red boxes and arrows interact with the N-terminal PilN peptide in the PilM structure and were mutated in the PilM variants analyzed. B) Alignment of N-termini of PilN proteins from *M. xanthus, P. aeruginosa, T. thermophilus* and *N. gonorrhoea.* The indicated 15 residues of *T. thermophilus* PilN were included in the PilM structure which is partially shown in (C). Conservation is indicated as in (A). C) Close-up view of 3D model "2ych" (Karuppiah & Derrick, 2011) showing the binding site on PilM (red) for the PilN peptide (grey) from *T. thermophilus*. The three residues that were substituted in *M. xanthus* during this study are highlighted in green. D) Immunoblot detecting YFP-PilM in the indicated strains

using GFP-specific antibodies. Blot was done as described in Figure 15B. * indicates degradation products of the fluorescently tagged proteins. E) Motility assays and localization of the indicated PilM proteins. Upper rows, motility assay for the indicated strains; scale bar 1 mm. Cells were treated as in Figure 15A. The two lower rows show fluorescence and phase contrast (Ph) microscopy images of the indicated strains. Scale bar 2 µm. Cells were treated as in Figure 29A.

2.9 PilN, PilO, PilP and PilQ form oligomers

While the previous experiments gave us useful insights about T4P protein interdependencies *in vivo*, they do not show direct interactions. To investigate in more details, which proteins may interact, we tested for direct protein interactions *in vitro,* using purified proteins and focusing on the proteins PilN/O/P/Q and TsaP. As most of the T4P proteins are embedded or attached to the IM or OM, only the soluble, periplasmic parts of the proteins were purified. In the case of PilN and PilO, the cytoplasmic N-terminus and the transmembrane helix were removed and the resulting proteins $PilN_{\Delta 42}$ and $PilO_{\Delta 37}$ were fused to a C-terminal His6-tag. For the lipoprotein PilP, we removed the type II signal peptide and added a His-tag. For PilQ, we decided to purify the periplasmic part including the B1, B2, N0 and N1 domains (compare Figure 4) and the resulting $PilQ_{20\text{-}656}$-His6 was used for the interaction studies. The first 19 amino acids were removed to prevent secretion of the protein upon overexpression in *E. coli*. All constructs were cloned under the T7 promoter and the resulting overexpression constructs were introduced into *E. coli* Rosetta 2 (DE3). This overexpression strain carries the T7 polymerase under the IPTG-inducable *lac*-promoter. The four proteins were overexpressed and purified under native conditions. Except for PilO, sufficient amounts of protein could be purified (~5-10 mg/500 ml culture; Figure 56A). To exclude aggregation and to analyze the oligomeric states of the proteins, we applied all purified proteins to a gel filtration column. The elution profiles for PilN, PilO and PilP showed two peaks corresponding by size to dimers and tetramers, respectively. For PilQ, only one peak could be detected, corresponding to PilQ dimers (Figure 56B-F). Dimerization of PilO has been reported before (Sampaleanu et al., 2009). To our knowledge, oligomers of PilQ, PilN or PilP have not been previously reported. As PilO purification yielded a large fraction of aggregated protein, we tried another approach for purification. We purified PilO under denaturing conditions, which resulted in larger amounts of purified protein (Figure 57A). We then dialyzed stepwise against buffer without detergents to allow refolding of the protein and applied the protein again on the gelfiltration column. The profile showed one main peak corresponding to the size of a tetramer. The fraction with the aggregated protein was lost, suggesting that the protein is a stable tetramer under the tested conditions (Figure

57B). Therefore, the second purification procedure under denaturing conditions and subsequent dialysis was chosen for further *in vitro* experiments.

Repeated attempts to purify PilM failed, either yielding insufficient protein, or, when larger tags e.g. GST- or MalE-tags were used, the purified protein aggregated (Figure 61D).

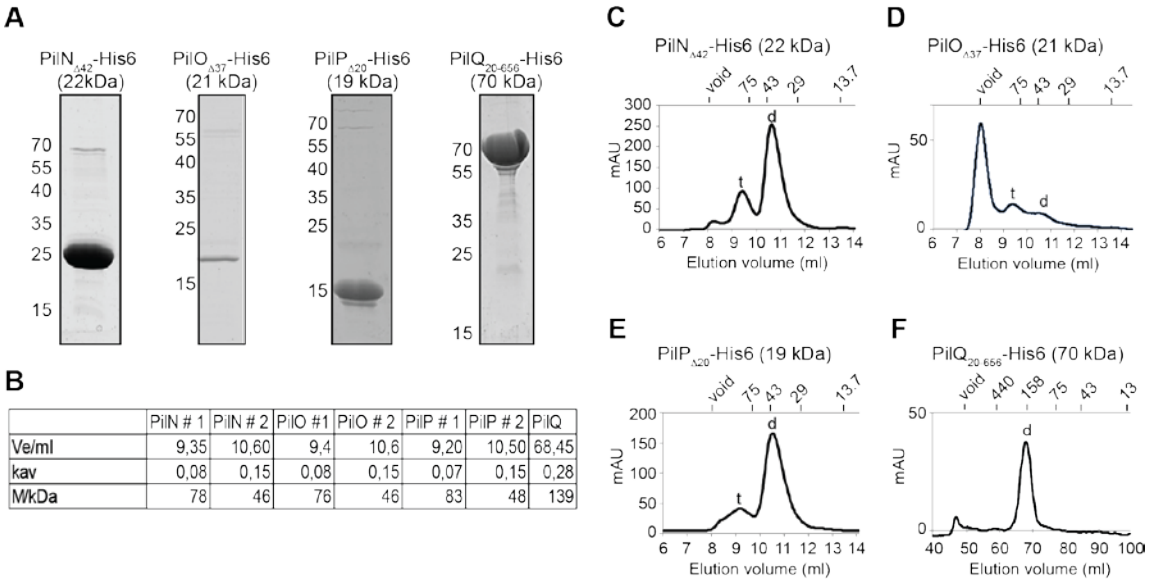

	PilN # 1	PilN # 2	PilO #1	PilO # 2	PilP # 1	PilP # 2	PilQ
Ve/ml	9,35	10,60	9,4	10,6	9,20	10,50	68,45
kav	0,08	0,15	0,08	0,15	0,07	0,15	0,28
M/kDa	78	46	76	46	83	48	139

Figure 56 - *In vitro* analysis of the periplasmic parts of PilN, PilO, PilP and PilQ. A) SDS–PAGE analysis of the indicated purified proteins after staining with Coomassie G-250. Positions of molecular markers are indicated on the left. Calculated molecular masses are shown in parentheses. B) Table showing the elution volumes (Ve), the partition coefficient (Kav) and the determined relative molecular weight (M) of the peaks detected by size-exclusion of the indicated proteins. Calculations are based on the calibration formular shown in Figure 67 and Figure 68. C-F) Periplasmic domains of PilN, PilO and PilP form dimers and tetramers in solution, while PilQ forms dimers. The diagrams show the elution profiles of the indicated His_6-tagged proteins from size-exclusion chromatography experiments (Superdex 75 10/300 GL for PilN$_{\Delta 42}$-His6, PilO$_{\Delta 37}$-His6, PilP$_{\Delta 20}$-His6 and HiLoad 16/60 Superdex 200 prep grade for PilQ20-656-His6). Molecular size markers are indicated at the top in kDa. Peaks marked "t" and "d" correspond to the size of a tetramer and dimer, respectively.

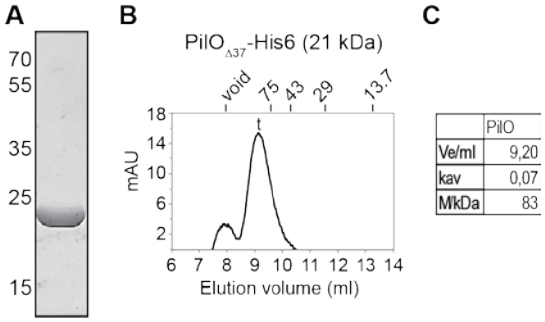

	PilO
Ve/ml	9,20
kav	0,07
M/kDa	83

Figure 57 - *In vitro* analysis of PilO$_{\Delta 37}$-His6. A) SDS–PAGE analysis of purified PilO$_{\Delta 37}$-His6 after staining with Coomassie G-250. Positions of molecular markers are indicated on the left. B) Size-exclusion profile with PilO$_{\Delta 37}$-His6 using the column Superdex 75 GL. Peak marked with "t" corresponds to the size of a tetramer. Molecular size markers are indicated at the top in kDa. Calculated molecular mass of PilO$_{\Delta 37}$-His6 is 21 kDa. C) Table showing the elution volume (Ve), the partition coefficient (Kav) and the determined relative molecular weight (M) of the peak detected by size exclusion of PilO$_{\Delta 37}$-His6.

2.10 PilN and PilO as well as PilP and PilQ interact directly

To investigate for direct protein interactions between the periplasmic parts of PilN, PilO, PilP, PilQ and TsaP, we used co-affinity purification. Binary protein combinations with different affinity tags were tested for interaction via co-purification on the respective affinity columns. Therefore, each protein except for PilQ was additionally overexpressed and purified with a MalE-tag (Figure 58).

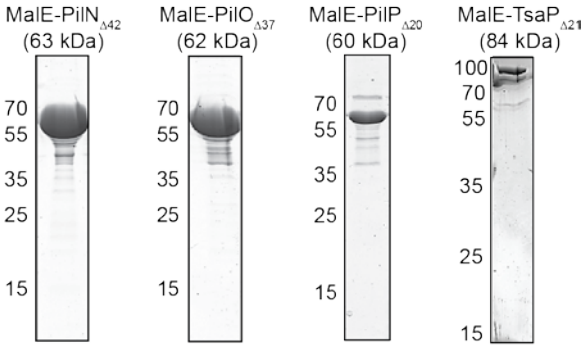

Figure 58 – SDS–PAGE analysis of the indicated purified proteins after staining with Coomassie G-250. Positions of molecular markers are indicated on the left. Calculated molecular masses are shown in parentheses.

His6- and MalE-tagged proteins were first purified separately and dialyzed against the respective buffer for the affinity columns. Similar amounts of purified proteins were mixed and applied to amylose and Ni^{2+}-NTA-columns, respectively. Then, we analyzed whether both proteins could be co-eluted from the columns. To test for unspecific binding to the column material, the His6-tagged proteins were applied separately on an amylose column and the MalE-tagged proteins on a Ni^{2+}-NTA column. An overview of all tested protein combinations is shown in Figure 59A. With this approach co-elution of PilN$_{\Delta 42}$-His6 and MalE-PilO$_{\Delta 37}$ (Figure 59B) as well as MalE-PilP$_{\Delta 20}$ and PilQ$_{20\text{-}656}$-His6 (Figure 59C) was detected, suggesting that the periplasmic parts of PilN and PilO, as well as the periplasmic parts of the lipoprotein PilP and the secretin PilQ interact. Due to the appearance of an unspecific band in the purified fraction of PilQ$_{20\text{-}656}$-His6 that runs at a very similar molecular weight to MalE-PilP$_{\Delta 20}$, we performed an immunoblot with PilP specific antibodies to confirm that the band in the elution fraction of MalE-PilP$_{\Delta 20}$ and PilQ$_{20\text{-}656}$-His6 on Ni^{2+}-NTA corresponds to PilP (Figure 59D). Further combinations, which did not show any co-elution were MalE-PilN$_{\Delta 42}$ and PilP$_{\Delta 20}$-His6, MalE-PilP$_{\Delta 20}$ and PilN$_{\Delta 42}$-His6, MalE-PilO$_{\Delta 37}$ and PilP$_{\Delta 20}$-His6, PilQ$_{20\text{-}656}$-His and MalE-TsaP$_{\Delta 21}$ (Figure 59E-I). It should be noted that negative interactions in this experimental setup might be due to steric hindrance caused by the used tags or that interactions require more than two interaction partners and thus different approaches should be used to verify further direct interactions.

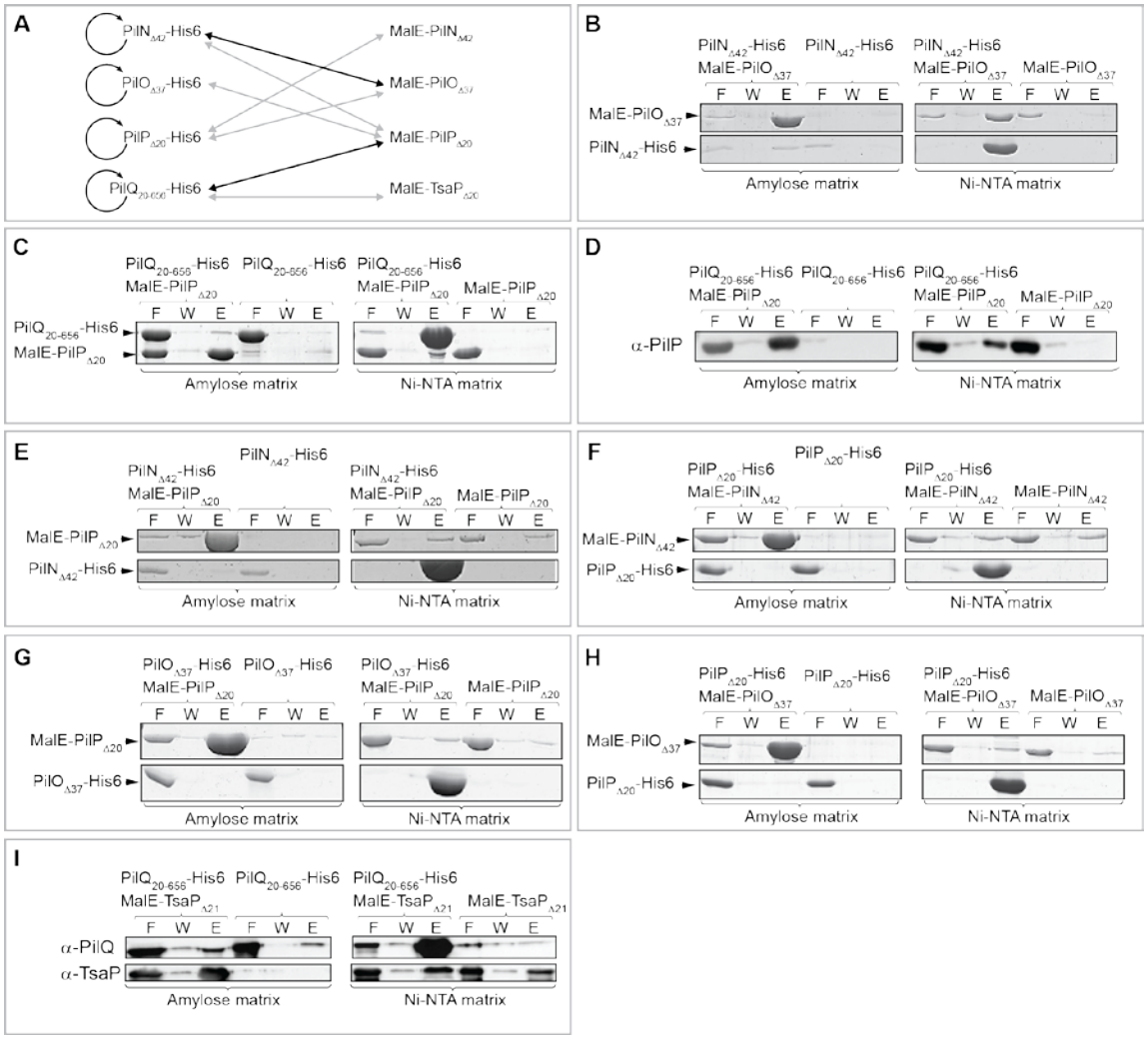

Figure 59 - PilP and PilQ as well as PilN and PilO interact directly. A) Diagram of proteins tested for direct interactions *in vitro*. Black lines indicate combinations of one or two proteins in which interactions were observed. Grey lines indicate the combinations tested for direct interactions with negative results. B) PilN and PilO interact directly. The indicated protein(s) were mixed and applied to amylose and Ni^{2+}-NTA matrices as indicated. Shown are relevant sections of Coomassie G-250-stained polyacrylamide gels of the flowthrough (F), wash (W) and elution (E) fractions with PilN$_{\Delta 42}$-His6 (23 kDa) and MalE-PilO$_{\Delta 37}$ (62 kDa). C) PilP and PilQ interact directly. The experiments were carried out and are presented as in B) except that gel sections with MalE-PilP$_{\Delta 20}$ (60 kDa) and PilQ$_{20-656}$-His6 (70 kDa) are shown. D) Samples from the experiment shown in (C) were stained with PilP-specific antibodies by immunoblotting. E-H) No co-purification of the indicated proteins could be observed. The experiments were carried out and are presented as in (B). I) No co-purification of PilQ$_{20-656}$-His6 and MalE-TsaP$_{\Delta 21}$ (84 kDa) could be observed. Immunoblots were performed to visualize the proteins using specific antibodies as indicated.

2.11 PilM is an actin-like ATPase

For further biochemical analysis of the T4P proteins, we investigated the function of the cytoplasmic protein PilM. PilM from *T. thermophilus* has been shown to possess an actin-like fold and to bind ATP with low affinities (Karuppiah & Derrick, 2011). In general, actin-like ATPases possess a tertiary structure with two connected

domains with a similar fold that build a binding pocket for ATP in their interdomain cleft (Bork *et al.*, 1992). Members of the family of actin-like ATPases like FtsA or MreB often share less than 20% sequence similarity, therefore it is difficult to identify new members of this family. There are five conserved sequence motifs called phosphate 1, connect 1, phosphate 2, adenosine and connect 2, which are important for ATP binding and hydrolysis (Bork et al., 1992). However, ATP hydrolysis could not be detected for all of the identified members of this protein family, implying a regulatory function upon ATP binding (Sanchez *et al.*, 1994). Crystallization experiments revealed a conformational change upon ATP binding, which could control the formation of filaments in the case of MreB from *Thermotoga maritima* (van den Ent *et al.*, 2001) or could generally control protein interactions, as is proposed for actin, hexokinases and Hsc70 (Holmes *et al.*, 1993).

We wanted to test if the potential ATPase or ATP-binding activity of PilM from *M. xanthus* is essential for its function in T4P-dependent motility. During my master studies, I performed site-directed mutagenesis of the predicted sequence motifs phosphate 1 (D46), phosphate 2 (N229) and adenosine (G332). In other actin-like ATPases, these three residues are important for ATP-binding or hydrolysis (Jensen & Gerdes, 1997, Sanchez et al., 1994, van den Ent & Lowe, 2000). The *M. xanthus* mutant proteins either failed to complement the motility phenotype of the Δ*pilM* mutant or only partially restored motility in this mutant. In the case of the phosphate 1 mutation D46A, the substitution led to the degradation of PilM, suggesting that this residue is essential for correct folding and stability of the protein. The other two mutations N229A and G332D did not cause any protein degradation (Friedrich, 2010). Therefore, we checked their localization. YFP-tagged WT PilM protein localizes in a bipolar manner, however, the mutant proteins fused to YFP localized in a diffuse manner throughout the cells. This raised the question, if the ATPase function is required to recruit PilM to the poles or if these mutations disturb possible protein interactions.

ATPase activity of PilM has not been demonstrated *in vitro*, so it was unclear if the mutant proteins were defective in ATPase activity or ATP binding. Therefore, we wanted to investigate the ATPase activity of PilM and the potential active-site mutants. PilM could not be purified in sufficient amounts under native conditions using a C- or N-terminal His-tag. Therefore, we tried larger tags to improve the solubility of the protein, and found that a glutathion-S-transferase (GST)-tag increased the solubility of the protein. After purification on a glutathione column, additional bands in the elution fraction (Figure 60A) were analyzed by mass spectrometry to check for contaminating proteins. No contaminating proteins could be detected, but degradation products of

either PilM or the GST-tag could be identified. Assuming that the elution fraction was pure, we tested ATP hydrolysis using a thin layer chromatography (TLC) method. Various concentrations of WT GST-PilM and the two mutants GST-PilM^{N229A} and GST-PilM^{G332D} were incubated with a mixture of unlabeled and radioactive labeled ATP ([α-^{32}P]ATP) for 10-30 min and then the adenine nucleotides were separated by TLC and visualized by phosphor imaging (Figure 60B). The enzyme apyrase was used as a positive control for this assay, to mark the positions of [α-^{32}P]ADP and [α-^{32}P]ATP. All three PilM proteins showed comparable [α-^{32}P]ADP signals. The positive control apyrase showed hydrolysis of [α-^{32}P]ATP to [α-^{32}P]ADP and presumably to [α-^{32}P]AMP and ^{32}P. Signals were quantified using the Multi Gauge program (Fujifilm). Signals for ADP and AMP were quantified together and divided by the signal for labeled ATP to obtain the relative accumulation of ADP and AMP. Note that due to the fact that the accumulation of ^{32}P was not quantified during the quantification procedure and most of the [α-^{32}P]ATP has already been converted to ^{32}P by the apyrase, the value for this sample does not reflect its appropriate activity and should be higher than shown in the graph. Increasing ATP hydrolysis occurred with increasing protein concentrations, but no difference between WT and mutant proteins was visible (Figure 60C), which suggests that the mutant proteins are able to hydrolyse ATP at comparable rates to the WT. It is also possible that only background hydrolysis was detected, due to an unknown contaminant that could not be measured via mass spectrometry.

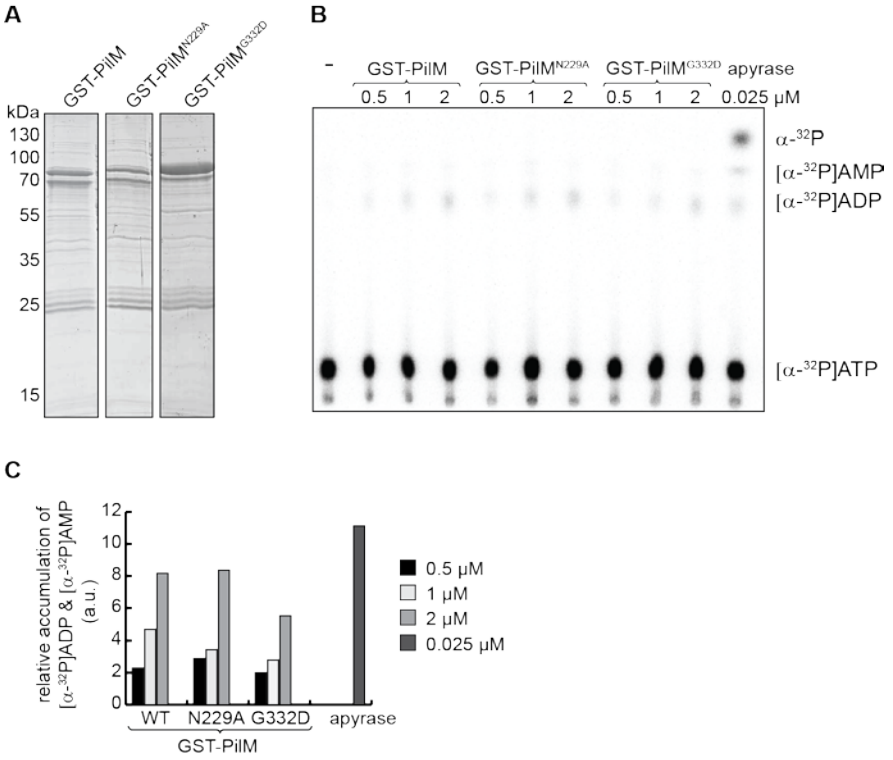

Figure 60 – ATPase assay with GST-PilM and mutant proteins. A) SDS–PAGE analysis of the indicated purified proteins after staining with Coomassie G-250. Positions of molecular markers are indicated on the left. The calculated molecular mass of all three proteins is 68 kDa. B) TLC assay with the indicated proteins and concentrations. The mixture of labeled and unlabelled nucleotides (ATP endconcentration 1 mM) was incubated for 30 min at RT with the different proteins. Nucleotides were separated on TLC plates, as indicated on the right. (-) indicates that no protein was added to the sample. C) Quantification of the TLC assay shown in B). Accumulation of labeled [α-^{32}P]ADP and [α-^{32}P]AMP relative to [α-^{32}P]ATP was quantified using the MultiGauge program. The value obtained for the negative control (-) was subtracted from all other values. Accumulation of ^{32}P was not considered. a.u. = arbitrary units.

To improve yield and purity of the proteins, we tested another tag, i.e. MalE. Overexpression and purification of the WT and mutant MalE-tagged proteins yielded larger amounts of soluble protein and fewer contaminating bands in comparison to the glutathione affinity chromatography (Figure 17A). This time, we used [γ-^{32}P]ATP for the TLC assay to detect the accumulation of ^{32}P. Again, no difference could be detected between WT and the mutant proteins (Figure 61B/C) and only slight increases in hydrolysis could be observed with increasing protein concentrations.

In addition to measuring ATP hydrolysis, we also wanted to quantify the rate at which PilM binds ATP using UV-cross-linking with 8-azido-[α-^{32}P]ATP and a photometrical assay using 2'-/3'-O-(N'- Methylanthraniloyl) adenosine-5'-O-triphosphate (MANT-ATP). 8-azido-α-^{32}P-ATP can be crosslinked to ATP-binding proteins by UV-irradiation and detected via phosphor imaging after separation by SDS-PAGE. MANT-

ATP is a fluorescent analogue of ATP, which can change its spectral properties upon protein binding. Both assays did not provide any evidence for ATP-binding by PilM (data not shown).

As all experiments concerning the enzymatic function of PilM were inconclusive, we analyzed the purified protein via size-exclusion chromatography to determine the oligomeric state of the proteins and to check for protein aggregates. As the name size-exclusion implies, proteins are separated by size in a gel filtration column. Each column has a certain range of protein sizes, which can be separated and proteins that aggregate due to misfolding or hydrophobic interactions are mostly too large for the column to separate and elute in the void volume of the column. The elution profile of WT MalE-PilM revelead that it only elutes in the void volume (Figure 61D), suggesting that the protein forms aggregates. The two mutant proteins were also analyzed via size-exclusion chromatography and showed a similar elution profile to the WT protein (data not shown). As many other actin-like ATPases polymerize upon ATP-binding, we analyzed PilM via negative stain electron microscopy (EM) to test if these aggregates were polymers. However, no polymers could be detected, suggesting that the protein is not stable under the used conditions. These results possibly explain the inconclusive results from the ATPase and ATP-binding assays because the analyzed proteins were unable to exhibit enzymatic activity due to misfolding. To analyze the enzymatic properties of PilM, further modifications to the proteins or protocols would be required to improve stability of PilM during the overexpression and purification procedures.

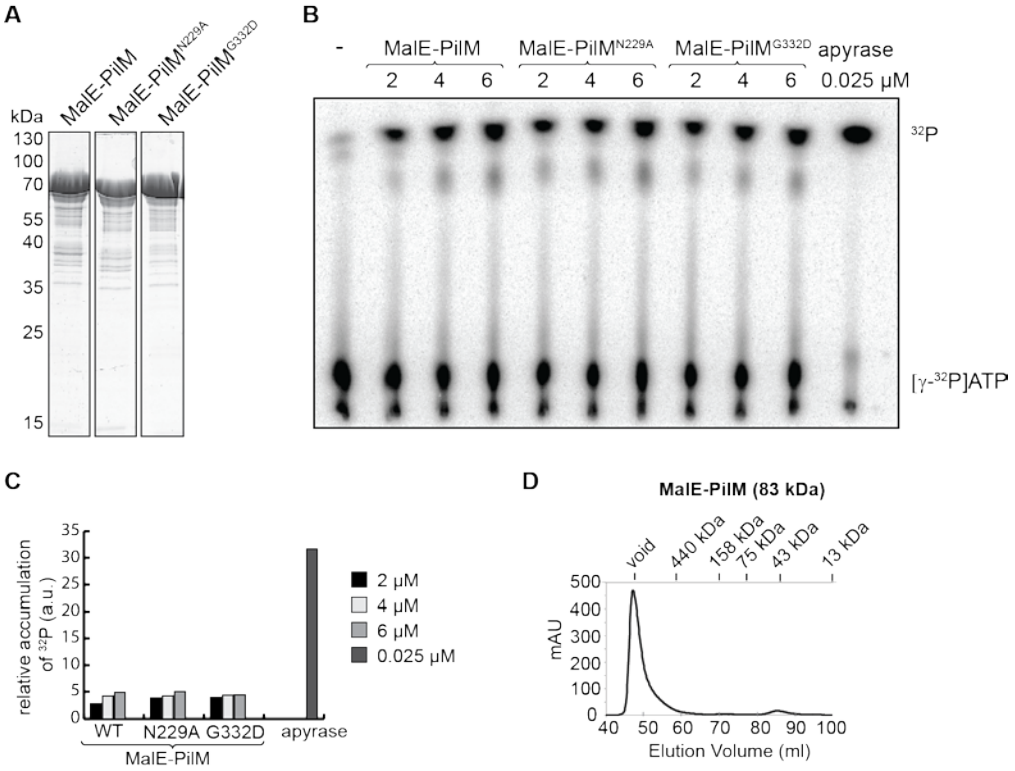

Figure 61 – ATPase assay with MalE-PilM and mutant proteins. A) SDS–PAGE analysis of the indicated purified proteins after staining with Coomassie G-250. Positions of molecular markers are indicated on the left. The calculated molecular mass of all three proteins is 83 kDa. B) TLC assay with the indicated proteins and concentrations. The mixture of labeled and unlabeled nucleotides (ATP endconcentration 1mM) was incubated for 30 min at 24°C with the different proteins. Nucleotides were separated on TLC plates, as indicated on the right. (–) indicates that no protein was added to the sample. C) Quantification of the TLC assay shown in B). Accumulation of ^{32}P relative to [γ-^{32}P]ATP was quantified using the MultiGauge program. The value obtained for the negative control (-) was subtracted from all other values. a.u. = arbitrary units. D) Purified MalE-PilM aggregates. The diagram shows the elution profile from the size-exclusion chromatography experiment using the Superdex 200 prep grade column. Molecular size markers are indicated at the top in kDa.

2.12 PilM-PilN$_{1-16}$ forms dimers and tetramers

Taking into account what we learned from previous experiments, namely that PilM might need the interaction with PilN to accumulate and localize, we speculated that PilM might be misfolded when missing its interaction partner PilN. Following up on this idea, we constructed a fusion protein with the 16 N-terminal amino acids of PilN fused to the C-terminus of PilM, assuming that the PilN-peptide will fold correctly in the binding pocket of PilM and subsequently stabilize PilM. Indeed, this strategy yielded larger amounts of soluble protein (Figure 62A), which was then applied to a gelfiltration column. His6-PilM-PilN$_{16}$ eluted as two clearly separated peaks (Figure 62B), corresponding to the sizes expected from dimers and monomers. The stabilizing effect of PilN on PilM emphasizes the direct interaction between PilM and PilN. Consistently, all proteins analyzed so far seem to be present as multimers, supporting the idea that

the T4P system is a large multimeric protein complex with dimers or tetramers forming the basic building blocks.

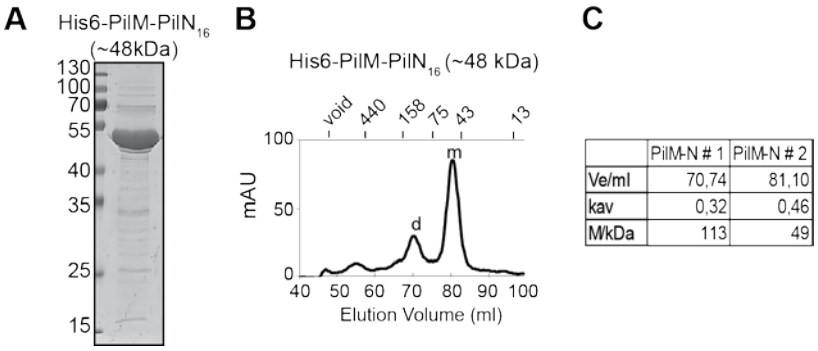

	PilM-N # 1	PilM-N # 2
Ve/ml	70,74	81,10
kav	0,32	0,46
M/kDa	113	49

Figure 62 - *In vitro* analysis of the fusion protein His6-PilM-PilN$_{16}$ A) SDS–PAGE analysis of the purified protein after staining with Coomassie G-250. Positions of molecular markers are indicated on the left. Calculated molecular mass is shown in parentheses. B) His6-PilM-PilN$_{16}$ forms dimers and monomers in solution. The diagram shows the elution profile from the size-exclusion chromatography experiment using the HiLoad 16/60 Superdex 200 prep grade. Molecular size markers are indicated at the top in kDa. Peaks marked "d" and "m" correspond to the size of a dimer and monomer, respectively. C) Table showing the elution volumes (Ve), the partition coefficients (Kav) and the determined relative molecular weights (M) of the peaks detected by size exclusion of His6-PilM-PilN$_{16}$.

2.13 Timing of polar PilQ localization

Since our data suggest that assembly of the T4P complex begins with the secretin PilQ in the OM, we wanted to investigate the mechanism by which PilQ becomes polarly localized.

Bioinformatic analysis of PilQ revealed that it has two amidase N-terminal (AMIN) domains, which are predicted to be involved in targeting periplasmic protein complexes to a specific region of the cell envelope. AMIN domains were discovered in the amidase AmiC and shown to be important for its recruitment to the septum during cell division by proteins involved in cell division (Bernhardt & de Boer, 2003). Later, these domains were shown to be more widely distributed in several protein families in addition to amidases, suggesting a more general targeting mechanism (de Souza *et al.*, 2008). The fact that PilQ has two AMIN domains, raises the question whether PilQ is recruited to the cell poles by an unknown protein during cell division, when new cell poles arise.

To address this question, we performed time-lapse microscopy on cells expressing PilQ-sfGFP and extra TgI and with images captured every 20 min. The high mobility of the *M. xanthus* cells during time-lapse microscopy made it difficult to follow the cells over a longer time period, as they frequently moved out of the visible area. Therefore, we introduced the fluorescent construct into the Δ*aglZ* strain, which cannot

move in terms of A-motility. PilQ-sfGFP was detected at midcell late during cell division in cells with a deep constriction or immediately after cell division. Two representative cells are shown in Figure 63. During cell division, cells stopped moving. 20-40 min after cell division and the appearance of the novel PilQ-sfGFP clusters, cells were again motile by T4P suggesting that oligomeric PilQ has assembled in the OM, allowing the subsequent assembly of T4P complexes. We conclude that oligomeric PilQ-sfGFP becomes polarly localized late during or immediately after cell division.

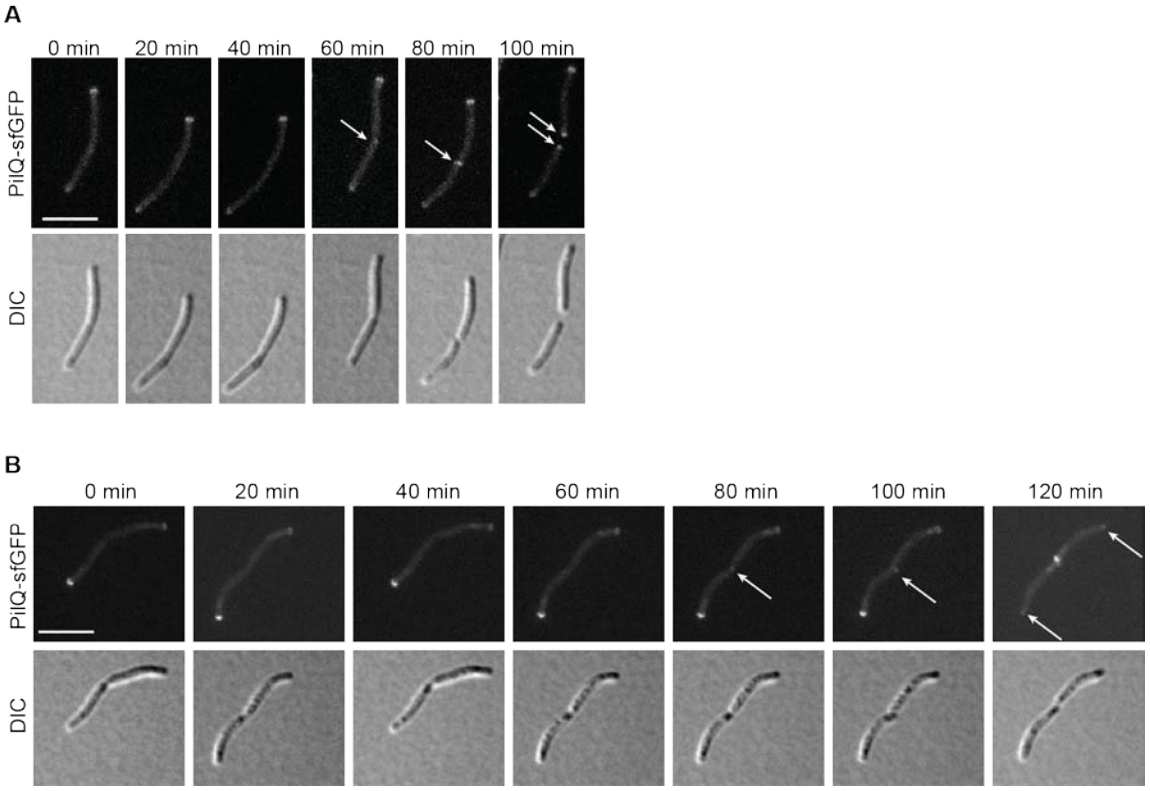

Figure 63 –PilQ localizes polarly late during or immediately after cell division. A-B) Cells from an exponentially growing culture were applied directly on a coverslip with a 0.1% CTT agarose pad and imaged by fluorescence and DIC microscopy at 20 min intervals. Arrows indicate newly formed polar clusters. Strain used, SA6060 (*ΔaglZ/tg*l, *pilQ-sfGFP*). The *ΔaglZ* mutation blocks gliding motility. Scale bars 5 µm.

3 Discussion

Due to their broad distribution among bacteria and their high functional diversity, T4P have became the subject of intensive research. *M. xanthus* uses T4P for surface associated movement. They are built at the leading cell pole and undergo cycles of extension, attachment to a surface and retraction, which pulls the cell forward. Although the T4P machinery localizes to both cell poles in *M. xanthus*, it is only activated at one pole to generate movement along the long axis of a cell. Upon a cellular reversal, T4P switch poles, meaning that they are disassembled at the old leading pole and assembled at the new leading cell pole. The dynamic cycles of T4P extension and retraction require the assembly of a molecular machine that includes at least 12 proteins, which span from the cytoplasm, over the IM, the periplasm to the OM. Although most of the proteins have been known for a long time, it has been elusive how and in which order the single proteins are connected to build up this multi-protein machinery to drive polymerization and depolymerization of T4P.

In this study, we elucidated the assembly process and functional interactions between T4P proteins. We propose that the T4P machinery is assembled in an outside-in manner and that multimeric PilQ in the OM functions as an assembly platform for additional components, which are added sequentially. Moreover, the two ATPases PilB and PilT, which provide the energy for T4P extension and retraction, respectively localize independently of all other T4P proteins.

3.1 PilM, PilN, PilO, PilP, PilQ, Tgl and TsaP are required for T4P dependent motility

To investigate the assembly of the T4P machinery, we needed a set of in-frame deletions of each protein involved in T4P assembly or function. Although in-frame deletions of *pilM, pilN, pilO, pilP* and *pilQ* were generated and shown to be deficient in S-motility (Bulyha, 2010, Wall et al., 1999), they had not been complemented to exclude polar effects. In this study, we show that each gene is required for S-motility and polar effects were not observed, as each mutant could be complemented by ectopic expression of the respective gene. In *P. aeruginosa*, motility of the *pilO* mutant could only be restored when all four genes *pilM, pilN, pilO* and *pilP* were provided in trans, suggesting that the relative stoichiometry of the proteins is crucial for complex formation (Ayers et al., 2009). As this was not the case in *M. xanthus*, the components are either not as senstitive to changes in protein levels or expression from the *pilA* promoter matched the native expression levels.

Then, we could show that in-frame deletions of the two genes that are not encoded in the *pil*-gene cluster, *tgl* and *tsaP*, lead to impairments of T4P-dependent

motility. While the *Δtgl* mutant was completely immobile on soft agar, as previously reported for the insertion mutant (Nudleman et al., 2006), the *ΔtsaP* mutant exhibited reduced motility (Binzen, 2012). EM analysis of the *ΔtsaP* mutant showed that the number of cells with T4P decreased significantly and furthermore, that the number of T4P per cell was down to one to two. Regarding the current model of TsaP being a secretin anchoring component in *N. gonorrhoeae* (Siewering et al., manuscript in preparation), we conclude that anchoring to the peptidoglycan layer or alignment of IM and OM subcomplexes might also be affected upon deletion of *tsaP* in *M. xanthus*. The presence of one to two pili in about 35 % of the cells in a Δ*tsaP* strain in *M. xanthus* might originate from the randomly aligned complexes, which would infrequently allow the polymerization and exit of T4P. Alternatively, T4P assembly and surface access might be fine, but T4P are pulled off upon retraction due to the missing anchoring to the peptidoglycan.

We were unable to generate an in-frame deletion of the prepilin peptidase *pilD*. Since other T4P proteins and motility in general are not essential for survival of *M. xanthus*, we speculate that PilD is involved in processing other proteins with a type III signal sequence that are either required for survival or the accumulation of these unprocessed proteins is toxic to the cells. Often the prepilin peptidase is shared between the T4P system and the T2SS (Strom et al., 1991). In *M. xanthus*, there is one paralog of *pilD* encoded in the T2SS gene cluster (Mxan_3105), however, this gene product is missing the two conserved cysteine pairs, which are required for the function of a prepilin peptidase (Seifer, 2011). Hence, we speculate that deletion of *pilD* also affects the function of the T2SS. To test whether the knock out of *pilD* is possible using the designed construct, one could introduce a second copy of *pilD* at the Mx8 attachment site and try again to delete the native *pilD*. If the generation of the in-frame deletion is possible under these conditions, the deletion procedure per se is fine and the inability to get an in-frame deletion mutant is presumably due to necessity for PilD in *M. xanthus*.

3.2 PilN, PilO, PilP, PilQ and TsaP localize bipolarly, whereas Tgl localizes throughout the cell

To investigate the assembly pathway of the T4P machinery, we aimed to systematically profile the stability and localization of all T4P proteins. To do so, we first had to develope or adapt localization tools for the different proteins. While most of the published localization patterns could be confirmed, Tgl did not display a unipolar localization as published by Nudleman et al. (2006). Analyzing the localization of Tgl by immunostaining and an sfGFP-fusion protein revealed fluorescent signals all over the

cell. Admittedly, in both approaches Tgl is not expressed at native levels. Overexpression from the *pilA* promoter might affect the localization of Tgl. It has been shown for components of the T4SS and T2SS that overexpression can lead to polar localization, although the proteins are usually distributed along the cell when expressed at native levels (Aguilar *et al.*, 2011, Lybarger *et al.*, 2009). However, we doubt that overexpression of Tgl could shift the localization pattern from a unipolar to a diffuse pattern without showing a stronger signal in the polar regions. Furthermore, a unipolar localization would imply that Tgl switches poles during a cellular reversal. We cannot think of a mechanism that allows a lipoprotein anchored in the OM to switch from one pole to another in the time period of a cellular reversal, which can be less than 30 seconds. An alternative mechanism could be that Tgl is only made during cell division, when the new cell pole requires the formation of PilQ multimers. This would imply that Tgl is degraded at the old pole resulting in a unipolar localization pattern. Blocking protein biosynthesis using chloramphenicol, we observed that Tgl is at least stable for 6 h. As one cell cycle is approximately 5 h, we conclude that this hypothesis cannot explain a unipolar localization pattern of Tgl. Another observation that supports the uniform localization of Tgl is the appearance of fluorescent signals exterior to the cells expressing Tgl-sfGFP. As Tgl is found in OM vesicles (OMVs), we propose that these signals originate from OMVs visualized by Tgl-sfGFP. These kinds of signals have been described in two recent publications upon membrane staining with a lipid bilayer dye or using sfGFP with a signal sequence for the OM (Ducret et al., 2013, Remis et al., 2013). Importantly, no such signals could be observed when periplasmic or IM fusion-proteins were used. This suggests that our observed fluorescent signals are showing full-length Tgl-sfGFP anchored in the OM.

The localization of Tgl throughout the envelope and the fact that Tgl is not encoded in the *pil*-gene cluster raises the question if Tgl acts exclusively on the T4P secretin or is a general pilotin for all secretins in *M. xanthus*. Two further secretin proteins are encoded in *M. xanthus,* presumably belonging to the T2SS. To our knowledge, it has never been tested if Tgl is involved in multimer formation of the T2SS secretin.

Investigating the localization of PilN, PilO, PilP and TsaP revealed that all four proteins localize to both cell poles as previously shown for PilC, PilM and PilQ (Bulyha et al., 2009, Nudleman et al., 2006), suggesting that PilN, PilO, PilP and TsaP belong to the stationary components, which do not switch poles during a cellular reversal. To localize PilQ we tried different methods and constructs, as we were unable to reproduce the data from Nudleman and colleagues using immunofluorescence.

Although the fusion construct PilQ-sfGFP could not restore motility in a *pilQ*-deletion strain, the fact that Tgl overexpression had a positive effect on the localization pattern of PilQ-sfGFP implies that the observed signal is not an artifact. As PilQ forms a multimeric channel, we speculate that multimer formation is disturbed due to steric clashes caused by the sfGFP-tag. Moreover, we detected stronger signals in a *pilQ*$^{+}$ strain compared to a *pilQ*$^{-}$ strain. This observation suggests that a mixture of PilQ and PilQ-sfGFP forming a potential multimeric channel in the OM can overcome the steric problems by incorporating the sfGFP-tagged protein only once in a while. Why the fusion localizes unipolarly in some cells, remains an open questions. We first thought that the signal might be enhanced at the cell pole where the T4P machinery is active. However, we could not detect a correlation between leading/lagging cell pole and the position of the cluster. Another explanation could be that accumulation of PilQ at the new cell pole after cell division is delayed due to the bulky sfGFP-tag. But then we would expect a correlation between “young”, short cells and a unipolar localization pattern. This was not the case (data not shown). At the moment, we cannot find a plausible explanation why the PilQ-sfGFP clusters are unevenly distributed among the two cell poles. However, the fact that Tgl can compensate for the unipolar distribution, suggests that multimer formation is the critical step.

3.3 Assembly of the T4P machinery starts from multimeric PilQ in the OM and proceeds inwards

To initially address the question of protein interactions, we used the indirect approach of mapping effects on stability caused by the absence of a certain protein. This approach is applicable for proteins of membrane complexes as the incorporation of single components into a protein complex can be dependent on an interaction partner. Upon interruption of this interaction, the protein is presumably degraded due to structural problems.

Based on the accumulation data, we found two types of proteins. The two ATPases PilB and PilT, as well as the IM protein PilC and the pilin subunit PilA accumulate independently of all other proteins and do not affect the accumulation of other proteins. For the remaining proteins PilM/N/O/P/Q, Tgl and TsaP, our results demonstrate that these seven proteins affect each other in terms of stability, suggesting that they interact to form a trans-envelope complex. Furthermore, we hypothesized an accumulation hierarchy from outside-in, as all detected effects were starting from the OM components (PilQ, Tgl), which affect periplasmic proteins (PilP), which then affect IM components (PilN/O), which in turn affect cytoplasmic components (PilM) but not vice versa. The fact that OM components affect the stability of

cytoplasmic proteins indicates that this experimental setup cannot distinguish between direct and indirect effects.

Specifically, PilN and PilO require each other for stability, supporting the data from *P. aeruginosa* where heterodimers of PilN/O were observed (Sampaleanu et al., 2009). PilM requires PilN/O/P/Q and Tgl for stability, suggesting that PilM cannot connect to the machinery until all other proteins are stably accumulating in the cell envelope. PilP stability depends on PilQ and Tgl, while PilP itself is required to accumulate PilM/N/O, indicating that PilP is mediating the connection between IM and OM complexes as it was proposed previously (Tammam et al., 2011).

We could show that Tgl and PilQ do not require any other component to be stable, which suggests that these two proteins fold independently. It is not clear if the effect of Tgl on the stability of PilM/N/O/P and TsaP is direct or indirect. Either Tgl is directly interacting with PilN/O/P or indirectly affecting these proteins via PilQ, as Tgl is required to assemble the PilQ-multimer. Hence, it might be that only PilQ in the multimeric state is able to connect to the protein complex in the IM and to TsaP, which is suggested to form a second ring structure around PilQ (Siewering et al., manuscript in preparation). TsaP does not follow the proposed accumulation hierarchy, as it was shown to depend on PilQ and Tgl, but does not seem to be connected to any of the other T4P proteins. Because TsaP has a peptidoglycan binding domain and is supposed to anchor the PilQ channel to the peptidoglycan layer, it might have a more structural and stabilizing role, independent of the IM components. Based on our results from the accumulation experiments, we hypothesized that PilM/N/O/P/Q, Tgl and TsaP interact and build a protein-complex spanning all subcellular compartments.

The localization experiments further elucidated the interconnections and interdependencies between all T4P proteins. One of the main findings of the localization experiments is that PilQ, which is the first protein of the accumulation hierarchy, localized independently of all other proteins except for Tgl. This supports the assumption that PilQ is the first component of the T4P machinery to localize to the poles, building an assembly platform in the OM for further components. Importantly, PilQ polar localization is abolished in the absence of Tgl. Since Tgl is required for PilQ multimer formation, we propose that only oligomeric PilQ is polarly localized. As Tgl is localized throughout the OM, we suggest that Tgl is not a polar targeting factor for PilQ.

Next, we found that polar PilP localization is dependent on PilN/O/Q and Tgl. Localization data for the *pilQ* and *tgl* mutant have to be taken with care, as PilP usually does not accumulate in these mutants. The fusion of PilP to sfGFP might rescue the

protein from degradation, but it does presumably not cure PilP from misfolding. Furthermore, the localization analysis of PilP-sfGFP in these mutants does not reflect the natural situation. Therefore, the diffuse localization of PilP-sfGFP in these two mutants can only confirm the results from the stability approach.

While PilP can accumulate without PilN/O, it is not capable of localizing to the poles. We suggest that PilN/O are required to mediate the incorporation of PilP into the protein-complex and if this is abolished due to the absence of PilN/O, PilP cannot be concentrated at the poles. These results entirely reflect the interdependencies, observed in the T2SS, as the localization of GspC, corresponding to PilP is also dependend on GspD (PilQ). Further, GspC (PilP) is partially mislocalized in the absence of GspL/M (PilMN/O), suggesting that these two proteins are important for the conformation of GspC, which is required for its maintenance at the correct position (Lybarger et al., 2009). Therefore, the T2SS is also proposed to be assembled from outside-in starting with the secretin and proceeding inwards.

Our localization studies on PilM revealed that it localizes independently of PilB/T/C/A and TsaP. Due to the instability of PilM in the absence of PilN/O/P/Q and Tgl, PilM localization could not be investigated in these strains. Therefore, a mutagenesis approach was used to analyze the connection of PilM to the IM complex via PilN. The mutagenesis experiments, as well as the stabilizing effect of the cytoplasmic N-terminus of PilN on PilM observed with the PilM-$PilN_{16}$ fusion, support the hypothesis that PilN is the direct interaction partner of PilM, as previously shown for *T. thermophilus* (Karuppiah & Derrick, 2011). Moreover, it revealed that this interaction is required for polar PilM localization and hence, for functionality of the whole T4P machinery.

The next important finding from the localization studies is that PilC, which accumulates independently of all other T4P-components seems to be a part of the PilN/O/P/Q/Tgl complex as its localization depends on the presence of these proteins. Interaction with the multi-protein complex is required for proper PilC localization. This localization experiment provides more information about the assembly of the whole T4P machinery, as we can conclude that first a stable protein complex needs to be established, starting with PilQ and Tgl in the OM, to which PilN/O/P can then connect to. Only if these proteins are assembled, PilC can be incorporated into the protein complex and stay at the poles. Based on the BACTH screen in *N. meningitidis* (Georgiadou et al., 2012), where they showed direct interaction between PilO and PilC (called PilG in *Neisseria*), we hypothesize that PilO is the direct interaction partner of PilC and all other observed effects might be indirect by affecting the stability of PilO.

Localizing TsaP in the *pil*-deletion mutants showed that it localizes to the poles in a PilQ- and Tgl-dependent manner. Again, TsaP is usually not stable in these mutants. Therefore, these results confirm the requirements of TsaP for PilQ and Tgl and hence, the PilQ multimer. Furthermore, the deletion of PilA decreased polar localization of TsaP. As the pilin subunits in the IM are distributed over the cell envelope, we speculate that it might be the polymerized pilus, which triggers polar TsaP localization probably indirectly through PilQ, which opens for the pilus to exit and this conformational change in PilQ might give rise to the interaction site for TsaP. However, if this is true, we would expect the same effect on TsaP localization in a strain, which cannot polymerize the pilins, like the Δ*pilB* mutant and this is not the case. To solve the interconnection between PilA and TsaP, further studies are required. Another effect, we cannot explain so far, is the dispersed localization of PilO-sfGFP in the absence of TsaP while all other components of the IM complex localize normally. Since all members of this protein complex are required for stability and correct polar localization, it is currently unclear, why only one member of the complex is mislocalized in the absence of TsaP.

Another mystery of the T4P machinery is how T4P and OM components of the machinery pass the peptidoglycan layer. TsaP has a peptidoglycan binding domain but does not provide a domain for peptidoglycan hydrolysis. We assume that at least one more protein is involved in the assembly process of T4P, which locally hydrolyzes the cell wall to allow the passage of PilQ and T4P. Alternatively, the envelope-spanning complex might be incorporated into the peptidoglycan layer during cell division.

To map further interactions, which could not be identified by the screens used here and to confirm the proposed interactions, based on our stability and localization data, we started to investigate direct protein-protein interactions. We could show direct interaction between PilP and PilQ using co-affinity purification. So far, direct interactions between PilP and PilN or PilO could not be observed for *M. xanthus*, but in *P. aeruginosa,* it has been shown that this interaction requires the heterodimer of PilN/O (Tammam et al., 2011). Hence, the interaction study should be repeated including all three proteins. The direct interaction between PilN and PilO could also be shown in *M. xanthus*, as both proteins were able to pull down each other. The positive interactions shown here, may explain the mutual dependencies observed by the stability approach. However, the negative results cannot be taken as an indication that the tested proteins do not interact, as they might be due to the bulky affinity tags. Furthermore, interactions may require more than two interaction partners, membrane association or in the case of PilQ and TsaP, multimer formation of PilQ. To fully

understand how the single proteins directly interact in the trans-envelope machinery, further interaction experiments are needed.

The assembly from outside-in might be a good way to ensure that the pilus is only made when all IM and OM components are connected and aligned. In contrast, the flagella system, which assembles inside-out, harbours a mechanism of regulatory feedback to coordinate flagellar gene expression with assembly. For instance, the completion of the hook structure serves as a checkpoint for the transcription of further flagellar components like the flagellin (Dasgupta *et al.*, 2003). This feedback mechanism ensures that proteins, which are required at a late stage of flagellar assembly do not accumulate before they are needed, allowing the assembly from inside-out. To our knowledge no such feedback mechanism has been described for the T2SS or the T4P system. We speculate that this could be the reason for the opposite assembly pathway.

Moreover, in *M. xanthus* the assembly pathway starting with the secretin might be beneficial to allow extracellular complementation by Tgl. While motility is not essential under laboratory conditions, it is important for the cooperative and coordinated movement of *M. xanthus* swarms to gather nutrients in their natural habitats. The transfer of proteins via OMVs and OM fusion guarantees mobility of the whole community. Assuming that the IM complex can only connect to the oligomeric PilQ ring, the assembly from outside-in would allow activation of the whole machinery by Tgl, which can be provided by the community in case of spontaneous mutations in the *tgl* gene.

For some secretins it has been suggested that OM insertion requires a pilotin protein and that lack of this protein leads to IM localization of the secretin monomers (Koo et al., 2008). In contrast, experiments from *N. meningitidis* showed that multimerization of PilQ depends on a member of the β-barrel assembly machinery (BAM) complex (Voulhoux *et al.*, 2003) which is usually involved in the correct folding and insertion of OM proteins with ß-barrel structure. Extracellular complementation by Tgl also suggests that PilQ monomers exist in the OM and are assembled after Tgl is transferred. Another observation that supports this idea is that piliation can be restored in a *pilW* (homolog of *tgl* in *N. meningitidis*) mutant in a retraction deficient background *ΔpilT* (Carbonnelle et al., 2006). Carbonnelle et al. suggest that PilQ can form multimers in the OM in the absence of PilW, which allow the passage of T4P, but these multimers are not stable enough to withstand the forces during T4P retraction and cannot be detected upon SDS-PAGE as they are not heat- and detergent resistant. It should be analyzed to which subcellular compartment PilQ localizes in the absence of

Tgl in *M. xanthus*. In general, the data obtained from gene deletions in a Δ*pilT* background would give important extra information on the role of certain components. Hence, several deletions should be redone in a retraction deficient background and reanalyzed in *M. xanthus*.

3.4 Polar targeting of the T4P machinery

We propose that the T4P machinery assembles from outside-in with PilQ being the first component to localize to the poles therefore determining the site for piliation. This raises the question how PilQ becomes polarly localized?

Using time-lapse microscopy, we observed polarly localized PilQ late during cell division or immediately after cell division suggesting that PilQ becomes incorporated in the OM during the late stages of cell division. Studying polar recruitment of other polarly localized envelope spanning machineries revealed different potential mechanisms. For flagella or Flp pili, further components were discovered to be essential for the polar localization, like CpaE for Flp pili (Perez-Cheeks *et al.*, 2012, Viollier *et al.*, 2002) or FlhF and FlhG for flagella (Murray & Kazmierczak, 2006, Pandza *et al.*, 2000, Kusumoto *et al.*, 2008). Hence, there might be a so far unknown interaction partner, which might target PilQ to the poles. Interestingly, both polar targeting systems of flagellar and Flp pili involved a *parA/minD*-like protein. In *M. xanthus*, there are four *parA* paralogs. It would be interesting to analyze, if any of these genes has an effect on the polar localization of T4P components.

Also membrane curvature may provide a mechanism for protein recruitment, as it has been shown for other proteins that their localization is dependent on either positive or negative membrane curvature (Ramamurthi *et al.*, 2009, Ramamurthi & Losick, 2009). To check if the PilQ localization depends on the stronger membrane curvature at the poles, we could introduce the PilQ-sfGFP fusion into *E. coli* and check if it also localizes to the poles. If it does so, *E. coli* cells could be treated with lysozyme to lose the rod shape and observe if the localization pattern changes. Similar experiments could be done in *M. xanthus*. Another possibility for PilQ recruitment to the poles might be the interaction with lipids, which are enriched at the cell poles, e.g. cardiolipin (Mileykovskaya & Dowhan, 2000). It has been shown for other systems that polar localization of a protein can be dependent on polar cardiolipin localization (Romantsov *et al.*, 2007). To check if this is the case for PilQ, we could delete the cardiolipin synthases in *M. xanthus* and check for PilQ localization. Finally, there is the possibility that a mechanism of site-directed or in our case pole-directed membrane insertion exists. So far, it is unclear if polarly localized proteins are first incorporated into the membrane all over and then transported to the pole or if they are directly

inserted in the polar regions. In bacteria this is a highly speculative field. However, we think that the transport of proteins in the membrane(s) is a very slow and energy consuming process. To answer this question one could perform experiments with fluorescently labeled, polarly localized proteins under an inducible promoter and follow the cells under the microscope to analyze if the fluorescent signal first appears throughout the cell envelope and gets concentrated at the pole or if the fluorescence directly appears in the polar regions.

Future work will be directed at understanding how oligomeric PilQ becomes polarly localized in *M. xanthus*.

3.5 How is the T4P envelope complex energized by the ATPases PilB and PilT?

Our localization data demonstrate that both ATPases, which localize mainly unipolarly and are dynamic during a cellular reversal (Bulyha et al., 2009), localize independently of all tested T4P proteins. Given that all other components localize to both poles it is not surprising that none of them is required for PilB/T unipolar localization. PilB/T require a higher level of regulation supporting unipolar localization of PilB/T to separate between leading and lagging cell pole and allow the relocation upon a cellular reversal. This function is accomplished by SofG and bactofilins together with the MglA/B module, which are required to target the proteins to the pole and sort the proteins to the leading or lagging cell pole, respectively (Bulyha et al., 2013). To our knowledge it is not clear, how the switch between T4P extension and retraction is accomplished. T4P are suggested to bind to the EPS of neighbouring cells, which triggers pilus retraction (Li et al., 2003). This raises the question, whether the pilus itself is capable of transducing a signal from its tip to the cytoplasm to initiate pilus retraction. Is there a feedback mechanism to ensure that pili are only retracted when they have attached to a surface? As T4P are only composed of PilA subunits in *M. xanthus*, we speculate that binding of the pilus tip to a surface might induce a structural change in the pilin subunit, which is then transferred from one subunit to another in a kind of chain reaction of conformational changes. Reaching the T4P machinery in the cell envelope, a switch mechanism could lead to the dissociation of proteins required for extension or alternatively, to the dissociation of proteins, which counteract retraction, hence, allowing the interaction with the retraction ATPase PilT and subsequent retraction. This feedback mechanism would be beneficial as retraction of each individual pilus could be coordinated individually when T4P have found a substrate to pull on. This hypothesis is in agreement with the observation of Skerker and Berg that labeled pili on *P. aeruginosa* cells extend and retract independently (Skerker & Berg,

2001). If T4P extend and retract independently, a regulation mechanism on a cellular level as proposed by Bulyha et al. (2009) including the dynamic and temporal accumulation of PilT at the leading cell pole, would not be required. PilB or PilT association might be individually regulated for each T4P. So, the unipolar localization of PilB is required to determine the active/leading cell pole, however, we question a spatial separation of the two ATPases to separate between extension and retraction. Considering the fact that T4P in *Neisserial* species are localized all over the cell envelope, we cannot think of a mechanism to alternately exclude and recruit PilT to the base of the pili. Another observation that supports the hypothesis that PilT association is only prevented by another component is that piliation can be restored for some of the *pil*-mutants in a retraction deficient background (*ΔpilT*) (Carbonnelle et al., 2006, Takhar et al., 2013). Hence, some of the components are required to counteract retraction and possibly prevent PilT docking onto the T4P machinery to allow extension of T4P. The fact that single deletions of these counteracting proteins lead to a non-piliated phenotype, suggests that PilT is present at the base of the pilus pulling all pili in or PilT excludes PilB from the machinery, therefore blocking polymerization of the pili. In case of the *pilQ/pilT* double mutant, which polymerizes T4P in the periplasmic space, PilT might be involved in a kind of feedback mechanism, which usually pulls in all pili or prevents polymerization of T4P when they cannot unhinderedly exit. This supports the assumption that the pilus can signal to the machinery to induce the switch between extension and retraction. Similarly, it has been shown that application of high external forces on T4P during retraction can induce pilus elongation by reversing the retraction mechanism. Clausen and colleagues propose a force-dependent molecular switch to prevent breakage of T4P (Clausen et al., 2009, Maier *et al.*, 2004). Furthermore, this suggests that T4P function needs to quickly adapt in response to environmental circumstances, allowing the fast switch between extension and retraction, which presumably requires access of both ATPases at the base of T4P.

If PilT association to the complex needs to be inhibited by other T4P proteins, the affinity of the retraction ATPase to the T4P machinery might be higher than that of the extension ATPase. Therefore, the high PilB levels and low PilT levels at the leading cell pole in *M. xanthus* might be required to establish a certain ratio between PilB and PilT to get the appropriate balance between extension and retraction. Alternatively, PilT levels at the leading cell pole might be lower, as less is required to initiate retraction. There are different models concerning the energy requirements for extension or retraction of T4P. One example is the Brownian ratchet model, which describes that the pilin subunits from an assembled pilus melt down spontanously into the membrane,

because the energy is stored in the polymerized pilus (Merz & Forest, 2002). This model could explain lower levels of PilT at the leading cell pole as PilT might only act as a kind of molecular switch to initiate retraction and retraction itself occurs automatically. However, this has never been analyzed or proven so far.

The unipolar localization of PilT with the large cluster at the lagging cell pole leads to the question if PilT fulfills a function at the lagging cell pole. Our first thoughts were about inhibiting T4P extension at the lagging cell pole. However, this seems unlikely as PilB, which provides the energy for extension is predominantly localized to the leading cell pole and if T4P extension could occur with low levels of PilB at the lagging cell pole, we would expect pili on both cell poles in a deletion mutant of *pilT* which is not the case. Interestingly, PilB and PilT have been shown to localize to both poles in *P. aeruginosa* (Chiang et al., 2005). To our knowledge, polarity switching has not been observed in *P. aeruginosa,* suggesting that the T4P machinery localizes only to one pole. Hence, partial localization of PilB and PilT to the lagging cell pole seems to be a general mechanism for T4P regulation and might not be related to the capability of *M. xanthus* to build T4P at both poles and switch the direction of movement.

The fact that PilB/T were not shown to be recruited by any of the tested T4P proteins, does not mean that there is no interaction between these proteins. Takhar proposed that PilC mediates the interaction with PilB and PilT and transduces the energy over the IM in *P. aeruginosa* (Takhar et al., 2013).

Referring to the evolutionary related T2SS (Filloux, 2004, Hobbs & Mattick, 1993), we hypothesize that PilM might also be involved in the interaction with PilB or PilT. In the T2SS, PilM and PilN are composed of one protein called GspL (Sampaleanu et al., 2009), which interacts, recruits and stimulates the ATPase activity of the secretion ATPase GspE (Camberg et al., 2007, Sandkvist et al., 1999) corresponding to PilB/T. Due to the high structural similarity between both systems, it is possible that the IM complex of the T4P-system composed of PilM/N/O/C and of the T2SS composed of GspL/M/F have similar functions. For the T2SS it is suggested that the IM complex is involved in transducing energy from the secretion ATPase GspE located in the cytoplasm across the IM via conformational changes in GspL. GspL was in turn shown to interact with the major pseudopilin GspG (Gray et al., 2011) and is therefore suggested to support pseudopilus assembly. In our studies we did not find any evidence for interactions between PilM/N and the pilin PilA or the ATPases PilB/T. However, we think that this is due to the fact that the interaction of PilA or PilB/T with the IM complex might be only transient therefore not affecting accumulation or localization of each other. Moreover, it should be tested whether the two ATPases can

be stimulated upon interaction with PilC or PilM/PilN, like it was shown for GspL and GspE from the T2SS. This could also shed some light on the interaction partner(s) docking the two ATPases so that they can energize the T4P machinery.

3.6 What is the function of the IM complex?

pilM/N/O/P are only conserved among T4aP systems. In contrast to T4bP systems, T4aP can be retracted, which raises the question if PilM/N/O/P are only needed for retraction of T4P. Deleting the genes *pilM/N/O/P* in a retraction deficient strain (Δ*pilT*) and subsequent EM analyisis to check for the presence of T4P will address this question. If the genes are involved in assembly, no T4P should be detectable whereas the presence of T4P would be an indication that the genes are possibly involved in counteracting retraction of T4P. We think that the proteins PilM/N/O/P have a role, which exceeds the function of structurally aligning and stabilizing. As the IM complex extends into the cytosol with PilM being actin-like (Karuppiah & Derrick, 2011), we assume that PilM can undergo conformational changes upon ATP binding, which might serve to mediate protein interactions, to transduce energy or cytosolic signals. For *P. aeruginosa* it was shown that *pilM/N/O/P* are conditionally dispensable for T4P assembly and PilC is suggested to interact with PilB/T to transduce the energy. In contrast, PilC is dispensible for piliation in *N. meningitidis*, but PilM/N/O/P are required for piliation. Perhaps both PilC and PilM/N/O/P provide the possibility to transduce energy over the IM, but in the different organisms, the tasks to transduce energy for extension or retraction were assigned to different proteins. So, PilC might interact with PilB to enable pilus extension and PilM might interact with PilT to enable pilus retraction or vice versa.

Regarding the determined oligomeric states of PilM/N/O/P/Q we speculate that the trans-envelope protein complex builds a more complex structure in the periplasmic space than previously suggested. If all components are similarly arranged like PilQ into ring like structures, we can think of PilM/N/O/P connecting the secretin to the cytoplasm, building a trans-periplasmic channel. This could either serve to form a scaffold for the growing pilus, which is directed to the secretin pore or to transduce the signal or energy to regulate the opening or closing of the secretin channel. To allow the passage of the fiber, the pore needs to open and close to prevent efflux of periplasmic molecules. If the IM complex is building a trans-periplasmic channel, this would easily allow the regulation of the pore from a mechanistical point of view.

Another potential role of the IM complex is the assistance in polymerization of the pilin subunits. In *N. meningitidis* and *P. aeruginosa*, proteins of the IM complex were shown to interact with the major pilin subunit (Georgiadou et al., 2012, Tammam

et al., 2013). This could either suggest that the proteins guide the assembled subunits to the pore or that they help to extract the pilin subunits from the IM for incorporation into the pilus. To further elucidate the function of the IM complex, the interaction between the ATPases and the proteins of the IM complex should be analyzed. As this interaction is presumably only transient, experiments should involve a cross-linking step.

3.7 Actin-like ATPase PilM is not stable *in vitro*

To further elucidate the function of the IM complex, we investigated the function of PilM. Sequence analysis revealed that PilM exhibits similarity to members of the family of actin-like ATPases, like FtsA or MreB. Mutagenesis of the functional motifs, predicted to be involved in ATP binding or hydrolysis revealed that they are important for function and localization of PilM (Friedrich, 2010). To verify whether these effects are due to impairment in ATP binding or hydrolysis, we aimed to purify PilM and the two mutant proteins $PilM^{N229A}$ and $PilM^{G332D}$ to analyze their enzymatic properties. All approaches used here, did not provide any evidence for ATP hydrolysis or binding of PilM when compared to the two mutant proteins. However, the size-exclusion chromatography revealed that the proteins used here, were aggregated, which means that they were presumably not correctly folded. Misfolding of PilM can be due to too fast overexpression so that the protein cannot fold properly and hydrophobic residues are exposed. As this study showed that PilM is not stable when missing its interaction partner PilN *in vivo*, we think that the interrupted interaction with PilN might be accountable for the aggregation behavior of PilM *in vitro*. Due to the misfolding of PilM, we cannot draw any conclusions from the performed assays. Within the scope of this study, we constructed a fusion protein of PilM with the first 16 amino acids of PilN. Size-exclusion chromatography showed that the purified fusion protein is not aggregating, but forms dimers and monomers in solution. As this is in agreement with the observations of oligomers of PilN, PilO and PilP, we suggest that PilM is correctly folded with the PilN-fusion. Hence, the fusion protein should be analyzed for ATP-hydrolysis or -binding. Though, the results should be taken with care, as it might be that the protein is in a constitutive active or inactive state, because PilN is artificially and permanently bound to PilM. It is unclear whether the ATPase function is providing energy for T4P function or simply a tool to coordinate protein-protein interactions. Conformational changes upon ATP binding and/or hydrolysis could create different interaction sites as proposed by Holmes et al. (1993). Some members of the actin-like ATPases polymerize upon ATP-binding, however, we were unable to detect polymers upon EM analysis of MalE-PilM aggregates. Furthermore, the observations of dimers of

the PilM-PilN fusion protein during size-exclusion chromatography leads us to the conclusion that PilM is not capable of forming polymers, like FtsA or MreB.

3.8 Functional diversity of the T4P machinery among different organisms

Studying a highly conserved machinery, we thought that knowledge from one organism might be easily transferred or applied to another one. Apparently, the recent results led us to the conclusion that despite conservation of the single subunits, the detailed interplay differs considerably.

The interdependencies among PilN/O/P, which we observed in *M. xanthus* are in agreement with the effects observed in *N. meningitidis* (Georgiadou et al., 2012). In contrast, while we observed that PilM requires PilN/O/P/Q for stability in *M. xanthus*, none of the proteins is required for PilM stability in *N. meningitidis.* In *P. aeruginosa* it was shown that PilN/O/P need PilM for stability and none of them is required for PilM accumulation (Ayers et al., 2009). Furthermore, absence of each of the proteins PilM/N/O/P results in the reduction of total amount of PilQ (Ayers et al., 2009). The differences among the single T4P components from the different organisms are illustrated in Figure 64. While we conducted a large-scale screen comprising 11 of the T4P proteins from *M. xanthus*, the screens from *N. meningitidis* and *P. aeruginosa* are not as comprehensive, as to our knowledge not all proteins have been tested for stability in all deletion backgrounds.

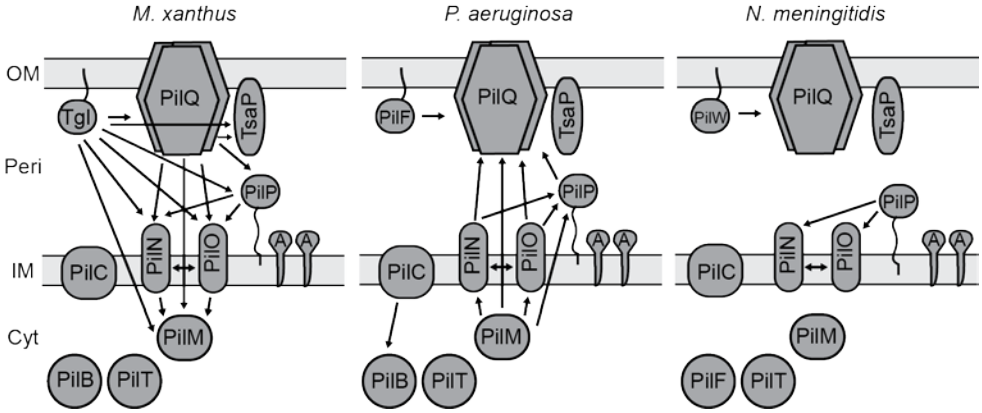

Figure 64 - The T4P machineries from *M. xanthus*, *P. aeruginosa* and *N. meningitidis* differ in the interplay of the single T4P proteins. Schematic T4P protein maps summarizing the stabilizing effects between single T4P proteins from the indicated organisms. Data for *P. aeruginosa* and *N. meningitidis* were obtained from Ayers et al. (2009) and Georgiadou et al. (2012), respectively. Not all proteins have been tested for stability in the absence of each T4P protein in *P. aeruginosa* and *N. meningitidis*.

While we propose an outside-in assembly for *M. xanthus*, studies on T4P from *Neisseria* species have shown that they most likely do not follow this assembly pathway. Analysis of a *pilQ/pilT* double mutant revealed the presence of pili, which

were trapped in the periplasmic space (Wolfgang et al., 2000), suggesting that the assembly machinery in the IM and cytoplasm is functional without the OM secretin. Although the single interdependencies among the proteins PilN/O/P in terms of stability reflect the situation observed in *M. xanthus*, both systems differ in the dependency of the IM complex on the secretin. Hence, the secretin-IM complex interaction(s) probably diverged in the different systems, which is in agreement with the sequence divergence among the N-terminal B1 and B2 domains of PilQ from different organisms (data not shown). To confirm our outside-in assembly pathway, which would not allow the production of T4P without the assembled secretin, we could construct a double deletion mutant of *pilQ* and *pilT* and analyze for T4P in the periplasmic space. Based on our model, periplasmic pili should not be present.

In conclusion, the interplay of the T4P proteins differs in *P. aeruginosa*, *M. xanthus* and *N. meningitidis*. In *Neisseria* and *Pseudomonas* species T4P are thought to fulfill similar functions in biofilm formation, DNA-uptake, adhesion to host cells and twitching motility. Although both machineries fulfill the same functions, they apparently diverged and developed different assembly mechanisms. Importantly, the mechanism of T4P polymerization seems to be highly conserved as pilins from *P. aeruginosa* can be polymerized by *N. gonorrhoeae* and similarly, the T2SS was shown to polymerize T4 pilins (Sauvonnet et al., 2000, Winther-Larsen *et al.*, 2007). While the T4P assembly machinery and certain accessory proteins differ in their detailed interplay, the main working mechanism of (pseudo)pilin polymerization seems to leave little room for variations.

3.9 Conclusion

In this study, we elucidated the assembly process and functional interactions between T4P proteins. We propose an assembly pathway starting in the OM with TgI, which assists in PilQ multimer formation (Figure 65i). TsaP is recruited by multimeric PilQ to the poles and possibly connects the PilQ complex to the peptidoglycan layer (Figure 65ii). PilP directly interacts with the periplasmic part of the PilQ complex and bridges the gap between OM and IM by presumably interacting with heterodimers of PilN and PilO (Figure 65iii). Having established the scaffold for the T4P envelope complex, PilC is connected to the machinery, presumably by direct interaction with PilO, and PilM is recruited to the poles by direct interaction with PilN (Figure 65iv).

After the completion of both T4P complexes at the poles, the machinery at the leading cell pole is alternately complemented by PilB or PilT to perform extension or retraction of T4P, respectively (Figure 65 iv, v).

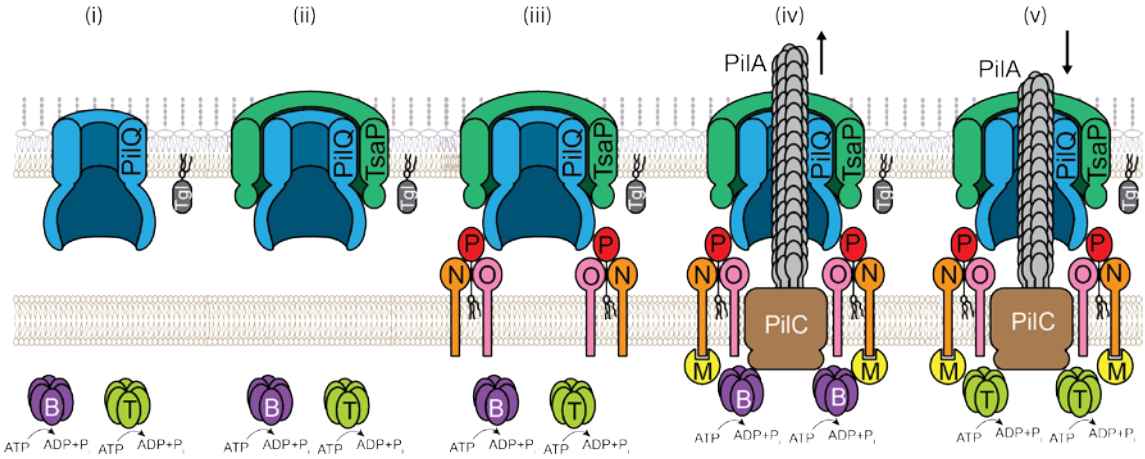

Figure 65 - Assembly model for the T4P machinery in *M. xanthus*. See text for details. Oligomers of PilM/N/O/P and peptidoglycan are not shown. Model designed by Dr. K. Wuichet (MPI Marburg), modified.

Whether the function of the IM complex of PilM/N/O/P is in gating the channel, transducing energy, switching between extension and retraction, help to extract pilins from the IM or to incorporate them into the pilus, remains to be elucidated.

In conclusion, this work gives novel insights into how the bacterial T4P machinery assembles and functions. As most of the proteins of the T4P machinery are highly conserved among different organisms, and their functionalities have been shown to be similar between species, we initially hypothesized that the findings from one system can be applied on other systems. Intriguingly, our work on *M. xanthus* T4P and comparison to studies from other organisms, suggests that there are distinct differences among the T4P systems concerning the interdependencies of single components of the T4P machinery. This implies that the different T4P systems diverged in the respective organisms to fit their specific lifestyles and habitats. Finally, the combination of our investigation on the T4P assembly and the numerous published results, does not support the idea of a general assembly model for T4P.

4 Materials and Methods

4.1 Chemicals and equipment

All chemicals, reagents, enzymes, kits and antibiotics used in this study are listed in Table 2 together with their suppliers. Technical equipment as well as the providing companies are listed in Table 3 and specific software used for data analysis is listed inTable 4.

Table 2 - Reagents, enzymes, antibiotics and kits

Reagents	**Supplier**
chemicals	Roth (Karlsruhe) Merck (Darmstadt) Sigma-Aldrich (Taufkirchen) Cambrex (Rockland, USA)
Media components, agar	Roth (Karlsruhe) Merck (Darmstadt) Difco (Heidelberg) Invitrogen (Darmstadt)
Oligonucleotides	Eurofins MWG Operon (Ebersberg) Sigma-Aldrich (Taufkirchen) Invitrogen (Karlsruhe)
SuperSignal chemiluminescence detection	Pierce/Thermo Scientific (Dreieich)
Rabbit antisera	Eurogentec (Seraing, Belgium)
Anti-GFP monoclonal antibody	Roche (Mannheim)
Rabbit anti-mouse IgG	DakoCytomation (Glostrup, Denmark)
Goat anti-rabbit IgG, goat anti-rabbit IgG DyLight 549	Pierce/Thermo Scientific (Dreieich)
Luminata Western HRP Substrate	Merck Millipore (Darmstadt)
PageRuler Plus Prestained Protein Ladder	Thermo Scientific (Dreieich)
HyperLadder I	Bioline (Luckenwalde)
2-log DNA Ladder	New England Biolabs (NEB) (Frankfurt a. M.)
Enzymes	
restriction enzymes	Fermentas (St. Leon-Rot) New England Biolabs (Frankfurt a. M.)
Antarctic Phosphatase	New England Biolabs (Frankfurt a. M.)
Phusion High-Fidelity DNA Polymerase	Thermo Scientific (Dreieich)
PfuUltra II DNA Polymerase	Invitrogen (Karlsruhe)
T4 DNA Ligase	Fermentas (St. Leon-Rot)
5 PRIME MasterMix	5 PRIME GmbH (Hamburg)

Antibiotics	
Kanamycin sulfate chloramphenicol ampicillin sodiumsulfate oxytetracycline dehydrate tetracycline	Roth (Karlsruhe)
Kits	
DNA purification gel extraction plasmid preparation	Qiagen (Hilden) Zymo Research HiSS Diagnostics GmbH (Freiburg) Macherey-Nagel (Düren)
MasterPure DNA purification kit	Epicentre Biotechnologies (Madison, USA)
SlowFade antifade kit	Molecular Probes/Invitrogen (Darmstadt)
QuickChange II XL site directed mutagenesis kit	Stratagene (Amsterdam)

Table 3 – Technical equipment

Application	**Device**	**Manufacturer**
Centrifugation	RC 5B plus Ultra Pro 80 Multifuge 1 S-R Biofuge fresco Biofuge pico Avanti J-26 XP Optima L-90K Centrifuge 5424 R	Sorvall / Thermo scientific (Dreieich) Heraeus / Thermo scientific (Dreieich) Beckman Coulter (Krefeld) Eppendorf (Hamburg)
PCR	Mastercycler personal Mastercycler epgradient	Eppendorf (Hamburg)
Thermomixer	Thermomixer compact Thermomixer comfort	Eppendorf (Hamburg)
DNA illumination and documentation	E-BOX VX2 imaging system	PeqLab (Eberhardzell)
DNA illumination	UVT_20 LE	Herolab (Wiesloch)
Cell disruption	Branson Sonifier 250	G. Heinemann (Schwäbisch Gmünd)
Protein electrophoresis	Mini-Protean® 3 Cell	Bio-Rad (München)
Determination of optical densities or nucleic acids absorption	Ultrospec 2100 pro Nanodrop ND-1000	Amersham Biosciences (Freiburg) Nanodrop (Wilmington, USA)

Electroporation	Gene Pulser® Xcell	Bio-Rad (München)
chemiluminescence detection	Luminescent Image Analyser LAS~4000	Fujifilm (Düsseldorf)
Western blotting	TransBlot® Turbo™Transfer System	Bio-Rad (München)
Size exclusion chromatography	ÄKTA purifier	Amersham Biosciences (Freiburg)
Microscopes and cameras	MZ75 stereomicroscope with the camera Leica DFC280 DM6000B microscope with the camera Cascade II DMI6000B microscope with adaptive focus control and Hamamatsu Flash 4.0 camera	Leica (Wetzlar) Photometrics (Tucson, USA) Leica (Wetzlar) Hamamatsu
Identification of proteins	4800 plus MALDI TOF/TOF Analyzer	Applied Biosystems (Darmstadt)
Immunofluorescence microscopy	Diagnostic microscope slides 12 well	Thermo Scientific (Dreieich)

Table 4 – Software for data analysis

Application	**Program**	**Supplier**
Fluorescence microscopy data analysis	Metamorph® v 7.5	Molecular Devices (Union city, CA)
Checking sequences, sequence alignments	Vector NTI advance software, suite 11	Invitrogen (Darmstadt)
Deconvolution	Huygens Essential 4.0.	Scientific Volume Imaging B.V (Hilversum, Netherlands)
View of crystal structures	PyMOL	DeLano Scientific LLC (South San Francisco, CA)

4.2 Media

E. coli cells were cultivated in lysogeny broth-medium (LB) whereas *M. xanthus* cells were grown in 1 % CTT-medium (Table 5). Antibiotics were added when appropriate (Table 6). For *M. xanthus* motility assays and microscopy the media shown in Table 7 were used.

Table 5 – Growth media for *E. coli* and *M. xanthus*

Media	Composition
LB-medium	1% (w/v) tryptone
	0.5% (w/v) yeast extract
	1% (w/v) NaCl
LB agar plates	LB-medium
	1.5 % (w/v) agar
1 % CTT	1% (w/v) Bacto casitone
	10 mM Tris-HCl pH 8.0
	1 mM potassium phosphate buffer pH 7.6
	8 mM MgSO4
CTT agar plates	1 % CTT medium
	1.5 % agar

Table 6 – Antibiotics used for *E. coli* and *M. xanthus*

Antibiotics	Final concentration	Dissolved in
E. coli		
Ampicillin sodium sulfate	100 µg/ml	H_2O
Chloramphenicol	30 µg/ml	99.99 % ethanol
Kanamycin sulfate	50 µg/ml	H_2O
Tetracyclin	15 µg/ml	99.99 % ethanol
M. xanthus		
Kanamycin sulfate	50 µg/ml	H_2O
Oxytetracycline	10 µg/ml	99.99 % methanol

Table 7 – Media used for motility assays and microscopy of *M. xanthus*

Media	Composition
A-motility plates (Hodgkin & Kaiser, 1977)	0.5 % CTT
	1.5 % select agar
S-motility plates (Hodgkin & Kaiser, 1977)	0.5 % CTT
	0.5 % select agar (Invitrogen)
A50 agar for microscopy	10 mM MOPS pH 7.2
	10 mM $CaCl_2$
	10 mM MgCl2
	50 mM NaCl
	1.5% (w/v) select agar (Invitrogen)
0.1 % CTT agarose for time lapse microscopy	10 mM Tris-HCl pH 7.6
	1 mM KH_2PO_4 pH 7.6
	8 mM $MgSO_4$
	0.1 % CTT
	1 % (w/v) SeaKem LE agarose (Cambrex)

4.3 Microbiological methods

4.3.1 Cultivation and storage of bacteria

E. coli strains were used for cloning of plasmid constructs as well as the expression of recombinant proteins. Cells were cultivated aerobically in LB-medium on horizontal shakers at 230 rpm and 37 °C or on LB-agar plates. The optical densities of *E. coli* cultures were measured photometrically at 600 nm.

M. xanthus strains were grown aerobically in 1 % CTT-medium at 32 °C on horizontal shakers at 220 rpm or on CTT-agar plates in the dark. To inoculate a *M. xanthus* culture, cells from a single colony were scraped form a CTT plate and first resuspended in 1 ml 1 % CTT-medium and then added to a bigger volume of medium. The optical density of *M. xanthus* cultures was measured photometrically at 550 nm.

All media and solutions were autoclaved for 20 min, 121 °C and 1 bar over pressure. Antibiotics were filtered using 0.22 µm pore size filters.
For long time storage of transformed *E. coli* strains, 1 ml over night culture was mixed with glycerol to a final concentration of 10 % and frozen in liquid nitrogen and stored at -80 °C. Similarly, to store *M. xanthus* strains 1 ml from an exponentially growing culture was mixed with glycerol to a final concentration of 4 %, frozen in liquid nitrogen and stored at -80 °C.

4.3.2 *E. coli* strains

Table 8 – *E. coli* strains used in this study

Strain	Relevant characteristics	Source or reference
Top10	F- *mcrA* Δ(*mrr-hsdRMS-mcrBC*), *80lacZΔM15ΔlacX74 recA1 deoR araD139 Δ(ara-leu)7697 galU galK rpsL* Str^R *endA1 nupG*	Invitrogen (Darmstadt)
Rosetta 2 (DE3)	F^-*ompT hsdS*$_B$($r_B^-m_B^-$) *gal dcm*(DE3) pRARE2(Cm^R)	Novagen/Merck (Darmstadt)

4.3.3 *M. xanthus* strains

Table 9 – *M. xanthus* strains used in this study

Strain	Relevant characteristics	Reference
DK1622	Wild type	(Kaiser, 1979)
DK8615	Δ*pilQ*	(Wall et al., 1999)
DK10409	Δ*pilT*	(Wu et al., 1997)
DK10410	Δ*pilA*	(Wu & Kaiser, 1996)
SA6011	Δ*tsaP*	(Binzen, 2012)
SA3002	Δ*pilM*	(Bulyha et al., 2009)
DK10416	Δ*pilB*	(Wu et al., 1997)
DK10417	Δ*pilC*	(Wu et al., 1997)

DK10405	Tc^r::*Δtgl*	(Nudleman et al., 2006)
SA3046	Δ*pilM*/P$_{pilA}$-*yfp-pilM* (pSC8)	(Bulyha et al., 2009)
SA3045	Δ*pilT/yfp-pilT* (pIB75)	(Bulyha et al., 2009)
SA6012	WT/P$_{pilA}$-*tsaP-mCherry* (pIMB3)	(Binzen, 2012)
SA6013	Δ*tsaP*/P$_{pilA}$-*tsaP-mCherry* (pIMB3)	(Binzen, 2012)
SA6015	*ΔpilQ*/P$_{pilA}$-*tsaP-mCherry* (pIMB3)	(Binzen, 2012)
SA3044	Δ*pilN*	I. Buylha (MPI, Marburg)
SA3001	Δ*pilO*	I. Buylha (MPI, Marburg)
SA3005	Δ*pilP*	I. Buylha (MPI, Marburg)
SA3006	Δ*pilQ* /P$_{pilA}$-*pilQ* (pIB55)	I. Buylha (MPI, Marburg)
SA3007	Δ*tgl* /P$_{pilA}$-*tgl* (pIB54)	I. Buylha (MPI, Marburg)
SA3053	Δ*pilM* /P$_{pilA}$-*pilM* (pSC2)	This work
SA4061	Δ*pilN* /P$_{pilA}$-*piN* (pSC37)	This work
SA4028	Δ*pilO* /P$_{pilA}$-*pilO* (pSC38)	This work
SA4029	Δ*pilP* /P$_{pilA}$-*pilP* (pSC39)	This work
SA4086	WT/P$_{pilA}$-*pilO-sfGFP* (pSC106)	This work
SA4088	Δ*pilO*/P$_{pilA}$-*pilO-sfGFP* (pSC106)	This work
SA6002	Δ*pilB*/P$_{pilA}$-*pilO-sfGFP* (pSC106)	This work
SA6005	Δ*pilT*/P$_{pilA}$-*pilO-sfGFP* (pSC106)	This work
SA6003	Δ*pilC*/P$_{pilA}$-*pilO-sfGFP* (pSC106)	This work
SA6001	Δ*pilA*/P$_{pilA}$-*pilO-sfGFP* (pSC106)	This work
SA4095	Δ*pilM*/P$_{pilA}$-*pilO-sfGFP* (pSC106)	This work
SA4096	Δ*pilN*/P$_{pilA}$-*pilO-sfGFP* (pSC106)	This work
SA4097	Δ*pilP*/P$_{pilA}$-*pilO-sfGFP* (pSC106)	This work
SA4098	Δ*pilQ*/P$_{pilA}$-*pilO-sfGFP* (pSC106)	This work
SA6051	Δ*tsaP*/P$_{pilA}$-*pilO-sfGFP* (pSC106)	This work
SA4067	WT/P$_{pilA}$-*pilP-sfGFP* (pSC102)	This work
SA4070	Δ*pilP*/P$_{pilA}$-*pilP-sfGFP* (pSC102)	This work
SA4078	Δ*pilB*/P$_{pilA}$-*pilP-sfGFP* (pSC102)	This work
SA4083	Δ*pilT*/P$_{pilA}$-*pilP-sfGFP* (pSC102)	This work
SA4079	Δ*pilC*/P$_{pilA}$-*pilP-sfGFP* (pSC102)	This work
SA4077	Δ*pilA*/P$_{pilA}$-*pilP-sfGFP* (pSC102)	This work
SA4080	Δ*pilM*/P$_{pilA}$-*pilP-sfGFP* (pSC102)	This work
SA4081	Δ*pilN*/P$_{pilA}$-*pilP-sfGFP* (pSC102)	This work
SA4082	Δ*pilO*/P$_{pilA}$-*pilP-sfGFP* (pSC102)	This work
SA4094	Δ*pilQ*/P$_{pilA}$-*pilP-sfGFP* (pSC102)	This work
SA6041	Δ*tsaP*/P$_{pilA}$-*pilP-sfGFP* (pSC102)	This work
SA6000	WT/P$_{pilA}$-*pilQ-sfGFP* (pSC110)	This work
SA4099	Δ*pilQ*/P$_{pilA}$-*pilQ-sfGFP* (pSC110)	This work

SA6026	WT/P_{pilA}-*tgl, pilQ-sfGFP* (pSC120)	This work
SA6027	Δ*pilQ*/P_{pilA}-*tgl, pilQ-sfGFP* (pSC120)	This work
SA6029	Δ*pilB*/P_{pilA}-*tgl, pilQ-sfGFP* (pSC120)	This work
SA6036	Δ*pilT*/P_{pilA}-*tgl, pilQ-sfGFP* (pSC120)	This work
SA6033	Δ*pilC*/P_{pilA}-*tgl, pilQ-sfGFP* (pSC120)	This work
SA6028	Δ*pilA*/P_{pilA}-*tgl, pilQ-sfGFP* (pSC120)	This work
SA6034	Δ*pilM*/P_{pilA}-*tgl, pilQ-sfGFP* (pSC120)	This work
SA6030	Δ*pilN*/P_{pilA}-*tgl, pilQ-sfGFP* (pSC120)	This work
SA6035	Δ*pilO*/P_{pilA}-*tgl, pilQ-sfGFP* (pSC120)	This work
SA6031	Δ*pilP*/P_{pilA}-*tgl, pilQ-sfGFP* (pSC120)	This work
SA6032	Δ*tsaP*/P_{pilA}-*tgl,pilQ-sfGFP* (pSC120)	This work
SA4060	Δ*pilMNOPQ*	This work
SA6024	Δ*pilBTCMNOPQ*	This work
SA6025	Δ*pilBTCMNOPQ*/ P_{pilA}-*yfp-pilT* (pIB75)	This work
SA6050	Δ*tsaP*/ P_{pilA}-*yfp-pilT* (pIB75)	This work
SA4076	Δ*tgl*/ P_{pilA}-*tgl-sfGFP* (pSC104)	This work
SA6044	*ΔpilB*/P_{pilA}-*tsaP-mCherry* (pIMB3)	This work
SA6048	*ΔpilT*/P_{pilA}-*tsaP-mCherry* (pIMB3)	This work
SA6045	*ΔpilC*/P_{pilA}-*tsaP-mCherry* (pIMB3)	This work
SA6043	*ΔpilA*/P_{pilA}-*tsaP-mCherry* (pIMB3)	This work
SA6046	*ΔpilM*/P_{pilA}-*tsaP-mCherry* (pIMB3)	This work
SA6049	*ΔpilN*/P_{pilA}-*tsaP-mCherry* (pIMB3)	This work
SA6047	*ΔpilO*/P_{pilA}-*tsaP-mCherry* (pIMB3)	This work
SA6022	*ΔpilP*/P_{pilA}-*tsaP-mCherry* (pIMB3)	This work
SA4057	*ΔpilM*/P_{pilA}-*yfp-pilM*^{D158A} (pSC96)	This work
SA4041	*ΔpilM*/P_{pilA}-*yfp-pilM*^{R388A} (pSC56)	This work
SA4058	*ΔpilM*/P_{pilA}-*yfp-pilM*^{D204A} (pSC97)	This work
SA4059	*ΔpilM*/P_{pilA}-*yfp-pilM*^{V204D} (pSC98)	This work
SA6053	*Δtgl*	This work
SA6059	*Δtgl*/ P_{pilA}-*tsaP-mCherry* (pIMB3)	This work
SA6056	Δ*tgl*/P_{pilA}-*pilP-sfGFP* (pSC102)	This work
SA6057	Δ*tgl*/P_{pilA}-*pilO-sfGFP* (pSC106)	This work
SA6058	Δ*tgl*/P_{pilA}-*yfp-pilT* (pIB75)	This work
SA6060	Δ*aglZ*/ P_{pilA}-*tgl, pilQ-sfGFP* (pSC120)	This work
SA6061	Δ*tgl*/P_{pilA}-*pilQ-sfGFP* (pSC110)	This work

4.3.4 Motility assay of *M. xanthus*

To analyze the ability of *M. xanthus* cells to move by A- or S-motility, cells from exponentially growing cultures were harvested and resuspended in 1% CTT to a

density of 7 × 10^9 cells/ml. 5 µl were spotted on 0.5% agar supplemented with 0.5% CTT to favor S-motility and 1.5% agar supplemented with 0.5% CTT to favor A-motility and incubated at 32 °C for 24 h in the dark. Colony edges were documented using a Leica MZ75 stereomicroscope equipped with a Leica DFC280 camera.

4.4 Molecular biological methods

4.4.1 Oligonucleotides and plasmids

All oligonucleotides used in this study are listed inTable 10 and Table 11. Sequences in bold display restriction sites used for cloning. Sequences in upper case indicate sequences complementary to the respective genes. Sequences in lower case show added sequences required for cloning. Underlined nucleotides were substituted during site-directed mutagenesis. Sequences in blue indicate sequences which are complimentary to fuse PCR products. Green sequences show an additional linker sequence.

Table 10 – oligonucleotides

Name	Nucleotide sequence 5'-3'
complementation under *pilA* promoter	
opilM-3	atcgg**aagctt**TCAGGCCAGCTTGTCGCC
opilM-4	atcgg**tctaga**GTGGTGCGAGGCTCCCGT
opilN-5	atcgg**tctaga**atgATGATTCGCATCAAC
opilN-6	atcgg**aagctt**TCAGATGGCGTAGTTGGA
opilO-5	atcgg**tctaga**atgGACAAGTACCTGGAT
opilO-6	atcgg**aagctt**CTATTTCTTCGAGTTCGA
opilP-5	atcgg**tctaga**ATGAAGACGTTCAAGGCC
opilP-6	atcgg**aagctt**CTACTCTCCGTAGTTCCT
oTgl-10	atcgg**tctaga**ATGTTCCGCCTTTCCACC
oTgl-12	atcgg**aagctt**CTACTAGAGCTTTTCCAGCAG
omxan_ 3001-1	atcgg**tctaga**ATGCGCTCCCGGATTCTC
omxan_ 3001-2	atcgg**aagctt**CAGCGGCTGGCCGAGGG
overexpression constructs	
opilM-14	atcgg**gaattc**gtgGTGCGAGGCTCCCGTCC
opilM-15	atcgg**gcggccgc**TCAGGCCAGCTTGTCGCC
opilM-30	atcgg**aagctt**TCAGGCCAGCTTGTCGCC
opilM-31	atcgg**gaattc**atgGTGCGAGGCTCCCGT

opilN-3	atc**ggatcc**catgGACCGACAGAGCGAGCTT
opilN-4	atc**aagctt**GATGGCGTAGTTGGAAGT
opilO-3	atc**ggatcc**catgCCCACGGAGGAAGAAATC
opilO-4	atc**aagctt**TTTCTTCGAGTTCGAGTT
opilP-3	atcgg**atccc**atgTACAGCTATGTGTACAAC
opilP-4	atc**aagctt**CTCTCCGTAGTTCCTGCC
opilP-8	atcgg**ggatcc**catgGAGGAGCCGCCGGCTCCT
opilP-9	atcgg**aagctt**CTCTCCGTAGTTCCTGCC
opilN-8	atcgg**gaattc**atgGACCGACAGAGCGAG
opilN-9	atcgg**aagctt**TCAGATGGCGTAGTTGGA
opilO-8	atcgg**gaattc**atgCCCACGGAGGAAGAA
opilO-9	atcgg**aagctt**CTATTTCTTCGAGTTCGA
opilP-10n	atcgg**gaattc**atgGAGGAGCCGCCGGCTCCT
opilP-11n	atcgg**aagctt**CTACTCTCCGTAGTTCCT
opilQ-17	atcgg**aagctt**CAGCGACCGGCTAAAGGA
opilQ-18	atcgg**gaattc**catgGTCGTTCTTGTGGGCGCC
omxan_ 3001-26	atcgg**gaattc**atgCAGCAGGAGAACGAGGAA
omxan_ 3001-27	atcgg**aagctt**TCAGCGGCTGGCCGAGGG
site-directed mutagenesis	
opilM-34	CGTGGGACTGGCGCTGGCGCGCCCGGGCGACAAG
opilM-35	CTTGTCGCCCGGGCGCGCCAGCGCCAGTCCCACG
opilM-43	CCCGGTGGTGGTGGCCGTGGATGCCTTCG
opilM-44	CGAAGGCATCCACGGCCACCACCACCGGG
opilM-45	GTGGTGGTGGACGACGATGCCTTCGCCG
opilM-46	CGGCGAAGGCATCGTCGTCCACCACCAC
opilM-41	GGACGTCAACATCGCCACGCAGATCCTCG
opilM-42	CGAGGATCTGCGTGGCGATGTTGACGTCC
fusion proteins	
osfGFP-1	atcgg**aagctt**ttaTTTGTAGAGCTCATCCAT
osfGFP-2	atcgg**ggatcc**ctggagggcccggcgggcctgATGAGCAAAGGAGAAGAACT
oPpilAforw	atcgg**gaattc**GCGGCGTTGAACGAGGGG
opilO-10	atcgg**ggatcc**TTTCTTCGAGTTCGAGTT
opilQ-15	atcgg**ggtacc**CAGAGTCTGCGCAATGGT

opilQ-21	atcgg**aagctt**CGCCCTCCAAGGCGCTCC
otgl-10	atcgg**tctaga**ATGTTCCGCCTTTCCACC
otgl-12	atcgg**aagctt**CTACTAGAGCTTTTCCAGCAG
opilP-12	atcgg**ggatcc**CTCTCCGTAGTTCCTGCC
otgl-13	atcgg**ggatcc**GAGCTTTTCCAGCAGCCT
opilN-29	**agctt**ggctccgccatgatgattcgcatcaacctgctgcccgtccgggcggtgaagaagcgttga**c**
opilN-30	**tcgag**tcaacgcttcttcaccgcccggacgggcagcaggttgatgcgaatcatcatggcggagcc**a**
opilM-49	atcgg**ggatcc**gatgGTGCGAGGCTCCCGT
opilM-50	atcgg**aagctt**ggcggagccGGCCAGCTTGTCGCCCGG
omxan_ 3001-3	atcgg**gaattc**GCGGCGTTGAACGAGGGG
omxan_ 3001-4	atcgg**ggattcc**GCGGCTGGCCGAGGGCGA
in frame deletions	
opilB-A	atcgg**gaattc**TGCCATCCGCGTCCAACTG
opilB-B	atcgg**gctagc**CAGTTCACCGAGTCGACC
opilC-C CS	atcgg**gctagc**TCGCTTGCCGGCGCCATC
opilC-D	atc**aagctt**AGCACCCGCGTGGGCGGC
opilB-E	GCATCGGCTTTCCCACCG
opilC-F	AGCAGACAGGGCGCCACC
opilT-E	CTCTCCACGCTGCACACC
opilT-H	AGGTTCCGGATTGCGGGG
opilT-F	TATCGAGGCACTGCACCA
opilM-A	atcgg**aagctt**GGGCTCACCGCAGAGGCC
opilM-Q-B	ctgccggttGTGCCTGGAGCCCGCCTG
opilM-Q-C	tccaggcacAACCGGCAGACCATTGCG
opilQ-D	atcgg**gaattc**CTCGGTCGACTTGCCGTT
opilT-A	atc**gaattc**CTCGCCCAGCGTCTGGCG
opilT-B NheI	atc**gctagc**GCGAAGCTGCGGCGGAGA
otgl-A	atcgg**aagctt**TACCGCGGGCTGCCCGCC
otgl-B	ccggcagtcCGAACAGGACGCGGTGGA
otgl-C	tcctgttcgGACTGCCGGAGGCTGCTG
otgl-D	atcgg**gaattc**ACGAGCCGGTCGGACTCG
otgl-E	GTGCGGGGCTTCGGGTAA

otgl-F	AAGCGCCGCTTGCTCTTG
otgl-G	AGCTCCAGGATGCGCTGC
otgl-H	TCACAGGTGGCGAAGGCT
omxan_3001-A	atcgg**aagctt**ACGAGCAGATGGAGATGT
omxan_3001-B	cgcgcccgcCATCAGCGAGGTGAGAAT
omxan_3001-C	tcgctgatgGCGGGCGCGTCGCCCTCG
omxan_3001-D	atcgg**gaattc**AGGAAGCCCTGATCCGGA
omxan_3001-E	TGGAGCGGGTGGCCCGGT
omxan_3001-F	ACACGCCCCCTCGGTCCA
omxan_3001-G	TGAGAGCGCTCCCGGTGA
omxan_3001-H	TGCCCACGAAGTCGGTGA
Primers used to verify integration at Mx8 phage attachment site	
attB right	GGAATGATCGGACCAGCTGAA
attB left	CGGCACACTGAGGCCACATA
attP right	GCTTTCGCGACATGGAGGA
attP left	GGGAAGCTCTGGGTACGAA

Table 11 – Sequencing primers

Name	Description	Nucleotide sequence (5'-3')
M13 uni (-43)	general sequencing primer for pBJ113, pBJ114, pSWU30	AGGGTTTTCCCAGTCACGACGTT
M13 rev (-49)	general sequencing primer for pBJ113, pBJ114, pSWU30	GAGCGGATAACAATTTCACACAGG
T7	sequencing pET24b$^+$ and pET45b$^+$	TAATACGACTCACTATAGGG
T7 term	sequencing pET24b$^+$ and pET45b$^+$	CTAGTTATTGCTCAGCGGT
malE	sequencing pMal-c2x	GGTCGTCAGACTGTCGATGAAGCC
M13 uni (-21)	sequencing pMal-c2x, pSK$^-$	TGTAAAACGACGGCCAGT
M13 rev (-29)	sequencing pSK$^-$	CAGGAAACAGCTATGACC
osfGFP rev	internal sequencing primer sfGFP	TTCACCCTCTCCACGGAC
PpilA for	internal sequencing primer P_{pilA}	GTGCGCACCTGGGTTGGCATGCG

KA-232	sequencing pSWU30	GCTTTACACTTTATGCTTCCGGCTCG
KA-316	internal sequencing primer mCherry	CTTGAAGCCCTCGGGGAAGGA
pGEX-for	sequencing pGEX-4T-1	GGAGCAGACAAGCCCGTCAGG
pGEX-rev	sequencing pGEX-4T-1	CAGGCTTTACACTTTATGCTTCCGGC

Table 12 – Plasmids used in this study

Plasmid	Characteristics	Reference
pSW105	Vector with Mx8 *attP* site and *pilA* promoter, Km^R	S. Weiss (MPI, Marburg)
pKA28	pSWU30 with *pomZ*-mCherry, Mx8 attP,Tet^R	(Treuner-Lange *et al.*, 2012)
pBJ114	Vector for in-frame deletion constructs, Km^R	(Julien *et al.*, 2000)
pBJ113	Vector for in-frame deletion constructs, Km^R	(Julien et al., 2000)
pET45 b^+	Expression vector, T7 promoter, N-term. His_6-tag, Amp^R	Merck Millipore
pSC8	pSWU30 – P_{pilA}-*yfp-pilM;* Tet^R	(Bulyha et al., 2009)
pIB75	pSWU30 – P_{pilA}-*yfp-pilT;* Tet^R	(Bulyha et al., 2009)
pMal-c2x	Expression vector , *tac* promoter, C-term. MBP-tag, Amp^R	New England biolabs
pET24 b^+	Expression vector, T7 promoter, C-term. His_6-tag, Km^R	Merck Millipore
pBluescript II SK- (pSK^-)	cloning vector, Amp^R	Fermentas
pSWU30	Vector with Mx8 *attP* site, Tet^R	
pET-21-sf-GFP	pET-21 - sfGFP, Amp^R	(Dinh & Bernhardt, 2011)
pSC2	pSW105 - *pilM;* Km^R	(Bulyha et al., 2009)
pIB54	pSW105 - *tgl,* Km^R	I. Bulyha (MPI Marburg)
pIB55	pSW105 - *pilQ,* Km^R	I. Bulyha (MPI Marburg)
pSC25	pSW105 - $pilM^{N229A}$	C. Friedrich (MPI Marburg)
pSC26	pSW105 - $pilM^{G332D}$	C. Friedrich (MPI Marburg)
pSC9	pET 45b^+- *pilM*	C. Friedrich (MPI Marburg)
pSC10	pGEX-4T-1 - *pilM*	C. Friedrich (MPI Marburg)
pIMB1	pBJ114 - *tsaP* in-frame deletion, Km^R	(Binzen, 2012)
pIMB2	pSC105 - *tsaP,* Km^R	(Binzen, 2012)
pIMB3	pSWU30 – P_{pilA}-*tsaP*-mCherry; Tet^R	(Binzen, 2012)
pSC32	pGEX-4T-1 - $pilM^{N229A}$	This work
pSC33	pGEX-4T-1 - $pilM^{G332D}$	This work
pSC34	pMal-c2x - *pilM*	This work
pSC35	pMal-c2x - $pilM^{N229A}$	This work
pSC36	pMal-c2x – $pilM^{G332D}$	This work
pSC37	pSW105 - *pilN,* Km^R	This work
pSC38	pSW105 - *pilO,* Km^R	This work
pSC39	pSW105 - *pilP,* Km^R	This work
pSC101	pSWU30 -sfGFP, Tet^R	This work
pSC102	pSC101 - P_{pilA}-*pilP*, Tet^R	This work
pSC104	pSC101 - P_{pilA}-*tgl*, Tet^R	This work
pSC106	pSC101 - P_{pilA}-*pilO*, Tet^R	This work
pSC110	pSC101 - P_{pilA}-*pilQ*, Tet^R	This work
pSC120	pSC101 - P_{pilA}-*tgl,pilQ*, Tet^R	This work
pSC11	pSK^- - *pilM*, Amp^R	This work
pSC56	pSC8 – $pilM^{R388A}$, Tet^R	This work
pSC97	pSC8 – $pilM^{D203A}$, Tet^R	This work
pSC98	pSC8 – $pilM^{V204D}$, Tet^R	This work
pSC5	pET24 b^+ - $pilN_{\Delta 42}$, Km^R	This work

pSC6	pET24 b^+ - *pilO*$_{\Delta 37}$, Km^R	This work
pSC7	pET24 b^+ - *pilP*$_{\Delta 55}$, Km^R	This work
pSC43	pET24 b^+ - *pilP*$_{\Delta 20}$, Km^R	This work
pSC44	pMal-c2x - *pilN*$_{\Delta 42}$, Amp^R	This work
pSC108	pET24b^+ - *pilQ*$_{20\text{-}656}$, Km^R	This work
pSC45	pMal-c2x - *pilO*$_{\Delta 37}$, Amp^R	This work
pSC46	pMal-c2x - *pilP*$_{\Delta 20}$, Amp^R	This work
pSC121	pMal-c2x - *tsaP*$_{\Delta 21}$, Amp^R	This work
pSC111	pET45b^+ - *pilM*-linker-*pilN*$_{1\text{-}16}$, Amp^R	This work
pSC83	pBJ114 - *pilBTC* in-frame deletion, Km^R	This work
pSC84	pBJ114 - *pilTC* in-frame deletion, Km^R	This work
pSC89	pBJ114 - *pilMNOPQ* in-frame deletion, Km^R	This work
pSC125	pBJ114 - *tgl* in-frame deletion, Km^R	This work

4.4.2 Construction of plasmids

Purified *M. xanthus* genomic DNA was used as a template to amplify the respective genes and regions. Plasmid DNA was used to amplify the gene for sfGFP. *E. coli* TOP10 was used for all cloning steps. All plasmids were confirmed to be correct by sequencing. DNA sequencing was performed by the company Eurofins MWG Operon (Ebersberg). Sequences were checked using the program ContigExpress of the VectorNTI advance suite 11 software (Invitrogen).

The plasmids **pSC5, pSC6, pSC7 and pSC43** were constructed for the overexpression of PilN$_{\Delta 42}$-His$_6$ (opilN-3 and opilN-4), PilO$_{\Delta 37}$-His$_6$ (opilO-3 and opilO-4), PilP$_{\Delta 55}$-His$_6$ (opilP-3 and opilP-4) and PilPΔ20-His$_6$ (opilP-8 and opilP-9). The truncated genes were amplified and digested with BamHI and HindIII and fused into the pET24b^+ vector.

pSC108 was constructed for the overexpression of the periplasmic part of PilQ. A part of the gene coding for amino acids 20-656 was amplified using the primers opilQ-17 and opilQ-18 carrying the EcoRI and HindIII restriction sites. After digestion, the gene product was fused into the pET24b^+.

To express the fusion protein His6-PilM-PilN$_{1\text{-}16}$ the plasmid **pSC111** was created in two steps. First, the sequence for the PilN-peptide was cloned into the pET45b^+ vector using two complementary primers covering the full gene sequence of the PilN-peptide which were already designed with overlapping ends of HindIII and XhoI restriction sites. Specifically, the primers opilN-29 and opilN-30 were mixed, heated up to 98 °C for 3 min and then cooled down to room temperature, allowing them to form a duplex and ligate the fragment into the pET45b^+ vector. *pilM* was subsequently cloned into this vector using opilM-49 and opilM-50 with opilM-50 carrying a linker sequence (ggcggagcc) and using the restriction sites BamHI and HindIII.

To construct the plasmids **pSC32** and **pSC33** for overexpression of GST-PilM^{N229A} and GST-PilM^{G332D}, the mutated genes were amplified with the primers opilM-14 and opilM-15 using the plasmids pSC25 and pSC26 as templates, respectively. After restriction digest with NotI and EcoRI, the genes were ligated into the pGEX-4t-1 vector.

For overexpression of MalE-tagged PilM, PilM^{N229A} and PilM^{G332D}, the plasmids **pSC34**, **pSC35** and **pSC36** were designed. The genes were amplified from genomic DNA or the plasmids pSC25 or pSC26, respectively. Gene products were digested with HindIII and EcoRI and subsequently fused into the pMal-2cx overexpression vector.

The plasmids **pSC44, pSC45, pSC46** and **pSC121** were constructed to overexpress MalE-PilN$_{\Delta 42}$ (opilN-8 and opilN-9), MalE-PilO$_{\Delta 37}$ (opilO-8 and opilO-9), MalE-PilP$_{\Delta 20}$ (opilP-10n and opilP-11n) and MalE-TsaP$_{\Delta 21}$ (omxan_3001-26 and omxan_3001-27). The truncated genes were amplified, digested with HindIII and EcoRI and cloned into the pMal-c2x expression vector.

Complementation constructs for *pilM, pilN, pilO, pilP* and *tsaP* were constructed by amplifying the respective genes using the primers: opilM-3 and opilM-4 (**pSC2**), opilN-5 and opilN-6 (**pSC37**), opilO-5 and opilO-6 (**pSC38**), opilP-5 and opilP-6 (**pSC39**) as well as omxan_3001- and omxan_3001 (**pIMB2**). All gene products were digested with XbaI and HindIII and cloned into the pSW105 vector.

To construct **pSC101**, the gene *sfGFP* was amplified from the vector pET21-sfGFP using the primers osfGFP-1 and osfGFP-2. The osfGFP-2 primer contained a linker (ctggagggcccggcgggcctg) which resembles the linker which was recommended by Dinh and Bernhardt (2011) and was optimized in terms of codon usage for *M. xanthus*. The PCR product was digested with BamHI and HindIII and cloned into the vector pSWU30.

To localize PilP, PilO, PilQ and Tgl via sfGFP-fusions, plasmids **pSC102, pSC106, pSC110** and **pSC104** were constructed, respectively. The *pilA* promoter with the full-length genes were each amplified from the respective complementation plasmid using the primers oPpilAforw and opilP-12, opilO-10, opilQ-15 or otgl-13, respectively. After digestion with EcoRI and BamHI, the gene products were cloned into the plasmid pSC101 carrying the *sfGFP* gene.

The second localization construct **pSC120** carried the genes for *tgl* and *pilQ* under the *pilA* promoter with *pilQ* fused C-terminally to *sfGFP*. *pilQ* was amplified with the upstream intergenic region between *pilP* and *pilQ* (57 bp) using the primers opilQ-21 and opilQ-15 carrying the restriction sites for HindIII and KpnI. *tgl* was amplified

using otgl-10 and otgl-12 carrying XbaI and HindIII. Both gene products were digested and cloned simultaneously in the vector pSC110 from which the *pilQ* gene has previously been removed with HindIII and XbaI.

The plasmids for site-directed mutagenesis of *pilM* (**pSC96, pSC97, pSC98, pSC56**) were constructed using the QuikChange II XL site directed mutagenesis protocol as described by the manufacturer (Stratagene). The mutations were introduced in the plasmid **pSC11** carrying the gene *pilM* which was cut from pSC2 with XbaI and HindIII and fused into the plasmid pSK$^-$. After introducing the mutations with the primer pairs opilM-41 and opilM-42 (D158A), opilM-34 and opilM-35 (R388A), opilM-43 and opilM-44 (D203A) and opilM-45 and opilM-46 (V204D), *pilM* was cut out by XbaI and HindIII and ligated into pSC8.

The deletion construct for *tgl* (full-length gene: 762 bp, deletion from 31-732 bp; **pSC125**) was cloned using the primers named otgl-A/B/C/D. Due to overlapping regions of the primers B and C, the gene products of the primer pairs A/B and C/D were fused in a third PCR using the primers A/D. After digestion with HindIII and EcoRI, the products were fused into the vector pBJ114. To delete multiple genes, as it was done for *pilMNOPQ* (deletion from position 49 bp in *pilM* to position 2676 bp in *pilQ*; **pSC89**), *pilBTC* (deletion form position 25 bp in *pilB* to position 1230 bp in *pilC*; **pSC83**), or *pilTC* (deletion from position 91 bp in *pilT* to position 1230 bp in *pilC,* **pSC84***)* the up- and downstream fragments were amplified with the primers opilM-A and opilM-Q-B and opilM-Q-C and opilM-Q-D for pSC89, with opilB-A, opilB-B and opilC-C_{CS}, opilC-D in the case of pSC83 and using opilT-A, opilT-B NheI, opilC-C_{CS} and opilC-D for pSC84 and subsequently cloned into the vector pBJ114 as described above.

4.4.3 Generation of *M. xanthus* in-frame deletions

The generation of in-frame deletions of specific regions on the chromosome was done as described (Shi *et al.*, 2008). Briefly, approximately 500 bp up- and downstream of the gene of interest were amplified using the primer pairs A/B and C/D. While primers A and D contain restriction sites for cloning into the vector pBJ114 (Km^R), primers B and C contain complementary sequences which allow the fusion of the two fragments A/B and C/D by a third PCR reaction using the primers A and D. The plasmids generated for in-frame deletions were all sequenced and correct plasmids were transformed into *M. xanthus*. Transformants were selected on kanamycin. The plasmid integrates into the chromosome via homologous recombination using either the up- or downstream site of the gene. Insertion of the plasmid was checked by PCR using the primer combinations E/M13for and F/M13rev (Figure 66). Depending on the

site of recombination different fragment sizes were obtained. After the successful integration of the plasmid, a second recombination must take place to loop out the plasmid. For this purpose the plasmid contains a second selection marker *galK* (galactokinase-encoding gene from *E. coli*). The galactokinase phosphorylates galactose to galactose-1-phosphat which accumulates to toxic levels in the cells as it cannot be metabollized by *M. xanthus*. Clones which contain the up- or downstream integration of the plasmid were grown over night in the presence of kanamycin to an optical density of 0.5-0.8 and different volumes (50, 100, 200 µl) were plated on CTT-plates containing 2.5 % galactose. Only cells which looped out the plasmid with the *galK* gene are able to grow on these plates. After this second homologous recombination there are theoretically 50 % of the cells which contain the in-frame deletion and 50 % of the cells are WT (Figure 66). Transformants were screened for growth on galactose and kanamycin and only clones which could grow on galactose but not on kanamycin were tested by PCR. External primers E and F and internal primers G and H were used to verify the in-frame deletion of the respective gene (Figure 66).

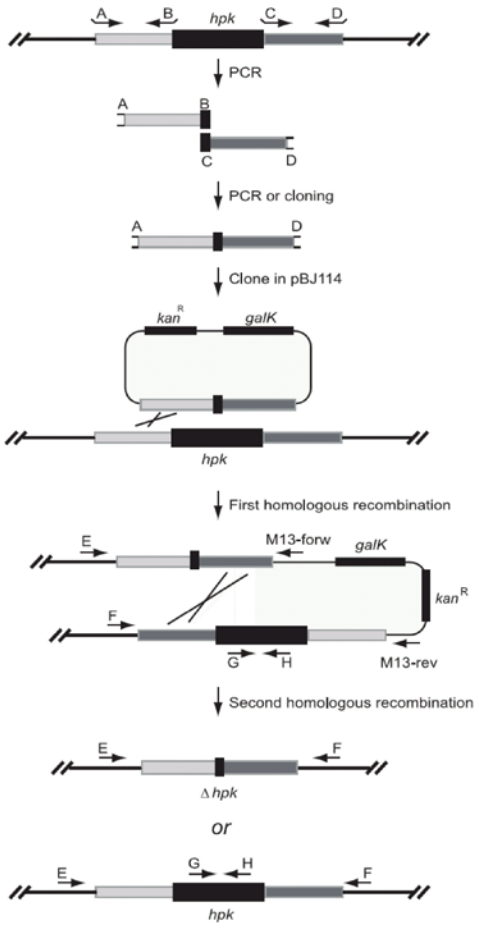

Figure 66 – Schematic illustration of in-frame deletion of the gene *hpk* in the chromosome of *M. xanthus*. Up- and downstream flanking regions of the gene to be deleted are shown in light and dark grey. Primers are indicated by black arrows. The black crosses stand for the homologous recombination events occurring during the deletion process. For simplicity, the first homologous recombination is only shown for the recombination occurring in the upstream flanking region. For details see text 4.4.3. This figure was reproduced from Shi et al. (2008).

4.4.4 DNA isolation from *E coli* and *M. xanthus*

To isolate plasmid DNA from *E. coli* the QIAprep Spin Miniprep Kit (Qiagen) or the NucleoSpin Plasmid QuickPure kit (Macherey-Nagel) was used. Genomic DNA from *M. xanthus* was isolated with the MasterPure DNA preparation Kit (Epicentre). Concentration and purity of the DNA was determined with the Nanodrop ND-1000 spectrophotometer. Crude genomic DNA of *M. xanthus* to do colony PCR was prepared by resuspending cells in 50 µl of ddH_2O, boiling for 5 min and spinning down the cell debris. 1.5 µl from the supernatant were used per PCR reaction.

4.4.5 Polymerase chain reaction (PCR)

To amplify specific DNA fragments a PCR was performed with the Phusion High-Fridelity DNA Polymerase in a 20 µl volume. For colony PCR the 5 PRIME MasterMix was used in a 20 µl volume. PCR reactions were prepared as described in Table 13.

Table 13 – Composition of PCR reactions for cloning or check PCR

Component	Volume	Final Concentration
PCR for cloning		
genomic DNA	1 µl	100 ng
10 µM primer	1 µl	0.5 µM
10 mM dNTPS (each)	0.4 µl	0.2 mM
5 x Phusion GC buffer	4 µl	1 x
5 x enhancer	4 µl	1 x
Phusion DNA polymerase	0.2 µl	1 unit/50 µl PCR
ddH_2O	to 20 µl	
check PCR		
crude genomic DNA	1.5 µl	~ 100 ng
5 PRIME Master Mix	8 µl	
10 µM primer	1 µl	0.5 µM
DMSO	2 µl	10 % (v/v)
ddH_2O	to 20 µl	

The following PCR programs were used in this study and modified in terms of annealing temperature and elongation time, based on the sequence of the primers or the length of the region to amplify (Table 14).

Table 14 – PCR programs

Step	Temparature	Time	
PCR for cloning			
Initial denaturation	98 °C	1 min	
Denaturation	98 °C	10 sec	30 x
Annealing	5 °C below melting temperature	30 sec	
Elongation	72 °C	30 sec/kb	
Final Elongation	72 °C	10 min	
Hold	4 °C	∞	
check PCR			
Initial denaturation	94 °C	3 min	
Denaturation	94 °C	30 sec	35 x
Annealing	5 °C below melting temperature	30 sec	
Elongation	72 °C	1 min/kb	
Final Elongation	72 °C	5 min	
Hold	4 °C	∞	

Correct product sizes were analyzed per agarose gel electrophoresis, excised from the gel and purified using the Zymoclean Gel DNA recovery kit (Zymo Research) or the NucleoSpin® Gel and PCR Clean-up (Macherey-Nagel).

4.4.6 Agarose gel electrophoresis

Correct DNA fragment sizes were visualized via agarose gel electrophoresis. DNA samples were mixed with 5 x DNA loading buffer (32.5 % saccharose, 5 mM EDTA, 5 mM Tris-HCl pH7.5, 0.15 % bromophenol blue) and separated on 1 % agarose gels with 0.01 % (v/v) ethidium bromide in 1 x TBE buffer (Invitrogen) at 120 V. As size standards the HyperLadder I (Bioline) or the 2-log DNA ladder (NEB) were used. Gels were documented with the E-BOX VX2 imaging system from PeqLab.

4.4.7 DNA restriction and ligation

Restriction of DNA fragments (0.5-2 µg) was performed at 37 °C for 1 h. Restricted DNA was purified using the DNA Clean & Concentrator kit (Zymo Research). Ligation reactions were done using the T4 DNA ligase (NEB) with ~50 ng of vector DNA and 3- to 5-fold molar excess of insert DNA. Ligations were performed for 1 h at roomtemperature or at 18 °C over night. T4 ligase was heat-inactivated at 65 °C for 10 min. Ligation mixtures were used for transformation into *E. coli* TOP10.

4.4.8 Preparation and transformation of chemical competent *E. coli* cells

Overnight cultures of *E. coli* TOP10 were used to inoculate 50 ml LB medium. Cells were grown to an OD_{600} of 0.5-0.7 and then harvested at 5000 x g for 10 min at 4°C. The cell pellet was resuspended in 25 ml ice cold 50 mM $CaCl_2$ solution. Cells were pelleted as described before and resuspended in 5 ml CaCl2 solution. After 10 min incubation on ice, 1ml 10 M glycerol was added and cells were aliquoted à 200 µl

and frozen in liquid nitrogen. Frozen aliquots were stored at -80 °C. One aliquot was used per transformation. Cells were thawed on ice and 20 µl of ligation mixture was added to the cells and mixed carefully. After incubation on ice for 30 min, cells were heat-shocked at 42 °C for 2 min. After 5 min incubation on ice, 1 ml LB-medium was added and cells were incubated for 30 min shaking at 37 °C. Then, cells were pelleted for 30 sec, the supernatant was discarded and cells were resuspended in 50 µl LB medium and plated on LB plates with appropriate antibiotics. Plates were incubated at 37 °C over night. Colonies were transferred to fresh agar plates and checked for the presence of the insert containing plasmid by restriction digest.

4.4.9 Preparation and transformation of electrocompetent *E. coli* cells

Overnight cultures of *E. coli* Rosetta 2 (DE3) were used to inoculate a culture in LB medium with chloramphenicol. Cells were grown to an OD_{600} of 0.5-0.7 and then harvested at 5000 x g for 10 min at 4°C. The cell pellet was washed two times in deionized water and then resuspended in water. Glycerol was added to a final concentration of 1.7 M and cells were aliquoted à 50 µl, frozen in liquid nitrogen and stored at -80 °C. For transformation 1 µl plasmid DNA was added to one cell aliquot, mixed and transferred into an electroporation cuvette (Bio-Rad, München). Cells were pulsed with 1.8 kV, 25 µF and 200 Ω. 1 ml LB medium was added and the cell suspension was then transferred into a sterile plastic tube and incubated for 1 h at 37˚C shaking at 230 rpm. 100 µl were plated on LB agar plates with appropriate antibiotics. The remaining 900 µl were pelleted and resuspended in 50 µl LB medium and plated as well. Plates were incubated at 37 °C over night.

4.4.10 Transformation of *M. xanthus* electrocompetent cells

For transformation of *M. xanthus* cells, 2 ml of an overnight culture OD550 0.6-0.9 were harvested at 13.000 x g for 2 min and the pellet was washed twice in 1 ml sterile ddH2O and resuspended in 50 µl H2O. 0.1 µg DNA for plasmids integrating at the Mx8 site and 1 µg of DNA for plasmids integrating at the endogenous site was added and the mixture was transferred into an electroporation cuvette. Cells were pulsed with 0.65 kV, 25 µF and 400 Ω. 1 ml CTT-medium was added and the cell suspension was transferred to a 25 ml Erlenmeyer flask and incubated at 32 °C, 230 rpm for 6h. 100 µl of the culture were plated directly on CTT-plates with the appropriate antibiotics. For the integration at the endogenous site the remaining 900 µl were also plated after concentrating the cells to a volume of 50-100 µl. Plates were incubated at 32 °C for 5-10 days and integration of the plasmid was verified by colony PCR (Table 13, Table 14).

4.5 Biochemical Methods

4.5.1 Purification of PilM, PilN, PilO, PilP, PilQ and TsaP

To purify $PilN_{\Delta 42}$-His6, $PilO_{\Delta 37}$-His6, $PilP_{\Delta 55}$-His6, $PilP_{\Delta 20}$-His6 and $PilQ_{20\text{-}656}$-His6 the overexpression constructs pSC5, pSC6, pSC7, pSC43 and pSC108 were transformed into Rosetta 2 (DE3)/pLysS strain (Novagen). Cells were grown in 0.5 or 1 L LB-medium with appropriate antibiotics at 37 °C to an OD_{600} 0.5-0.7, induced with 0.1 mM IPTG and grown at 18 °C over night. Cells were harvested at 10.000 x g for 20 min at 4 °C and resuspended in 35 ml lysis buffer (50 mM NaH_2PO_4, 300 mM NaCl, 10 mM Imidazol; pH8) with protease inhibitors (Complete Protease Inhibitor Cocktail Tablets from Roche). Cells were disrupted by sonication (medium tip, duty cycle 50 %, output control 4, 2 x 5 min). Cell debris were removed by centrifugation at 4000 x g for 10 min. The lysate was further centrifuged at 160.000 x g for 1h at 4 °C. The supernatant containing all soluble proteins was mixed with the equilibrated Ni^{2+}-NTA agarose (Qiagen) and incubated gently shaking at 4°C for 30-60 min. The mixture was loaded on a Pierce centrifuge column. After collecting the flow through, the column was washed twice with 20 ml lysis buffer. Bound protein was eluted with 2 times 1 ml lysis buffer containing 250 mM imidazol. For the generation of specific antibodies against $PilN_{\Delta 42}$-His6 and $PilP_{\Delta 55}$-His6, size exclusion chromatography (HiLoad Superdex 200 prep grade for PilN; HiLoad Superdex 75 prep grade for PilP) was performed to further purify both proteins. Both proteins were sent to Eurogentec (Seraing, Belgium) for antibody production.

To purify $PilO_{\Delta 37}$-His under denaturing conditions, a 1 L culture was grown and treated as before. After the ultracentrifugation the pellet was resuspended in buffer B (100 mM NaH_2PO_4, 10 mM Tris, 8 M Urea; pH 8) and incubated for 1 h at room temperature. After centrifugation at 160.000 x g for 1h the supernatant was mixed with pre-equilibrated Ni-NTA agarose and incubated for 30-60 min at room temperature. The mixture was loaded on a column and the flow through was collected. After washing twice with 20 ml buffer C (buffer B; pH 6.3), the protein was eluted with 1 ml buffer D (buffer B, pH 5.9) and three times 1 ml buffer E (buffer B, pH 4.5). Elution fractions of PilO purified under denaturing conditions were dialyzed against lysis buffer in three steps (4 M Urea, 2 M Urea, 0 M Urea, by mixing buffer B and lysis buffer in different ratios) using the Slide-A-Lyzer MINI Dialysis devices.

For the purification of GST-tagged proteins, the plasmids pSC10, pSC32 and pSC33 were introduced into Rosetta 2 (DE3). 500 ml cultures were grown and harvested as described before. Purification was performed in 40 ml PBS buffer (137 mM NaCl, 2.7 mM KCl, 10 mM Na_2HPO_4, 1.8 mM KH_2PO_4, pH 7.4). Cells were

sonicated and harvested as described before. The soluble proteins after ultra centrifugation are mixed with 1-2 ml of pre-equilibrated glutathione sepharose and incubated for 30-60 min at 4 °C. The mixture was loaded on a Pierce centrifuge column. After collecting the flow through, the column was washed twice with 25 ml PBS. Bound proteins were eluted in three steps, each with 1-2 ml 50 mM Tris-HCl pH8 with increasing concentrations of glutathione (5 mM, 10 mM, 20 mM).

To purify MalE-PilM, MalE-PilM^{N229A}, MalE-PilM^{G332D}, MalE-PilN$_{\Delta 42}$, MalE-PilO$_{\Delta 37}$, MalE-PilP$_{\Delta 20}$ and MalE-TsaP$_{\Delta 21}$ the overexpression constructs pSC34, pSC35, pSC36, pSC44, pSC45, pSC46 and pSC121 were transformed into Rosetta 2 (DE3)/pLysS strain (Novagen). Cells were grown and harvested as described before. The cell pellet was resuspended in 35 ml CB1 buffer (20 mM Tris-HCl pH7.4, 200 mM NaCl, 1 mM DTT, 1 mM EDTA) with protease inhibitors, sonicated and centrifuged as described for the His-tagged proteins. The supernatant was mixed with equilibrated amylose matrix (NEB) and incubated for 30-60 min at 4 °C. The mixture was loaded on a Pierce centrifuge column. After collecting the flow through, the column was washed twice with 20 ml CB1 buffer. Bound protein was eluted with 3 times 1 ml CB2 buffer (CB1 buffer with 10 mM maltose). Yield and purity of the proteins were verified by SDS-PAGE.

4.5.2 Co-Purification experiments

After purification of individual proteins, as described in 4.5.1, they were split and dialyzed against lysis buffer for Ni^{2+}-NTA chromatography or CB1 buffer for amylose chromatography. Proteins in the same buffer were mixed to the same final equimolar concentration, incubated for 1-2 h at 4 °C, and applied to a Ni^{2+}-NTA-agarose or an amylose column. Similar volumes of the flow through, wash and elution fractions were separated by SDS-PAGE and visualized by Coomassie G-250 staining.

4.5.3 SDS Polyacrylamide Gel Electrophoresis (SDS-PAGE)

To visualize and separate proteins by size, SDS-PAGE (Laemmli, 1970) 14 % or 8 % polyacrylamide gels were used. To denature proteins, they were mixed with 5 x loading buffer (50% (v/v) glycerol, 250 mM Tris-HCl pH 6.8, 10 mM EDTA, 10% (w/v) SDS, 0.5 M DTT, 1% (w/v) bromphenol blue) and heated at 98˚C for 5 min before loading o a gel. Gels were run in a Bio-Rad electrophoresis chambers at 150 V in 1 x Tris Glycin SDS (TGS) buffer from BioRad. As protein marker, the PageRuler Prestained Protein Ladder from Fermentas was used. Proteins were stained with PageBlue protein staining solution (Pierce) containing coomassie G-250. Gels were shortly boiled in the staining solution and incubated for 10-30 min. Destaining was performed by washing or boiling in water.

4.5.4 Determination of protein concentration by Bradford (Bradford, 1976)

To determine protein concentrations, the Bradford reagent (Bio-Rad) was used. Bovine serum albumin (BSA) was used to generate a protein standard curve. Protein concentrations were determined in duplicates in 1 ml reaction volumes. Samples were incubated with the Bradford reagent for 15 min at room temperature in the dark. The absorbance was determined at 595 nm with the Ultrospec 2100 pro spectrophotometer. Protein concentrations were calculated based on the linear slope of the standard curve.

4.5.5 ATPase assay

ATPase assay was carried out in buffer with 50mM Tris-HCl pH 7.5, 50 mM KCl, 10mM $MgCl_2$ and 1mM DTT. Different concentrations of PilM were incubated with 1 mM of an ATP-mix (endconcentration) with radioactive labeled ATP [α-^{32}P]-ATP (110 Tbq/mmol, Hartmann Analytic, diluted 1:50 in the ATP-mix) for 10 min to 1 hour. Labeled adenine nucleotides were separated by thin layer chromatography (TLC). 0.5µL of the protein-nucleotide-mixture were applied to a poly-ethyleneimine-cellulose F TLC plate (Merck, Darmstadt) with 2.4M formic acid as the solvent system. Labeled nucleotides on the TLC plate were visualized and quantified by phosphor imaging and analyzed using ImageQuant software. As positive control for this assay and to mark the positions of [α-^{32}P]-ADP, [α-^{32}P]-ATP or [α-^{32}P], the Apyrase Grade VII from potato (Sigma-Aldrich, Taufkirchen) was used.

4.5.6 Immunoblot analysis

Immunoblotting was performed to detect proteins by specific antibodies. First, the protein solution or proteins from cell extract (protein from 7 $\times 10^7$ cells loaded per lane) were separated by SDS-PAGE like described in 4.5.3 and then transferred to a nitrocellulose membrane using the Trans-Blot TurboTM Transfer System (BioRad) at 1,3 A, 25 V for 7 min with buffer containing 300 mM Tris and 300 mM Glycin, pH 9. After protein transfer the membrane was blocked in 5 % non-fat milk powder (w/v) in 1 x TTBS buffer (0.05% (v/v) Tween 20, 20 mM Tris-HCl, 137 mM NaCl pH 7) for 1 h at room temperature or over night at 4 °C. After washing with 1 x TTBS buffer, the primary antibody (rabbit) was added in proper dilutions (Table 15) in 1 x TTBS supplemented with 2 % non-fat milk powder for 2 h at room temperature. After washing again with 1 x TTBS the secondary anti-rabbit immunoglobulin G peroxidase conjugate (Sigma) was added in a 1:15.000 dilution and incubated for 1 h at room temperature. Before detecting the signals, the membrane was washed again with 1 x TTBS. Then, the blot was developed with the Luminata Western HRP Substrate (Merck Millipore) and visualized with the luminescent image analyzer LAS-4000 (Fujifilm).

Table 15 – Antibody dilutions for immunoblotting

Antibody	α-PilA	α-PilB	α-PilC	α-PilM	α-PilN	α-PilO	α-PilP	α-PilQ
dilution	1:5000	1:5000	1:5000	1:2000	1:2000	1:2000	1:5000	1:10.000

Antibody	α-PilT	α-Tgl	α-TsaP	α-mCherry
dilution	1:3000	1:2000	1:3000	1:5000

For detection of YFP- or GFP-tagged proteins, monoclonal anti-GFP mouse antibodies (Roche) and peroxidase-conjugated rabbit anti-mouse immunoglobulin G secondary antibodies (DakoCytomation) were used.

4.5.7 Size-exclusion chromatography.

Purified proteins were applied to HiLoad 16/60 Superdex 200 prep grade (SD200) or Superdex 75 10/300GL (SD75) size exclusion columns equilibrated with lysis buffer using the ÄKTA purifier (Amersham Biosciences) and the unicorn 4.10 software. The SD200 column was calibrated with ferritin (440 kDa), aldolase (158 kDa), conalbumin (75 kDa) and carbonic anhydrase (29 kDa) (GE Healthcare) using the same buffer and conditions (Figure 67). For the SD75 conalbumin (75 kDa), ovalbumin (43 kDa), carbonic anhydrase (29 kDa), ribonuclease A (13.7 kDa) and apronitin (6.5 kDa) were used for calibration (Figure 68). Blue dextran (GE Healthcare) was used to determine the void volume of the columns. For the SD200 the determined void volume was 48 ml and for the SD75 8,2 ml. The partition coefficient Kav is calculated from the following formular:

$$Kav = \frac{Ve - V0}{Vt - V0}$$

The elution volume (Ve) is measured from the size exclusion chromatogram and relates to the molecular size of the molecule. The void volume (V0) is the elution volume of molecules that are excluded from the size exclusion medium because they are larger than the largest pores in the matrix and pass straight through the packed column. The formular from the calibration graphs is used to calculate the molecular weight of the applied proteins from their Kav, calculated from their Ve.

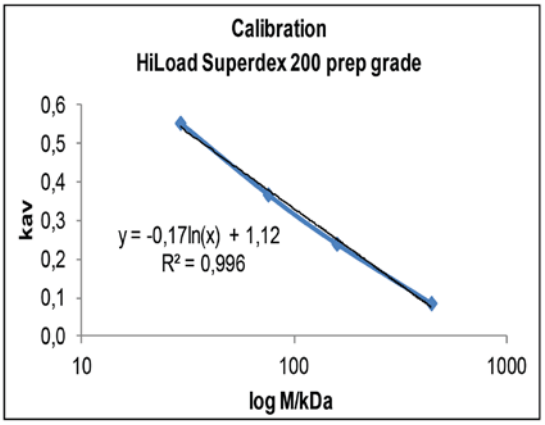

	ferretin	aldolase	conalbumin	carbonic anhydrase
M/kDa	440	158	75	29
Ve/ml	54,27	65,36	74,58	87,95
kav	0,09	0,24	0,37	0,55

Figure 67 - Calibration graph for the HiLoad Superdex 200 prep grade size exclusion column. Partition coefficient (Kav) is plotted against the logarithm of molecular weight (M). The table below shows the data with the molecular weight of the applied proteins, the elution volume (Ve) and the respective calculated Kav. The formular of the logarithmic trendline is indicated with the coefficient of determination R^2.

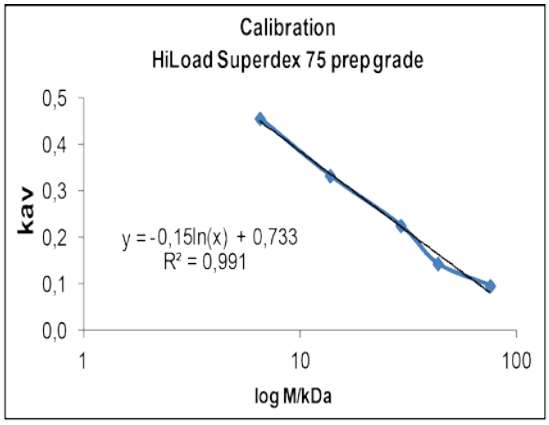

	conalbumin	ovalbumin	carbonic anhydrase	ribonuclease A	apronitin
M/kDa	75,00	43,00	29,00	13,70	6,50
Ve/ml	9,70	10,45	11,75	13,45	15,40
kav	0,10	0,14	0,23	0,33	0,46

Figure 68 - Calibration graph for the HiLoad Superdex 75 prep grade size exclusion column. For details compare Figure 67.

4.6 Microscopy

4.6.1 Live-cell imaging

For phase-contrast and fluorescence microscopy cells from exponentially growing cultures were transferred to a thin 1.5% agar pad with A50 buffer (10 mM MOPS pH 7.2, 10 mM $CaCl_2$, 10 mM $MgCl_2$, 50 mM NaCl) on a glass slide, and covered with a coverslip. Cells were immediately visualized with a Leica DM6000B microscope using a Leica Plan Apo 100x/NA 1.40 phase-contrast oil objective and imaged with a Roper Photometrics® Cascade II 1024 camera or a Leica DFC350FX camera. Images were recorded and processed with Metamorph (Molecular Devices).

For time-lapse recordings, cells were applied directly on a 0.1% CTT agarose pad on a coverslip at 32 °C, images recorded every 20 min using a temperature-controlled Leica DMI6000B microscope with an adaptive focus control and a motorized stage and a Hamamatsu Flash 4.0 camera, and images processed using the Leica MM AF software package. For each protein, polar fluorescent clusters were defined in WT assessing the intensity, position and shape and all other strains were compared to WT.

4.6.2 Immunofluorescence

Immunofluorescence microscopy was done essentially as described (Mignot et al., 2005). Briefly, exponentially growing *M. xanthus* cells were fixed with 3.2% (α-PilC, α-PilM, α-PilN, α-TsaP, α-PilQ) or 1.6% (α-PilB, α-Tgl) paraformaldehyde and 0.008% glutaraldehyde. Fixed cells were spotted on a poly-L-lysine treated 12-well diagnostic slide (Thermo Scientific) and permeabilized with GTE-buffer (50 mM glucose, 20 mM Tris-HCl, 10 mM EDTA, pH 7.5) for 5 min. After blocking with 2% BSA in PBS buffer (137 mM NaCl, 2.7 mM KCl, 10 mM Na_2HPO_4, 1.8 mM KH_2PO_4, pH 7.4) for 20 min, primary antibody was diluted 1:2000 (for α-PilQ 1:5000) in 2% BSA/PBS overnight at 4 °C. After washing with PBS, secondary antibody Alexa Fluor® 594 goat anti-rabbit IgG (Molecular Probes®, Life Technologies) was added for 2 h diluted 1:200 in 2% BSA/PBS. After washing with PBS, Slow Fade Anti Fade Reagent (Molecular Probes®, Life Technologies) was added to each well and cells covered with a coverslip. Cells were imaged as described.

4.6.3 Transmission electron microscopy (TEM)

For fixation, glutaraldehyde was added to an exponentially growing culture to a final concentration of 2.5% (v/v) to fix cells. 5 µl aliquots were applied to carbon-coated grids (400 square mesh). To visualize T4P, cells were not fixed and directly applied from liquid culture. After washing two times on a drop of double-distilled water, the samples were negatively stained with 2 % (w/v) uranyl acetate and air dried. Transmission electron microscopy was performed on a JEOL JEM-2100 at an acceleration voltage of 120 kV and images captured with a 2k x 2k fast scan CCD camera F214.

4.7 Bioinformatic analyses

M. xanthus gene and protein sequences were obtained using the Gene search tool from the J. Craig Venter Institute (JCVI) Comprehensive microbial Resource (CMR) server (http://cmr.jcvi.org/tigr-scripts/CMR/CmrHomePage.cgi). The Basic Local Alignment Search Tool (BLAST) was used to search for homologue nucleotide or protein sequences (http://blast.ncbi.nlm.nih.gov/Blast.cgi). Functional domains were

identified using the Simple Modular Architecture Research Tool (SMART) (http://smart.embl.de/). Transmembrane helices, signal peptides type I and II were predicted using the TMHMM Server v. 2.0 (http://www.cbs.dtu.dk/services/TMHMM/), SignalP 4.1 Server (http://www.cbs.dtu.dk/services/SignalP/) and LipoP 1.0 Server (http://www.cbs.dtu.dk/services/LipoP/), respectively. Sequence alignment based on secondary structure prediction was done with the PROMALS3D: multiple sequence and structure alignment server (http://prodata.swmed.edu/promals3d/promals3d.php) as well as the HHpred - Homology detection & structure prediction by HMM-HMM comparison (http://toolkit.tuebingen.mpg.de/hhpredd). The SWISS-Model Server (http://swissmodel.expasy.org/) was used for automated homology-modelling based on known crystal structures. 3D structures were analyzed with the PyMol program.

5 References

Abendroth, J., M. Bagdasarian, M. Sandkvist & W. G. Hol, (2004) The structure of the cytoplasmic domain of EpsL, an inner membrane component of the type II secretion system of *Vibrio cholerae*: an unusual member of the actin-like ATPase superfamily. *J Mol Biol* **344**: 619-633.

Aguilar, J., T. A. Cameron, J. Zupan & P. Zambryski, (2011) Membrane and core periplasmic *Agrobacterium tumefaciens* virulence Type IV secretion system components localize to multiple sites around the bacterial perimeter during lateral attachment to plant cells. *MBio* **2**: e00218-00211.

Andrade, M. A., C. Perez-Iratxeta & C. P. Ponting, (2001) Protein repeats: structures, functions, and evolution. *J Struct Biol* **134**: 117-131.

Arts, J., R. van Boxtel, A. Filloux, J. Tommassen & M. Koster, (2007) Export of the pseudopilin XcpT of the *Pseudomonas aeruginosa* type II secretion system via the signal recognition particle-Sec pathway. *J Bacteriol* **189**: 2069-2076.

Astling, D. P., J. Y. Lee & D. R. Zusman, (2006) Differential effects of chemoreceptor methylation-domain mutations on swarming and development in the social bacterium *Myxococcus xanthus*. *Mol Microbiol* **59**: 45-55.

Audette, G. F., R. T. Irvin & B. Hazes, (2004) Crystallographic analysis of the *Pseudomonas aeruginosa* strain K122-4 monomeric pilin reveals a conserved receptor-binding architecture. *Biochemistry* **43**: 11427-11435.

Averhoff, B. & A. Friedrich, (2003) Type IV pili-related natural transformation systems: DNA transport in mesophilic and thermophilic bacteria. *Arch Microbiol* **180**: 385-393.

Ayers, M., L. M. Sampaleanu, S. Tammam, J. Koo, H. Harvey, P. L. Howell & L. L. Burrows, (2009) PilM/N/O/P proteins form an inner membrane complex that affects the stability of the *Pseudomonas aeruginosa* type IV pilus secretin. *J Mol Biol* **394**: 128-142.

Balakrishna, A. M., Y. Y. Tan, H. Y. Mok, A. M. Saxena & K. Swaminathan, (2006) Crystallization and preliminary X-ray diffraction analysis of *Salmonella typhi* PilS. *Acta Crystallogr Sect F Struct Biol Cryst Commun* **62**: 1024-1026.

Balasingham, S. V., R. F. Collins, R. Assalkhou, H. Homberset, S. A. Frye, J. P. Derrick & T. Tonjum, (2007) Interactions between the lipoprotein PilP and the secretin PilQ in *Neisseria meningitidis*. *J Bacteriol* **189**: 5716-5727.

Berleman, J. E., T. Chumley, P. Cheung & J. R. Kirby, (2006) Rippling is a predatory behavior in *Myxococcus xanthus*. *J Bacteriol* **188**: 5888-5895.

Berleman, J. E., J. Scott, T. Chumley & J. R. Kirby, (2008) Predataxis behavior in *Myxococcus xanthus*. *Proc Natl Acad Sci U S A* **105**: 17127-17132.

Berleman, J. E., J. J. Vicente, A. E. Davis, S. Y. Jiang, Y. E. Seo & D. R. Zusman, (2011) FrzS regulates social motility in *Myxococcus xanthus* by controlling exopolysaccharide production. *PLoS One* **6**: e23920.

Bernhardt, T. G. & P. A. de Boer, (2003) The *Escherichia coli* amidase AmiC is a periplasmic septal ring component exported via the twin-arginine transport pathway. *Mol Microbiol* **48**: 1171-1182.

Berry, J.-L., M. M. Phelan, R. F. Collins, T. Adomavicius, T. Tønjum, S. A. Frye, L. Bird, R. Owens, R. C. Ford, L.-Y. Lian & J. P. Derrick, (2012) Structure and assembly of a trans-periplasmic channel for type IV pili in *Neisseria meningitidis*. *PLoS Pathog* **8**: e1002923.

Biais, N., D. L. Higashi, J. Brujic, M. So & M. P. Sheetz, (2010) Force-dependent polymorphism in type IV pili reveals hidden epitopes. *Proc Natl Acad Sci U S A* **107**: 11358-11363.

Biais, N., B. Ladoux, D. Higashi, M. So & M. Sheetz, (2008) Cooperative retraction of bundled type IV pili enables nanonewton force generation. *PLoS Biol* **6**: e87.

Binzen, I., (2012) Analyse der Lokalisation und Funktion des SaaP-Homologs Mxan_3001 in *Myxococcus xanthus*. *Bachelor thesis, Philipps-Universität Marburg*.

Black, W. P., Q. Xu & Z. Yang, (2006) Type IV pili function upstream of the Dif chemotaxis pathway in *Myxococcus xanthus* EPS regulation. *Mol Microbiol* **61**: 447-456.

Black, W. P. & Z. Yang, (2004) *Myxococcus xanthus* chemotaxis homologs DifD and DifG negatively regulate fibril polysaccharide production. *J Bacteriol* **186**: 1001-1008.

Blackhart, B. D. & D. R. Zusman, (1985) "Frizzy" genes of *Myxococcus xanthus* are involved in control of frequency of reversal of gliding motility. *Proc. Natl. Acad. Sci. USA* **82**: 8771-8774.

Bork, P., C. Sander & A. Valencia, (1992) An ATPase domain common to prokaryotic cell cycle proteins, sugar kinases, actin, and hsp70 heat shock proteins. *Proc Natl Acad Sci U S A* **89**: 7290-7294.

Bradford, M. M., (1976) A rapid and sensitive method for the quantitation of microgram quantities of protein utilizing the principle of protein-dye binding. *Anal Biochem* **72**: 248-254.

Bradley, D. E., (1980) A function of *Pseudomonas aeruginosa* PAO polar pili: twitching motility. *Can J Microbiol* **26**: 146-154.

Brown, D. R., S. Helaine, E. Carbonnelle & V. Pelicic, (2010) Systematic functional analysis reveals that a set of seven genes is involved in fine-tuning of the multiple functions mediated by type IV pili in *Neisseria meningitidis*. *Infect Immun* **78**: 3053-3063.

Buddelmeijer, N., M. Krehenbrink, F. Pecorari & A. P. Pugsley, (2009) Type II secretion system secretin PulD localizes in clusters in the *Escherichia coli* outer membrane. *J Bacteriol* **191**: 161-168.

Buist, G., A. Steen, J. Kok & O. P. Kuipers, (2008) LysM, a widely distributed protein motif for binding to (peptido)glycans. *Mol Microbiol* **68**: 838-847.

Bulyha, I., (2010) Regulation of type IV pili localization in *Myxococcus xanthus*. *PhD thesis, Philipps-Universität Marburg*.

Bulyha, I., S. Lindow, L. Lin, K. Bolte, K. Wuichet, J. Kahnt, C. van der Does, Thanbichler & L. Søgaard-Andersen, (2013) Two small GTPases act in concert with the bactofilin cytoskeleton to regulate dynamic bacterial cell polarity. *Dev. Cell* **25**: 119–131.

Bulyha, I., C. Schmidt, P. Lenz, V. Jakovljevic, A. Hone, B. Maier, M. Hoppert & L. Søgaard-Andersen, (2009) Regulation of the type IV pili molecular machine by dynamic localization of two motor proteins. *Mol Microbiol* **74**: 691-706.

Bustamante, V. H., I. Martinez-Flores, H. C. Vlamakis & D. R. Zusman, (2004) Analysis of the Frz signal transduction system of *Myxococcus xanthus* shows the importance of the conserved C-terminal region of the cytoplasmic chemoreceptor FrzCD in sensing signals. *Mol Microbiol* **53**: 1501-1513.

Caberoy, N. B., R. D. Welch, J. S. Jakobsen, S. C. Slater & A. G. Garza, (2003) Global mutational analysis of NtrC-like activators in *Myxococcus xanthus*: Identifying activator mutants defective for motility and fruiting body development. *Journal of Bacteriology* **185**: 6083-6094.

Camberg, J. L., T. L. Johnson, M. Patrick, J. Abendroth, W. G. J. Hol & M. Sandkvist, (2007) Synergistic stimulation of EpsE ATP hydrolysis by EpsL and acidic phospholipids. *EMBO J* **26**: 19-27.

Carbonnelle, E., S. Helaine, X. Nassif & V. Pelicic, (2006) A systematic genetic analysis in *Neisseria meningitidis* defines the Pil proteins required for assembly, functionality, stabilization and export of type IV pili. *Mol Microbiol* **61**: 1510-1522.

Carbonnelle, E., S. Helaine, L. Prouvensier, X. Nassif & V. Pelicic, (2005) Type IV pilus biogenesis in *Neisseria meningitidis*: PilW is involved in a step occurring after pilus assembly, essential for fibre stability and function. *Mol Microbiol* **55**: 54-64.

Cehovin, A., P. J. Simpson, M. A. McDowell, D. R. Brown, R. Noschese, M. Pallett, J. Brady, G. S. Baldwin, S. M. Lea, S. J. Matthews & V. Pelicic, (2013) Specific DNA recognition mediated by a type IV pilin. *Proc Natl Acad Sci U S A* **110**: 3065-3070.

Chiang, P., M. Habash & L. L. Burrows, (2005) Disparate subcellular localization patterns of *Pseudomonas aeruginosa* Type IV pilus ATPases involved in twitching motility. *J Bacteriol* **187**: 829-839.

Cisneros, D. A., P. J. Bond, A. P. Pugsley, M. Campos & O. Francetic, (2012a) Minor pseudopilin self-assembly primes type II secretion pseudopilus elongation. *EMBO J* **31**: 1041-1053.

Cisneros, D. A., G. Pehau-Arnaudet & O. Francetic, (2012b) Heterologous assembly of type IV pili by a type II secretion system reveals the role of minor pilins in assembly initiation. *Mol Microbiol* **86**: 805-818.

Clausen, M., M. Koomey & B. Maier, (2009) Dynamics of type IV pili is controlled by switching between multiple states. *Biophys J* **96**: 1169-1177.

Collins, R. F., L. Davidsen, J. P. Derrick, R. C. Ford & T. Tonjum, (2001) Analysis of the PilQ secretin from *Neisseria meningitidis* by transmission electron microscopy reveals a dodecameric quaternary structure. *J Bacteriol* **183**: 3825-3832.

Collins, R. F., S. A. Frye, S. Balasingham, R. C. Ford, T. Tonjum & J. P. Derrick, (2005) Interaction with type IV pili induces structural changes in the bacterial outer membrane secretin PilQ. *J Biol Chem* **280**: 18923-18930.

Collins, R. F., S. A. Frye, A. Kitmitto, R. C. Ford, T. Tonjum & J. P. Derrick, (2004) Structure of the *Neisseria meningitidis* outer membrane PilQ secretin complex at 12 A resolution. *J Biol Chem* **279**: 39750-39756.

Collins, R. F., M. Saleem & J. P. Derrick, (2007) Purification and three-dimensional electron microscopy structure of the *Neisseria meningitidis* type IV pilus biogenesis protein PilG. *J Bacteriol* **189**: 6389-6396.

Comer, J. E., M. A. Marshall, V. J. Blanch, C. D. Deal & P. Castric, (2002) Identification of the *Pseudomonas aeruginosa* 1244 pilin glycosylation site. *Infect Immun* **70**: 2837-2845.

Craig, L. & J. Li, (2008) Type IV pili: paradoxes in form and function. *Curr Opin Struct Biol* **18**: 267-277.

Craig, L., M. E. Pique & J. A. Tainer, (2004) Type IV pilus structure and bacterial pathogenecity. *Nat. Rev. Microbiol.* **2**: 363-378.

Craig, L., R. K. Taylor, M. E. Pique, B. D. Adair, A. S. Arvai, M. Singh, S. J. Lloyd, D. S. Shin, E. D. Getzoff, M. Yeager, K. T. Forest & J. A. Tainer, (2003) Type IV pilin structure and assembly: X-ray and EM analyses of Vibrio cholerae toxin-coregulated pilus and *Pseudomonas aeruginosa* PAK pilin. *Mol Cell* **11**: 1139-1150.

Craig, L., N. Volkmann, A. S. Arvai, M. E. Pique, M. Yeager, E. H. Egelman & J. A. Tainer, (2006) Type IV pilus structure by cryo-electron microscopy and crystallography: implications for pilus assembly and functions. *Mol Cell* **23**: 651-662.

Criss, A. K., K. A. Kline & H. S. Seifert, (2005) The frequency and rate of pilin antigenic variation in *Neisseria gonorrhoeae*. *Mol Microbiol* **58**: 510-519.

Dasgupta, N., M. C. Wolfgang, A. L. Goodman, S. K. Arora, J. Jyot, S. Lory & R. Ramphal, (2003) A four-tiered transcriptional regulatory circuit controls flagellar biogenesis in *Pseudomonas aeruginosa*. *Mol Microbiol* **50**: 809-824.

de Souza, R. F., V. Anantharaman, S. J. de Souza, L. Aravind & F. J. Gueiros-Filho, (2008) AMIN domains have a predicted role in localization of diverse periplasmic protein complexes. *Bioinformatics* **24**: 2423-2426.

Dinh, T. & T. G. Bernhardt, (2011) Using superfolder green fluorescent protein for periplasmic protein localization studies. *J Bacteriol* **193**: 4984-4987.

Ducret, A., B. Fleuchot, P. Bergam & T. Mignot, (2013) Direct live imaging of cell-cell protein transfer by transient outer membrane fusion in *Myxococcus xanthus*. *Elife* **2**: e00868.

Dworkin, M., (1996) Recent advances in the social and developmental biology of the myxobacteria. *Microbiol Rev* **60**: 70-102.

Faast, R., M. A. Ogierman, U. H. Stroeher & P. A. Manning, (1989) Nucleotide sequence of the structural gene, tcpA, for a major pilin subunit of *Vibrio cholerae*. *Gene* **85**: 227-231.

Farinha, M. A., B. D. Conway, L. M. Glasier, N. W. Ellert, R. T. Irvin, R. Sherburne & W. Paranchych, (1994) Alteration of the pilin adhesin of *Pseudomonas aeruginosa* PAO results in normal pilus biogenesis but a loss of adherence to human pneumocyte cells and decreased virulence in mice. *Infect Immun* **62**: 4118-4123.

Feilmeier, B. J., G. Iseminger, D. Schroeder, H. Webber & G. J. Phillips, (2000) Green fluorescent protein functions as a reporter for protein localization in *Escherichia coli*. *J Bacteriol* **182**: 4068-4076.

Filloux, A., (2004) The underlying mechanisms of type II protein secretion. *Biochim Biophys Acta* **1694**: 163-179.

Francetic, O., N. Buddelmeijer, S. Lewenza, C. A. Kumamoto & A. P. Pugsley, (2007) Signal recognition particle-dependent inner membrane targeting of the PulG Pseudopilin component of a type II secretion system. *J Bacteriol* **189**: 1783-1793.

Friedrich, C., (2010) Analyse der Funktion von PilM, PilN, PilO und PilP in *Myxococcus xanthus*. *Master thesis, Philipps-Universität Marburg*.

Georgiadou, M., M. Castagnini, G. Karimova, D. Ladant & V. Pelicic, (2012) Large-scale study of the interactions between proteins involved in type IV pilus biology in *Neisseria meningitidis*: characterization of a subcomplex involved in pilus assembly. *Mol Microbiol* **84**: 857-873.

Ghosh, A. & S. V. Albers, (2011) Assembly and function of the archaeal flagellum. *Biochem Soc Trans* **39**: 64-69.

Giltner, C. L., Y. Nguyen & L. L. Burrows, (2012) Type IV pilin proteins: versatile molecular modules. *Microbiol Mol Biol Rev* **76**: 740-772.

Golovanov, A. P., S. Balasingham, C. Tzitzilonis, B. T. Goult, L. Y. Lian, H. Homberset, T. Tonjum & J. P. Derrick, (2006) The solution structure of a domain from the *Neisseria meningitidis* lipoprotein PilP reveals a new beta-sandwich fold. *J Mol Biol* **364**: 186-195.

Gray, M. D., M. Bagdasarian, W. G. Hol & M. Sandkvist, (2011) In vivo cross-linking of EpsG to EpsL suggests a role for EpsL as an ATPase-pseudopilin coupling protein in the Type II secretion system of *Vibrio cholerae*. *Mol Microbiol* **79**: 786-798.

Hagblom, P., E. Segal, E. Billyard & M. So, (1985) Intragenic recombination leads to pilus antigenic variation in *Neisseria gonorrhoeae*. *Nature* **315**: 156-158.

Hartung, S., A. S. Arvai, T. Wood, S. Kolappan, D. S. Shin, L. Craig & J. A. Tainer, (2011) Ultrahigh resolution and full-length pilin structures with insights for filament assembly, pathogenic functions, and vaccine potential. *J Biol Chem* **286**: 44254-44265.

Henrichsen, J., (1972) Bacterial surface translocation: a survey and a classification. *Bacteriol Rev* **36**: 478-503.

Henrichsen, J., (1983) Twitching motility. *Annu Rev Microbiol* **37**: 81-93.

Hobbs, M. & J. S. Mattick, (1993) Common components in the assembly of type 4 fimbriae, DNA transfer systems, filamentous phage and protein-secretion apparatus: a general system for the formation of surface-associated protein complexes. *Mol Microbiol* **10**: 233-243.

Hodgkin, J. & D. Kaiser, (1977) Cell-to-cell stimulation of movement in nonmotile mutants of *Myxococcus*. *Proc Natl Acad Sci U S A* **74**: 2938-2942.

Hodgkin, J. & D. Kaiser, (1979) Genetics of Gliding Motility in *Myxococcus xanthus* (Myxobacterales) - Two Gene Systems Control Movement. *Molecular & General Genetics* **171**: 177-191.

Holmes, K. C., C. Sander & A. Valencia, (1993) A new ATP-binding fold in actin, hexokinase and Hsc70. *Trends Cell Biol* **3**: 53-59.

Hu, W., M. Hossain, R. Lux, J. Wang, Z. Yang, Y. Li & W. Shi, (2011) Exopolysaccharide-independent social motility of *Myxococcus xanthus*. *PLoS One* **6**: e16102.

Inclan, Y. F., S. Laurent & D. R. Zusman, (2008) The receiver domain of FrzE, a CheA-CheY fusion protein, regulates the CheA histidine kinase activity and downstream signalling to the A- and S-motility systems of *Myxococcus xanthus*. *Mol Microbiol* **68**: 1328-1339.

Inclan, Y. F., H. C. Vlamakis & D. R. Zusman, (2007) FrzZ, a dual CheY-like response regulator, functions as an output for the Frz chemosensory pathway of *Myxococcus xanthus*. *Mol Microbiol* **65**: 90-102.

Jain, S., K. B. Moscicka, M. P. Bos, E. Pachulec, M. C. Stuart, W. Keegstra, E. J. Boekema & C. van der Does, (2011) Structural characterization of outer membrane components of the type IV pili system in pathogenic *Neisseria*. *PLoS One* **6**: e16624.

Jakovljevic, V., S. Leonardy, M. Hoppert & L. Søgaard-Andersen, (2008) PilB and PilT are ATPases acting antagonistically in type IV pili function in *Myxococcus xanthus*. *J. Bacteriol.* **190**: 2411-2421.

Jelsbak, L. & L. Sogaard-Andersen, (2003) Cell behavior and cell-cell communication during fruiting body morphogenesis in *Myxococcus xanthus*. *J Microbiol Methods* **55**: 829-839.

Jensen, R. B. & K. Gerdes, (1997) Partitioning of plasmid R1. The ParM protein exhibits ATPase activity and interacts with the centromere-like ParR-parC complex. *J Mol Biol* **269**: 505-513.

Julien, B., A. D. Kaiser & A. Garza, (2000) Spatial control of cell differentiation in *Myxococcus xanthus*. *Proc. Natl. Acad. Sci. USA* **97**: 9098-9103.

Kachlany, S. C., P. J. Planet, R. Desalle, D. H. Fine, D. H. Figurski & J. B. Kaplan, (2001) flp-1, the first representative of a new pilin gene subfamily, is required for non-specific adherence of *Actinobacillus actinomycetemcomitans*. *Mol Microbiol* **40**: 542-554.

Kaimer, C., J. E. Berleman & D. R. Zusman, (2012) Chemosensory signaling controls motility and subcellular polarity in *Myxococcus xanthus*. *Curr Opin Microbiol* **15**: 751-757.

Kaiser, D., (1979) Social gliding is correlated with the presence of pili in *Myxococcus xanthus*. *Proc Natl Acad Sci U S A* **76**: 5952-5956.

Karuppiah, V. & J. P. Derrick, (2011) Structure of the PilM-PilN inner membrane type IV pilus biogenesis complex from *Thermus thermophilus*. *J Biol Chem* **286**: 24434-24442.

Karuppiah, V., D. Hassan, M. Saleem & J. P. Derrick, (2010) Structure and oligomerization of the PilC type IV pilus biogenesis protein from *Thermus thermophilus*. *Proteins* **78**: 2049-2057.

Kearns, D. B. & L. J. Shimkets, (2001) Lipid chemotaxis and signal transduction in *Myxococcus xanthus*. *Trends Microbiol* **9**: 126-129.

Keilberg, D., K. Wuichet, F. Drescher & L. Sogaard-Andersen, (2012) A response regulator interfaces between the Frz chemosensory system and the MglA/MglB GTPase/GAP module to regulate polarity in *Myxococcus xanthus*. *PLoS Genet* **8**: e1002951.

Kim, K., J. Oh, D. Han, E. E. Kim, B. Lee & Y. Kim, (2006) Crystal structure of PilF: functional implication in the type 4 pilus biogenesis in *Pseudomonas aeruginosa*. *Biochem Biophys Res Commun* **340**: 1028-1038.

Klausen, M., A. Aaes-Jorgensen, S. Molin & T. Tolker-Nielsen, (2003) Involvement of bacterial migration in the development of complex multicellular structures in *Pseudomonas aeruginosa* biofilms. *Mol Microbiol* **50**: 61-68.

Konovalova, A., S. Lobach & L. Sogaard-Andersen, (2012) A RelA-dependent two-tiered regulated proteolysis cascade controls synthesis of a contact-dependent intercellular signal in *Myxococcus xanthus*. *Mol Microbiol* **84**: 260-275.

Konovalova, A., T. Petters & L. Søgaard-Andersen, (2010) Extracellular biology of *Myxococcus xanthus*. *FEMS Microbiol. Rev.* **34**: 89–106.

Koo, J., S. Tammam, S. Y. Ku, L. M. Sampaleanu, L. L. Burrows & P. L. Howell, (2008) PilF is an outer membrane lipoprotein required for multimerization and localization of the *Pseudomonas aeruginosa* Type IV pilus secretin. *J Bacteriol* **190**: 6961-6969.

Korotkov, K. V., T. L. Johnson, M. G. Jobling, J. Pruneda, E. Pardon, A. Heroux, S. Turley, J. Steyaert, R. K. Holmes, M. Sandkvist & W. G. Hol, (2011) Structural and functional studies on the interaction of GspC and GspD in the type II secretion system. *PLoS Pathog* **7**: e1002228.

Korotkov, K. V., M. Sandkvist & W. G. Hol, (2012) The type II secretion system: biogenesis, molecular architecture and mechanism. *Nat Rev Microbiol* **10**: 336-351.

Kühn, J., A. Briegel, E. Mörschel, J. Kahnt, K. Leser, S. Wick, G. J. Jensen & M. Thanbichler, (2010) Bactofilins, a ubiquitous class of cytoskeletal proteins mediating polar localization of a cell wall synthase in *Caulobacter crescentus*. *EMBO J* **29**: 327-339.

Kurre, R., A. Hone, M. Clausen, C. Meel & B. Maier, (2012) PilT2 enhances the speed of gonococcal type IV pilus retraction and of twitching motility. *Mol Microbiol* **86**: 857-865.

Kusumoto, A., A. Shinohara, H. Terashima, S. Kojima, T. Yakushi & M. Homma, (2008) Collaboration of FlhF and FlhG to regulate polar-flagella number and localization in *Vibrio alginolyticus*. *Microbiology* **154**: 1390-1399.

Laemmli, U. K., (1970) Cleavage of structural proteins during the assembly of the head of bacteriophage T4. *Nature* **227**: 680-685.

Lancero, H. L., S. Castaneda, N. B. Caberoy, X. Ma, A. G. Garza & W. Shi, (2005) Analysing protein-protein interactions of the *Myxococcus xanthus* Dif signalling pathway using the yeast two-hybrid system. *Microbiology* **151**: 1535-1541.

Leonardy, S., I. Bulyha & L. Sogaard-Andersen, (2008) Reversing cells and oscillating motility proteins. *Mol Biosyst* **4**: 1009-1014.

Leonardy, S., G. Freymark, S. Hebener, E. Ellehauge & L. Sogaard-Andersen, (2007) Coupling of protein localization and cell movements by a dynamically localized response regulator in *Myxococcus xanthus*. *EMBO J* **26**: 4433-4444.

Leonardy, S., M. Miertzschke, I. Bulyha, E. Sperling, A. Wittinghofer & L. Sogaard-Andersen, (2010) Regulation of dynamic polarity switching in bacteria by a Ras-like G-protein and its cognate GAP. *EMBO Journal* **29**: 2276-2289.

Li, J., E. H. Egelman & L. Craig, (2012) Structure of the Vibrio cholerae Type IVb Pilus and stability comparison with the *Neisseria gonorrhoeae* type IVa pilus. *J Mol Biol* **418**: 47-64.

Li, Y., H. Sun, X. Ma, A. Lu, R. Lux, D. Zusman & W. Shi, (2003) Extracellular polysaccharides mediate pilus retraction during social motility of *Myxococcus xanthus*. *Proc Natl Acad Sci U S A* **100**: 5443-5448.

Linderoth, N. A., P. Model & M. Russel, (1996) Essential role of a sodium dodecyl sulfate-resistant protein IV multimer in assembly-export of filamentous phage. *J Bacteriol* **178**: 1962-1970.

Lybarger, S. R., T. L. Johnson, M. D. Gray, A. E. Sikora & M. Sandkvist, (2009) Docking and assembly of the type II secretion complex of *Vibrio cholerae*. *J Bacteriol* **191**: 3149-3161.

Maier, B., M. Koomey & M. P. Sheetz, (2004) A force-dependent switch reverses type IV pilus retraction. *Proc Natl Acad Sci U S A* **101**: 10961-10966.

Martin, P. R., M. Hobbs, P. D. Free, Y. Jeske & J. S. Mattick, (1993) Characterization of pilQ, a new gene required for the biogenesis of type 4 fimbriae in *Pseudomonas aeruginosa*. *Mol Microbiol* **9**: 857-868.

Martin, P. R., A. A. Watson, T. F. McCaul & J. S. Mattick, (1995) Characterization of a five-gene cluster required for the biogenesis of type 4 fimbriae in *Pseudomonas aeruginosa*. *Mol Microbiol* **16**: 497-508.

Mattick, J. S., (2002) Type IV pili and twitching motility. *Annu Rev Microbiol* **56**: 289-314.

Mauriello, E. M., D. P. Astling, O. Sliusarenko & D. R. Zusman, (2009) Localization of a bacterial cytoplasmic receptor is dynamic and changes with cell-cell contacts. *Proc Natl Acad Sci U S A* **106**: 4852-4857.

Mauriello, E. M. F., F. Mouhamar, B. Nan, A. Ducret, D. Dai, D. R. Zusman & T. Mignot, (2010) Bacterial motility complexes require the actin-like protein, MreB and the Ras homologue, MglA. *Embo Journal* **29**: 315-326.

Merz, A. J. & K. T. Forest, (2002) Bacterial surface motility: slime trails, grappling hooks and nozzles. *Curr Biol* **12**: R297-303.

Merz, A. J., M. So & M. P. Sheetz, (2000) Pilus retraction powers bacterial twitching motility. *Nature* **407**: 98-102.

Mignot, T., J. P. Merlie, Jr. & D. R. Zusman, (2005) Regulated pole-to-pole oscillations of a bacterial gliding motility protein. *Science* **310**: 855-857.

Mignot, T., J. P. Merlie, Jr. & D. R. Zusman, (2007a) Two localization motifs mediate polar residence of FrzS during cell movement and reversals of *Myxococcus xanthus*. *Mol Microbiol* **65**: 363-372.

Mignot, T., J. W. Shaevitz, P. L. Hartzell & D. R. Zusman, (2007b) Evidence that focal adhesion complexes power bacterial gliding motility. *Science* **315**: 853-856.

Mileykovskaya, E. & W. Dowhan, (2000) Visualization of phospholipid domains in *Escherichia coli* by using the cardiolipin-specific fluorescent dye 10-N-nonyl acridine orange. *J Bacteriol* **182**: 1172-1175.

Morand, P. C., E. Bille, S. Morelle, E. Eugene, J. L. Beretti, M. Wolfgang, T. F. Meyer, M. Koomey & X. Nassif, (2004) Type IV pilus retraction in pathogenic *Neisseria* is regulated by the PilC proteins. *EMBO J* **23**: 2009-2017.

Mulder, L., B. Lefebvre, J. Cullimore & A. Imberty, (2006) LysM domains of Medicago truncatula NFP protein involved in Nod factor perception. Glycosylation state, molecular modeling and docking of chitooligosaccharides and Nod factors. *Glycobiology* **16**: 801-809.

Murray, T. S. & B. I. Kazmierczak, (2006) FlhF is required for swimming and swarming in *Pseudomonas aeruginosa*. *J Bacteriol* **188**: 6995-7004.

Nan, B. & D. R. Zusman, (2011) Uncovering the Mystery of Gliding Motility in the Myxobacteria. *Annual Review Genetics, Vol 45* **45**: 21-39.

Nan, B. Y., J. Chen, J. C. Neu, R. M. Berry, G. Oster & D. R. Zusman, (2011) Myxobacteria gliding motility requires cytoskeleton rotation powered by proton motive force. *Proceedings of the National Academy of Sciences of the United States of America* **108**: 2498-2503.

Nan, B. Y., E. M. F. Mauriello, I. H. Sun, A. Wong & D. R. Zusman, (2010) A multi-protein complex from *Myxococcus xanthus* required for bacterial gliding motility. *Molecular Microbiology* **76**: 1539-1554.

Nariya, H. & M. Inouye, (2008) MazF, an mRNA interferase, mediates programmed cell death during multicellular *Myxococcus* development. *Cell* **132**: 55-66.

Nishiyama, K., S. Mizushima & H. Tokuda, (1992) The carboxyl-terminal region of SecE interacts with SecY and is functional in the reconstitution of protein translocation activity in *Escherichia coli*. *J Biol Chem* **267**: 7170-7176.

Nudleman, E., D. Wall & D. Kaiser, (2005) Cell-to-cell transfer of bacterial outer membrane lipoproteins. *Science* **309**: 125-127.

Nudleman, E., D. Wall & D. Kaiser, (2006) Polar assembly of the type IV pilus secretin in *Myxococcus xanthus*. *Mol Microbiol* **60**: 16-29.

Nunn, D. N. & S. Lory, (1991) Product of the *Pseudomonas aeruginosa* gene *pilD* is a prepilin leader peptidase. *Proc Natl Acad Sci U S A* **88**: 3281-3285.

O'Connor, K. A. & D. R. Zusman, (1991) Development in *Myxococcus xanthus* involves differentiation into two cell types, peripheral rods and spores. *J Bacteriol* **173**: 3318-3333.

O'Toole, G. A. & R. Kolter, (1998) Flagellar and twitching motility are necessary for *Pseudomonas aeruginosa* biofilm development. *Mol. Microbiol.* **30**: 295-304.

Overgaard, M., S. Wegener-Feldbrugge & L. Sogaard-Andersen, (2006) The orphan response regulator DigR is required for synthesis of extracellular matrix fibrils in *Myxococcus xanthus*. *J Bacteriol* **188**: 4384-4394.

Pandza, S., M. Baetens, C. H. Park, T. Au, M. Keyhan & A. Matin, (2000) The G-protein FlhF has a role in polar flagellar placement and general stress response induction in *Pseudomonas putida*. *Mol Microbiol* **36**: 414-423.

Parge, H. E., K. T. Forest, M. J. Hickey, D. A. Christensen, E. D. Getzoff & J. A. Tainer, (1995) Structure of the fibre-forming protein pilin at 2.6 A resolution. *Nature* **378**: 32-38.

Park, H. S. M., M. Wolfgang & M. Koomey, (2002) Modification of type IV pilus-associated epithelial cell adherence and multicellular behavior by the PilU protein of *Neisseria gonorrhoeae*. *Infection and Immunity* **70**: 3891-3903.

Pathak, D. T., X. Wei, A. Bucuvalas, D. H. Haft, D. L. Gerloff & D. Wall, (2012) Cell contact-dependent outer membrane exchange in myxobacteria: genetic determinants and mechanism. *PLoS Genet* **8**: e1002626.

Peabody, C. R., Y. J. Chung, M.-R. Yen, D. Vidal-Ingigliardi, A. P. Pugsley & M. H. Saier Jr., (2003) Type II protein secretion and its relationship to bacterial type IV pili and archaeal flagella. *Microbiology* **149**: 3051-3072.

Pelicic, V., (2008) Type IV pili: e pluribus unum? *Mol Microbiol* **68**: 827-837.

Perez-Cheeks, B. A., P. J. Planet, I. N. Sarkar, S. A. Clock, Q. Xu & D. H. Figurski, (2012) The product of *tadZ*, a new member of the *parA/minD* superfamily, localizes to a pole in *Aggregatibacter actinomycetemcomitans*. *Mol Microbiol* **83**: 694-711.

Planet, P. J., S. C. Kachlany, R. DeSalle & D. H. Figurski, (2001) Phylogeny of genes for secretion NTPases: identification of the widespread tadA subfamily and development of a diagnostic key for gene classification. *Proc Natl Acad Sci U S A* **98**: 2503-2508.

Py, B., L. Loiseau & F. Barras, (2001) An inner membrane platform in the type II secretion machinery of Gram-negative bacteria. *EMBO Rep* **2**: 244-248.

Ramamurthi, K. S., S. Lecuyer, H. A. Stone & R. Losick, (2009) Geometric cue for protein localization in a bacterium. *Science* **323**: 1354-1357.

Ramamurthi, K. S. & R. Losick, (2009) Negative membrane curvature as a cue for subcellular localization of a bacterial protein. *Proc Natl Acad Sci U S A* **106**: 13541-13545.

Ramboarina, S., P. J. Fernandes, S. Daniell, S. Islam, P. Simpson, G. Frankel, F. Booy, M. S. Donnenberg & S. Matthews, (2005) Structure of the bundle-forming pilus from enteropathogenic *Escherichia coli*. *J Biol Chem* **280**: 40252-40260.

Reichow, S. L., K. V. Korotkov, W. G. Hol & T. Gonen, (2010) Structure of the cholera toxin secretion channel in its closed state. *Nat Struct Mol Biol* **17**: 1226-1232.

Remis, J. P., D. Wei, A. Gorur, M. Zemla, J. Haraga, S. Allen, H. E. Witkowska, J. W. Costerton, J. E. Berleman & M. Auer, (2013) Bacterial social networks: structure

and composition of *Myxococcus xanthus* outer membrane vesicle chains. *Environ Microbiol*.

Rodriguez-Soto, J. P. & D. Kaiser, (1997) Identification and localization of the Tgl protein, which is required for *Myxococcus xanthus* social motility. *J Bacteriol* **179**: 4372-4381.

Romantsov, T., S. Helbig, D. E. Culham, C. Gill, L. Stalker & J. M. Wood, (2007) Cardiolipin promotes polar localization of osmosensory transporter ProP in *Escherichia coli*. *Mol Microbiol* **64**: 1455-1465.

Rosenberg, E., K. H. Keller & M. Dworkin, (1977) Cell density-dependent growth of *Myxococcus xanthus* on casein. *J Bacteriol* **129**: 770-777.

Rumszauer, J., C. Schwarzenlander & B. Averhoff, (2006) Identification, subcellular localization and functional interactions of PilMNOWQ and PilA4 involved in transformation competency and pilus biogenesis in the thermophilic bacterium *Thermus thermophilus* HB27. *FEBS J* **273**: 3261-3272.

Russel, M., (1998) Macromolecular assembly and secretion across the bacterial cell envelope: type II protein secretion systems. *J Mol Biol* **279**: 485-499.

Sager, B. & D. Kaiser, (1994) Intercellular C-signaling and the traveling waves of *Myxococcus*. *Genes Dev* **8**: 2793-2804.

Sakai, D., T. Horiuchi & T. Komano, (2001) ATPase activity and multimer formation of PilQ protein are required for thin pilus biogenesis in plasmid R64. *J Biol Chem* **276**: 17968-17975.

Sampaleanu, L. M., J. B. Bonanno, M. Ayers, J. Koo, S. Tammam, S. K. Burley, S. C. Almo, L. L. Burrows & P. L. Howell, (2009) Periplasmic domains of *Pseudomonas aeruginosa* PilN and PilO form a stable heterodimeric complex. *J Mol Biol* **394**: 143-159.

Sanchez, M., A. Valencia, M. J. Ferrandiz, C. Sander & M. Vicente, (1994) Correlation between the structure and biochemical activities of FtsA, an essential cell division protein of the actin family. *EMBO J* **13**: 4919-4925.

Sandkvist, M., M. Bagdasarian, S. P. Howard & V. J. DiRita, (1995) Interaction between the autokinase EpsE and EpsL in the cytoplasmic membrane is required for extracellular secretion in *Vibrio cholerae*. *EMBO J* **14**: 1664-1673.

Sandkvist, M., L. P. Hough, M. M. Bagdasarian & M. Bagdasarian, (1999) Direct interaction of the EpsL and EpsM proteins of the general secretion apparatus in *Vibrio cholerae*. *J Bacteriol* **181**: 3129-3135.

Satyshur, K. A., G. A. Worzalla, L. S. Meyer, E. K. Heiniger, K. G. Aukema, A. M. Misic & K. T. Forest, (2007) Crystal structures of the pilus retraction motor PilT suggest large domain movements and subunit cooperation drive motility. *Structure* **15**: 363-376.

Sauvonnet, N., G. Vignon, A. P. Pugsley & P. Gounon, (2000) Pilus formation and protein secretion by the same machinery in *Escherichia coli*. *EMBO J* **19**: 2221-2228.

Segal, E., E. Billyard, M. So, S. Storzbach & T. F. Meyer, (1985) Role of chromosomal rearrangement in *N. gonorrhoeae* pilus phase variation. *Cell* **40**: 293-300.

Seifer, P., (2011) Analyse der Lokalisation und Funktion von PilD in *Myxococcus xanthus*. *Bachelor thesis, Philipps-Universität Marburg*.

Sheth, H. B., L. M. Glasier, N. W. Ellert, P. Cachia, W. Kohn, K. K. Lee, W. Paranchych, R. S. Hodges & R. T. Irvin, (1995) Development of an anti-adhesive vaccine for *Pseudomonas aeruginosa* targeting the C-terminal region of the pilin structural protein. *Biomed Pept Proteins Nucleic Acids* **1**: 141-148.

Shi, W., T. Kohler & D. R. Zusman, (1993) Chemotaxis plays a role in the social behaviour of *Myxococcus xanthus*. *Mol Microbiol* **9**: 601-611.

Shi, W. & D. R. Zusman, (1993) The two motility systems of *Myxococcus xanthus* show different selective advantages on various surfaces. *Proc. Natl. Acad. Sci. USA* **90**: 3378-3382.

Shi, X., S. Wegener-Feldbrugge, S. Huntley, N. Hamann, R. Hedderich & L. Sogaard-Andersen, (2008) Bioinformatics and experimental analysis of proteins of two-component systems in *Myxococcus xanthus*. *J Bacteriol* **190**: 613-624.

Shimkets, L. J., (1999) Intercellular signaling during fruiting-body development of *Myxococcus xanthus*. *Annu Rev Microbiol* **53**: 525-549.

Shimkets, L. J. & D. Kaiser, (1982) Induction of coordinated movement of *Myxococcus xanthus* cells. *J Bacteriol* **152**: 451-461.

Skare, J. T. & K. Postle, (1991) Evidence for a TonB-dependent energy transduction complex in *Escherichia coli*. *Mol Microbiol* **5**: 2883-2890.

Skerker, J. M. & H. C. Berg, (2001) Direct observation of extension and retraction of type IV pili. *Proc Natl Acad Sci U S A* **98**: 6901-6904.

Strom, M. S. & S. Lory, (1991) Amino acid substitutions in pilin of *Pseudomonas aeruginosa*. Effect on leader peptide cleavage, amino-terminal methylation, and pilus assembly. *J Biol Chem* **266**: 1656-1664.

Strom, M. S., D. Nunn & S. Lory, (1991) Multiple roles of the pilus biogenesis protein *pilD*: involvement of *pilD* in excretion of enzymes from *Pseudomonas aeruginosa*. *J Bacteriol* **173**: 1175-1180.

Strom, M. S., D. N. Nunn & S. Lory, (1993) A single bifunctional enzyme, PilD, catalyzes cleavage and N-methylation of proteins belonging to the type IV pilin family. *Proc Natl Acad Sci U S A* **90**: 2404-2408.

Sun, D. X., J. M. Seyer, I. Kovari, R. A. Sumrada & R. K. Taylor, (1991) Localization of protective epitopes within the pilin subunit of the *Vibrio cholerae* toxin-coregulated pilus. *Infect Immun* **59**: 114-118.

Sun, H., D. R. Zusman & W. Shi, (2000) Type IV pilus of *Myxococcus xanthus* is a motility apparatus controlled by the *frz* chemosensory system. *Curr. Biol.* **10**: 1143-1146.

Sun, M. Z., M. Wartel, E. Cascales, J. W. Shaevitz & T. Mignot, (2011) Motor-driven intracellular transport powers bacterial gliding motility. *Proceedings of the National Academy of Sciences of the United States of America* **108**: 7559-7564.

Takhar, H. K., K. Kemp, M. Kim, P. L. Howell & L. L. Burrows, (2013) The platform protein is essential for type IV pilus biogenesis. *J. Biol. Chem.* **288**: 9721-9728.

Tammam, S., L. M. Sampaleanu, J. Koo, K. Manoharan, M. Daubaras, L. L. Burrows & P. L. Howell, (2013) PilMNOPQ from the *Pseudomonas aeruginosa* type IV pilus system form a transenvelope protein interaction network that interacts with PilA. *J Bacteriol* **195**: 2126-2135.

Tammam, S., L. M. Sampaleanu, J. Koo, P. Sundaram, M. Ayers, P. Andrew Chong, J. D. Forman-Kay, L. L. Burrows & P. L. Howell, (2011) Characterization of the PilN, PilO and PilP type IVa pilus subcomplex. *Mol Microbiol* **82**: 1496-1514.

Treuner-Lange, A., K. Aguiluz, C. van der Does, N. Gómez-Santos, A. Harms, D. Schumacher, P. Lenz, M. Hoppert, J. Kahnt, J. Muñoz-Dorado & L. Søgaard-Andersen, (2012) PomZ, a ParA-like protein, regulates Z-ring formation and cell division in *Myxococcus xanthus*. *Mol. Microbiol.* **In press**.

Trindade, M. B., V. Job, C. Contreras-Martel, V. Pelicic & A. Dessen, (2008) Structure of a widely conserved type IV pilus biogenesis factor that affects the stability of secretin multimers. *J Mol Biol* **378**: 1031-1039.

Turner, L. R., J. C. Lara, D. N. Nunn & S. Lory, (1993) Mutations in the consensus ATP-binding sites of XcpR and PilB eliminate extracellular protein secretion and pilus biogenesis in *Pseudomonas aeruginosa*. *J Bacteriol* **175**: 4962-4969.

van den Ent, F., L. A. Amos & J. Lowe, (2001) Prokaryotic origin of the actin cytoskeleton. *Nature* **413**: 39-44.

van den Ent, F. & J. Lowe, (2000) Crystal structure of the cell division protein FtsA from *Thermotoga maritima*. *EMBO J* **19**: 5300-5307.

Viollier, P. H., N. Sternheim & L. Shapiro, (2002) Identification of a localization factor for the polar positioning of bacterial structural and regulatory proteins. *Proc Natl Acad Sci U S A* **99**: 13831-13836.

Voulhoux, R., M. P. Bos, J. Geurtsen, M. Mols & J. Tommassen, (2003) Role of a highly conserved bacterial protein in outer membrane protein assembly. *Science* **299**: 262-265.

Wall, D. & D. Kaiser, (1998) Alignment enhances the cell-to-cell transfer of pilus phenotype. *Proc Natl Acad Sci U S A* **95**: 3054-3058.

Wall, D. & D. Kaiser, (1999) Type IV pili and cell motility. *Mol Microbiol* **32**: 1-10.

Wall, D., P. E. Kolenbrander & D. Kaiser, (1999) The *Myxococcus xanthus pilQ (sglA)* gene encodes a secretin homolog required for type IV pilus biogenesis, social motility, and development. *J Bacteriol* **181**: 24-33.

Ward, M. J., H. Lew & D. R. Zusman, (2000) Social motility in *Myxococcus xanthus* requires FrzS, a protein with an extensive coiled-coil domain. *Mol Microbiol* **37**: 1357-1371.

Wei, X., D. T. Pathak & D. Wall, (2011) Heterologous protein transfer within structured myxobacteria biofilms. *Mol Microbiol* **81**: 315-326.

Whitchurch, C. B., M. Hobbs, S. P. Livingston, V. Krishnapillai & J. S. Mattick, (1991) Characterisation of a *Pseudomonas aeruginosa* twitching motility gene and evidence for a specialised protein export system widespread in eubacteria. *Gene* **101**: 33-44.

Whitchurch, C. B. & J. S. Mattick, (1994) Characterization of a gene, *pilU*, required for twitching motility but not phage sensitivity in *Pseudomonas aeruginosa*. *Mol Microbiol* **13**: 1079-1091.

Winther-Larsen, H. C., M. C. Wolfgang, J. P. van Putten, N. Roos, F. E. Aas, W. M. Egge-Jacobsen, B. Maier & M. Koomey, (2007) Pseudomonas aeruginosa Type IV pilus expression in *Neisseria gonorrhoeae*: effects of pilin subunit composition on function and organelle dynamics. *J Bacteriol* **189**: 6676-6685.

Wireman, J. W. & M. Dworkin, (1977) Developmentally induced autolysis during fruiting body formation by *Myxococcus xanthus*. *J Bacteriol* **129**: 798-802.

Wolfgang, M., H. S. Park, S. F. Hayes, J. P. van Putten & M. Koomey, (1998) Suppression of an absolute defect in type IV pilus biogenesis by loss-of-function mutations in *pilT*, a twitching motility gene in *Neisseria gonorrhoeae*. *Proc Natl Acad Sci U S A* **95**: 14973-14978.

Wolfgang, M., J. P. van Putten, S. F. Hayes, D. Dorward & M. Koomey, (2000) Components and dynamics of fiber formation define a ubiquitous biogenesis pathway for bacterial pili. *EMBO J* **19**: 6408-6418.

Wolgemuth, C., E. Hoiczyk, D. Kaiser & G. Oster, (2002) How myxobacteria glide. *Current Biology* **12**: 369-377.

Wu, S. S. & D. Kaiser, (1996) Markerless deletions of pil genes in *Myxococcus xanthus* generated by counterselection with the *Bacillus subtilis sacB* gene. *J Bacteriol* **178**: 5817-5821.

Wu, S. S. & D. Kaiser, (1997) Regulation of expression of the *pilA* gene in *Myxococcus xanthus*. *Journal of Bacteriology* **179**: 7748-7758.

Wu, S. S., J. Wu, Y. L. Cheng & D. Kaiser, (1998) The *pilH* gene encodes an ABC transporter homologue required for type IV pilus biogenesis and social gliding motility in *Myxococcus xanthus*. *Mol Microbiol* **29**: 1249-1261.

Wu, S. S., J. Wu & D. Kaiser, (1997) The *Myxococcus xanthus pilT* locus is required for social gliding motility although pili are still produced. *Mol Microbiol* **23**: 109-121.

Yamagata, A., E. Milgotina, K. Scanlon, L. Craig, J. A. Tainer & M. S. Donnenberg, (2012) Structure of an essential type IV pilus biogenesis protein provides insights into pilus and type II secretion systems. *J Mol Biol* **419**: 110-124.

Yang, Z., Y. Geng, D. Xu, H. B. Kaplan & W. Shi, (1998) A new set of chemotaxis homologues is essential for *Myxococcus xanthus* social motility. *Mol Microbiol* **30**: 1123-1130.

Yang, Z., R. Lux, W. Hu, C. Hu & W. Shi, (2010) PilA localization affects extracellular polysaccharide production and fruiting body formation in *Myxococcus xanthus*. *Mol Microbiol*.

Zhang, Y., M. Franco, A. Ducret & T. Mignot, (2010) A bacterial Ras-like small GTP-binding protein and its cognate GAP establish a dynamic spatial polarity axis to control directed motility. *PLoS Biol* **8**: e1000430.

Zhang, Y., M. Guzzo, A. Ducret, Y. Z. Li & T. Mignot, (2012) A dynamic response regulator protein modulates G-protein-dependent polarity in the bacterium *Myxococcus xanthus*. *PLoS Genet* **8**: e1002872.

Zusman, D. R., A. E. Scott, Z. Yang & J. R. Kirby, (2007) Chemosensory pathways, motility and development in *Myxococcus xanthus*. *Nat Rev Microbiol* **5**: 862-872.

Acknowledgments/ Danksagung

Zu allererst möchte ich mich bei meiner Betreuerin Prof. Dr. Lotte Søgaard-Andersen bedanken, die mich während meiner akademischen Laufbahn stets unterstützt und angetrieben hat.

Für die Übernahme des Zweitgutachtens möchte ich mich ganz herzlich bei PD Dr. Sonja-Verena Albers bedanken.

Mein Dank gilt ebenfalls den Mitgliedern meines Prüfungs- und IMPRS-Kommittees: Prof. Dr. Andrea Maisner, Prof. Dr. Michael Bölker, Prof. Dr. Erhard Bremer, PD Dr. Sonja-Verena Albers und Dr. Chris van der Does.

Für die Finanzierung meiner Dissertation möchte ich mich bei der International Max Planck Research School for Environmental, Cellular and Molecular Microbiology, als auch beim Sonderforschungsbereich 987 „Microbial Diversity in Environmental Signal Response“ bedanken.

Bei Dr. Andreas Klingl möchte ich mich für die angenehme Zusammenarbeit und für die tollen EM-Bilder bedanken.

[redacted]

Curriculum vitae

Erklärung

Hiermit versichere ich, dass ich die vorliegende Dissertation mit dem Titel „Deciphering the assembly pathway of Type IV pili in *Myxococcus xanthus*“ selbstständig verfasst, keine anderen als die im Text angegebenen Hilfsmittel verwendet und sämtliche Stellen, die im Wortlaut oder dem Sinn nach anderen Werken entnommen sind, mit Quellenangaben kenntlich gemacht habe. Die Dissertation wurde in der jetzigen oder einer ähnlichen Form noch bei keiner anderen Hochschule eingereicht und hat noch keinen sonstigen Prüfungszwecken gedient.

Ort, Datum

Carmen Friedrich